NOISE ABATEMENT AND INTERNAL VIBRATIONAL ABSORPTION IN POTENTIAL STRUCTURAL MATERIALS

L. Kaufman, et al

Manlabs, Incorporated

Prepared for:

Advanced Research Projects Agency
Army Materials and Mechanics Research Center

March 1975

AMMRC CTR 75-4

NOISE ABATEMENT AND INTERNAL VIBRATIONAL ABSORPTION IN POTENTIAL STRUCTURAL MATERIALS

March 1975

L. Kaufman, S. A. Kulin, P. P. Neshe

ManLabs, Inc.
21 Erie Street
Cambridge, Massachusetts 02139

Semi-Annual Report Contract Number DAAG46-74-C-0048

Sponsored by: Defense Advanced Research Projects Agency
ARPA Order No. 2555

Program Code No. A13719
Effective Date of Contract: 1 December 1973
Contract Expiration Date: 30 June 1975
Amount of Contract: $275,454.00
Contract Period Covered by Report: 1 September 1974 to 1 March 1975

Approved for public release; distribution unlimited.

Prepared for

ARMY MATERIALS AND MECHANICS RESEARCH CENTER
Watertown, Massachusetts 02172

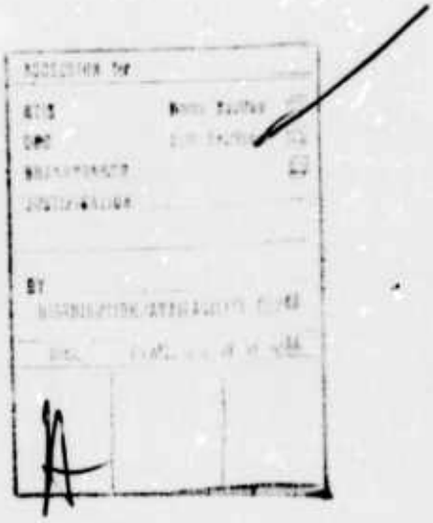

The view and conclusions contained in this document are those of the authors and should not be interprated as necessarily representing the official policies, either expressed or implied, of the Defense Advanced Research Projects Agency of the U. S. Government.

Mention of any trade names or manufacturers in this report shall not be construed as advertising nor as an official indorsement or approval of such products or companies by the United States Govarnment.

DISPOSITION INSTRUCTIONS

Destroy this report when it is no longer needed.
Do not return it to the originator.

UNCLASSIFIED

SECURITY CLASSIFICATION OF THIS PAGE (When Data Entered)

REPORT DOCUMENTATION PAGE

READ INSTRUCTIONS BEFORE COMPLETING FORM

1 REPORT NUMBER: AMMRC CTR 75-4

2 GOVT ACCESSION NO.:

3 RECIPIENT'S CATALOG NUMBER:

4 TITLE (and Subtitle): NOISE ABATEMENT AND INTERNAL VIBRATIONAL ABSORPTION IN POTENTIAL STRUCTURAL MATERIALS

5 TYPE OF REPORT & PERIOD COVERED: Semi-Annual Report 1 Sept. 1974--1 March 1975

6 PERFORMING ORG. REPORT NUMBER:

7 AUTHOR(s): L. Kaufman, S. A. Kulin, P. P. Neshe

8 CONTRACT OR GRANT NUMBER(s): DAAG46-74-C-0048

9 PERFORMING ORGANIZATION NAME AND ADDRESS:

10 PROGRAM ELEMENT, PROJECT, TASK AREA & WORK UNIT NUMBERS: See Item 18

11 CONTROLLING OFFICE NAME AND ADDRESS: Army Materials and Mechanics Research Center, Watertown, Massachusetts 02172

12 REPORT DATE: March 1975

13 NUMBER OF PAGES: 131

14 MONITORING AGENCY NAME & ADDRESS (if different from Controlling Office):

15 SECURITY CLASS. (of this report): Unclassified

15a DECLASSIFICATION/DOWNGRADING SCHEDULE:

16 DISTRIBUTION STATEMENT (of this Report)

Approved for public release; distribution unlimited.

17 DISTRIBUTION STATEMENT (of the abstract entered in Block 20, if different from Report)

18 SUPPLEMENTARY NOTES

ARPA Order: 2555
Program Code: A13719
AMCMS Code: 690000.21.10846
Agency Accession: DA OE 4778

19 KEY WORDS (Continue on reverse side if necessary and identify by block number)

Titanium-nickel alloys
Vibration damping
Sound transmission
Internal friction

20 ABSTRACT (Continue on reverse side if necessary and identify by block number)

The results obtained during the initial phase of this study indicate that structural changes which occur during phase transformations (particularly those of a thermoelastic nature) can offer a significant means for absorbing acoustical energy. In particular the complete set of resistivity, modulus, heat capacity and damping measurements performed on the 55 w/o Ni-45 w/o Ti alloy shows that over a useful temperature range between 12°C and 32°C high yield strength and high damping can be combined.

DD FORM 1 JAN 73 1473 EDITION OF 1 NOV 65 IS OBSOLETE

UNCLASSIFIED

SECURITY CLASSIFICATION OF THIS PAGE (When Data Entered)

Moreover, present results indicate that plastic deformation can be employed to expand the temperature range over which the attractive properties can be combined and to increase the strength levels.

Although the above mentioned desirable characteristics appear attainable, the mechanistic origin of the damping remains a mystery. The present results show that damping increases above the M_S temperature. Although twin formation readily occurs below M_S, no discernable structural changes occur above M_S. Hence the only postulated source for enhanced damping at temperatures above M_S is some precursor mechanism like soft mode formation. Externally applied tensile stresses characteristic of those employed in the damping measurements (up to 5500 psi) were found to have a negligible effect on M_S.

Preliminary studies of iron-platinum, copper-aluminum-nickel, cobalt-nickel and cobalt-iron alloys suggest that other examples of high strength-high damping materials based on structural transformations may be developed. In particular, a range of cobalt-iron alloys has been identified which exhibits loss factors that are five to fifty times higher than commercially available materials. Although the strength of this alloy is currently low, mechanisms exist for increasing the strength. These methods are currently under investigation.

TABLE OF CONTENTS

LIST OF TABLES

LIST OF FIGURES

LIST OF FIGURES (continued)

LIST OF FIGURES (continued)

LIST OF FIGURES (continued)

LIST OF FIGURES (continued)

LIST OF FIGURES (continued)

I. INTRODUCTION

Machinery contains parts that are subjected to periodic stresses resulting in acoustic waves which are set in motion in the solid components. When these waves reach a free surface in contact with the air, noise is produced. Since the energy in the acoustic waves is generally a small fraction of the total energy output of a machine, conversion of this energy to heat becomes an effective method of noise reduction with only an insignificant accompanying temperature rise. Damping materials with good structural properties are required to fulfill this function.

A number of damping materials like TiNi, Mn-Cu, Cu-Al-Ni, Co-Ni and Fe-Co alloys have been identified but the fundamental atomic processes causing the damping have not been clearly defined. Anharmonicity must be present to convert the acoustic waves into heat and atomic models employed to explain damping include twin boundary movement, stacking fault movement, phase boundary movement and magnetostrictive effects. The discovery of new damping alloys has been rather accidental and the ability to tailor an alloy to a specific engineering requirement demands considerable research into the understanding of the atomic mechanisms.

The present study is aimed at rectifying this situation by providing insight into possible mechanisms of acoustic absorption. The ultimate goal of the study is identification of alloys which can reduce vibration and noise associated with the operation of devices containing rapidly moving components. In some cases, notably helicopter and submarine propulsion systems, such reductions could result in a marked improvement of performance, lifetime and operating characteristics. Development of structural materials with high damping or noise absorption capacities offers a convenient method for attaining this objective. The present report summarizes the progress made during the past six-month period of an investigation of methods for achieving high internal damping in potential structural materials. This study has been conducted by ManLabs, Inc.

with the cooperation of groups at the Metallurgy Department of M.I.T., the Physics of Solids Group at Army Materials and Mechanics Research Center, and at Bolt, Beranek and Newman Inc. The initial objective of the program is to identify the basic mechanisms for achieving high internal damping and thereby identify potential materials approaches in noise and vibration reduction technology.

The results presented in the current report, obtained in studies of Ni-Ti, Cu-Al-Ni and Fe-Pt alloys, illustrate how phase transformations can be employed to achieve high vibrational damping. In addition preliminary experiments on nickel and a cobalt nickel alloy show that magnetostrictive effects can be employed to produce enhanced acoustical absorption. Moreover, the initial results obtained with cobalt-iron alloys have produced very high damping behavior.

Comparison of the damping capacity (or loss factor) and yield strength of cold worked Ni-Ti and Co-Fe alloys with commercially available alloys shows that opportunities exist for achieving higher damping capacity/strength characteristics than are presently available. In particular alloys in the composition range near 80 w/o cobalt-20 w/o iron have been found to exhibit loss factors that are five to fifty times higher than commercially available materials. Although the strength of these alloys in the high damping conditions is low, mechanisms exist for increasing the strength. These mechanisms are currently under investigation.

II. MEASUREMENT OF TRANSFORMATION BEHAVIOR AND STRENGTH OF A 55Ni-45Ti ALLOY

A substantial portion of the activities during this reporting period have been directed toward establishing whether the damping phenomenon observed in NiTi is directly related to the onset of transformation or if it occurs in a temperature range above M_S where atomic shuffles are thought to take place. In order to test the latter hypothesis it was decided to perform simultaneous measurements of the electrical resistance and acoustic emission of NiTi samples as a function of temperature. The measurements were conducted on the standard "reed" samples which BBN requires for measurements of damping capacity as a function of temperature. The resistivity of a typical NiTi 55 a/o alloy is shown in Figure 1 as a function of temperature cycling through the transition range. Simultaneous metallographic and resistance measurements do not disclose actual formation of the daughter or martensite phase in the region where the resistance increases. This is where the "atomic shuffles" are supposed to take place. In order to determine if these "soft mode displacements" lead to enhanced damping, specimens were temperature cycled many times to obtain a well defined resistivity peak. The peak in the cooling curve represents the M_S temperature as defined by the temperature at which the first observable surface relief forms on cooling (1-3).*

The present results obtained by BBN indicate that the increase in damping capacity begins in the temperature regime above M_S corresponding to the region of increasing electrical resistivity during cooling of the NiTi alloy.

In order to perform the above noted experiments, a precision electrical resistivity apparatus was constructed using the double Kelvin Bridge principle. This apparatus uses an L&N type K-3 potentiometer, a standard cell, constant voltage supply, a

---

*Underscored numbers in parentheses denote references.

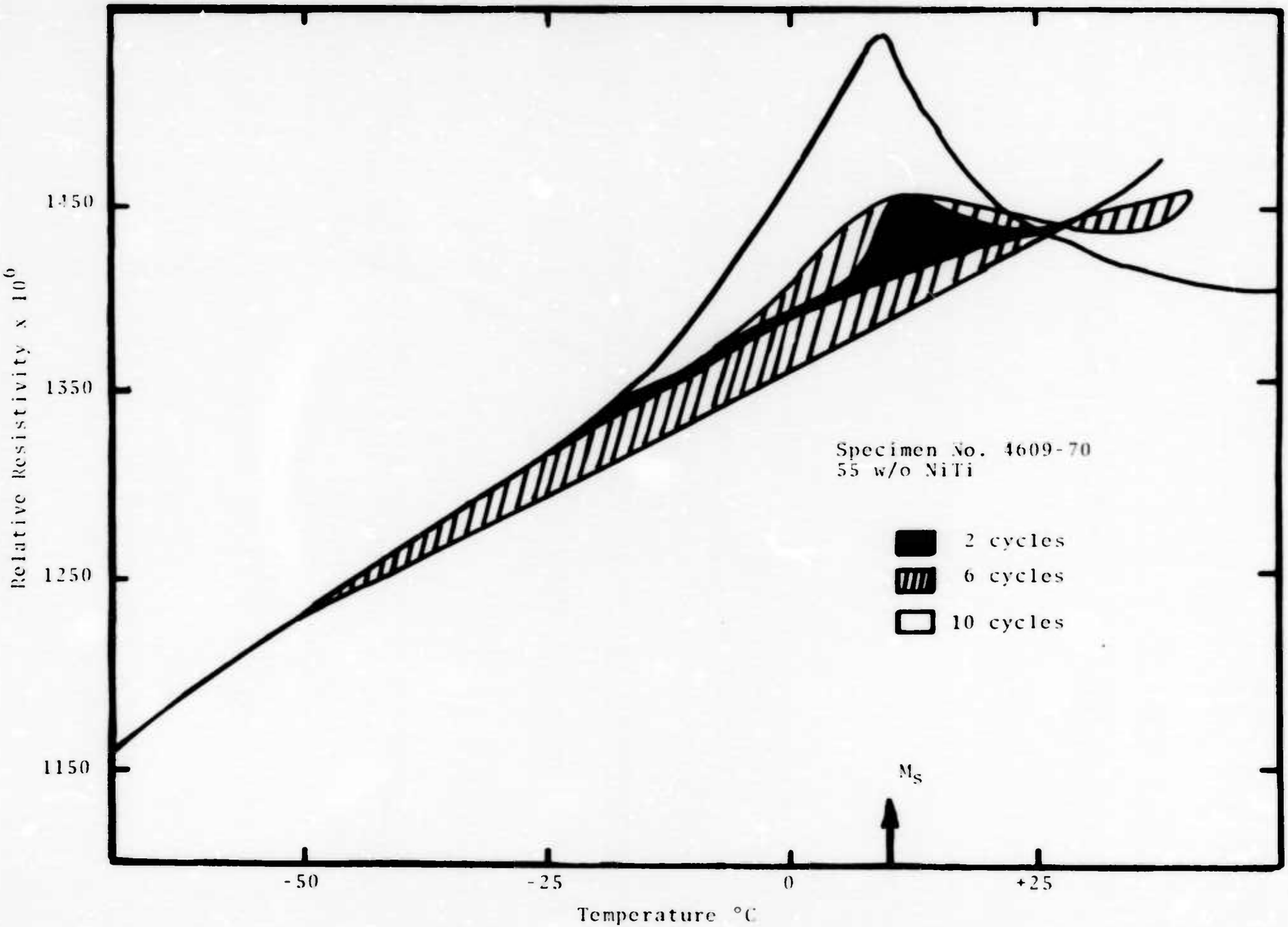

Figure 1. Electrical Resistivity versus Temperature for a 55 w/o NiTi Alloy as a Function of Number of Temperature Cycles.

regulated power supply, a L&N resistance standard and a L&N D.C. null detector. The precision of measurement obtained is of the order of 1×10^{-6} ohm-cm.

An acoustic apparatus was designed and constructed to yield information as to the types of martensitic transformations occuring, i.e. burst phenomena, thermoelastic, etc. This equipment uses a wire hook-up from a crystal transducer to the specimen. Standard amplifier and loud speaker are connected to the transducer. In addition, an Esterline Angus high speed recorder was connected so that a permanent record could be made of the acoustic emissions from the specimen during temperature cycling through the temperature range of interest. No acoustic emissions have been observed to date in experiments performed on NiTi samples as cycled through the "soft-mode" and the martensitic transformation temperature ranges. In contrast, much acoustic activity was detected during transformation in experiments using 70 Fe-30 Ni alloys in which "burst-type" martensitic transformation is known to occur (4). The above experiments indicate that the mechanism of martensitic transformation in the highly damping NiTi alloys is of the thermo-elastic mode.

In order to establish a stable transformation behavior as a baseline treatment for samples to be treated prior to various measurements, multiple temperature cycles between -65°C and +90°C were employed. The cycling treatment consisted of immersion in a Dow Corning 200-10CS/Dry Ice mixture held at -65°C and a second Dow Corning 200-10CS bath at 90°C. A ten-minute cycle is employed in this treatment. Figure 2 shows the resistance-temperature curve obtained after seventy-six cycles. Since these characteristics are well defined, a treatment of 50-70 cycles was selected as the basis for preparation of specimens to be evaluated by calorimetry, damping and Young's modulus measurements over the -65°C to 90°C temperature range.

A second series of experiments designed to evaluate the effects of cold work on the transformation characteristics was

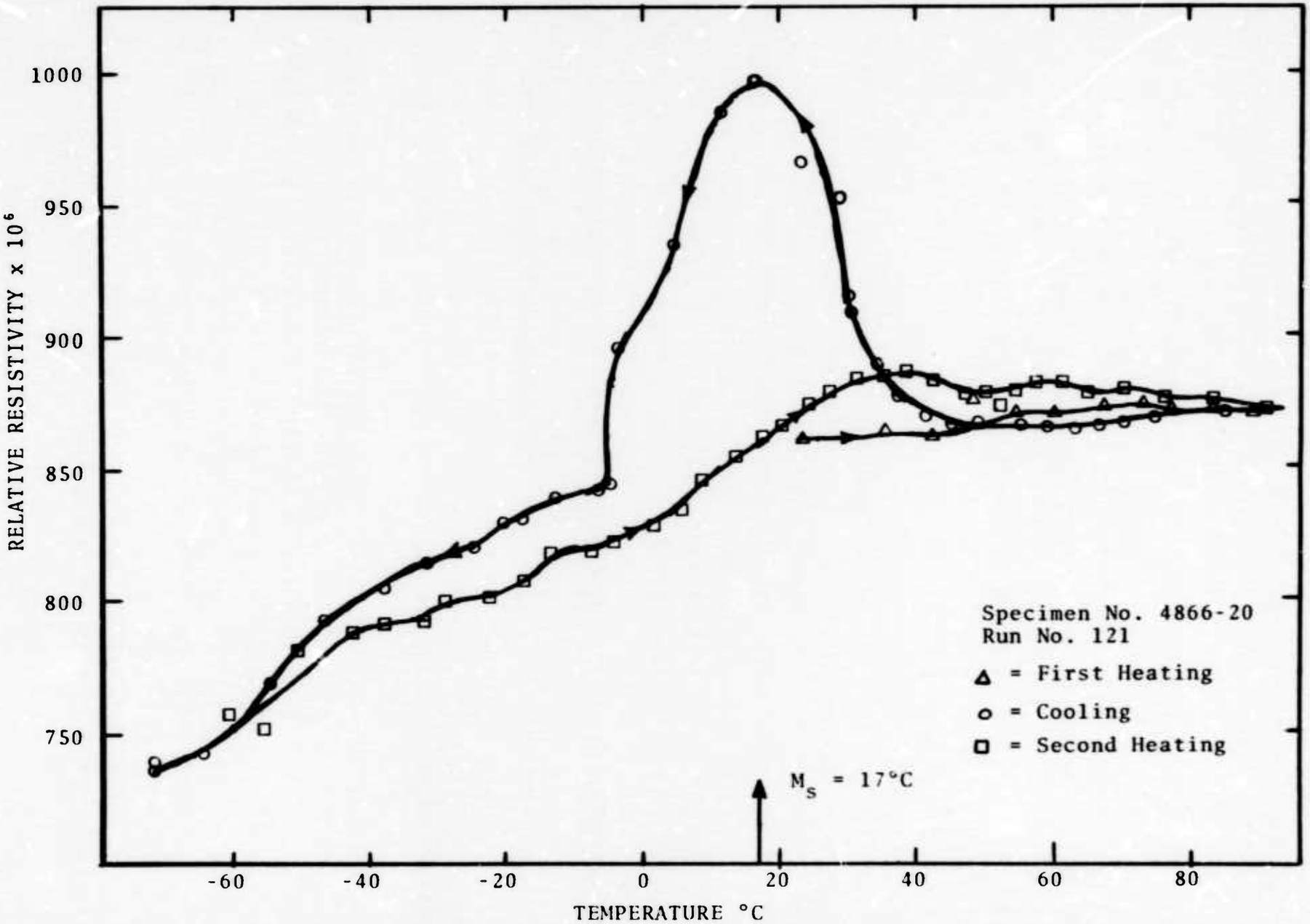

Figure 2. Electrical Resistivity versus Temperature for a 55 w/o NiTi Alloy as a Function of Temperature after 76 cycles between -65°C and +90°C.

carried out. These studies were conducted by heat treating strips of 55 w/o NiTi (4866) by annealing at 790°C for thirty minutes, quenching in water and cycling between -65°C and +90°C fifty times. Following this treatment the electrical resistance of the 190 mil x 250 mil x 5.5 inch strip was measured as a function of temperature. Figure 3 shows the results of this test. Subsequently, the strip was deformed by rolling at room temperature. This treatment was followed by a second set of fifty temperature cycles between -65°C and +90°C. Finally the resistance-temperature characteristics were measured again. Three levels of deformation were employed in this series of tests. These corresponded to 3.2%, 7% and 15.2%. The resultant measurements (obtained on three different bars) are shown in Figures 4-6. These curves show that deformation in the 0-7% range broadens the temperature range of the transformation while 15% deformation seems to obscure the change of resistance with transformation or eliminate the transformation entirely. These test bars were examined by determining their damping characteristics so that the effect of deformation on damping could be evaluated. The results have been combined to determine the optimum treatment which can be employed to achieve attractive damping and strength characteristics.

Due to the difficulty in machining NiTi specimens, it was decided to determine the possible usefulness of a flat-type specimen as compared with the standard reed-type specimens employed for damping capacity measurements in the BBN Resonant Dwell Apparatus. Specimens of each type were fabricated and were temperature cycled (up to seventy-six cycles) to yield stable temperature resistivity curves prior to measurement of damping capacity as a function of temperature by BBN. The results of the damping studies on the flat-type specimens did not compare favorably with the standard reed-type samples. As a consequence, the latter configuration will be employed exclusively.

Since the present study is designed to investigate the mechanism of damping in NiTi and the current results (presented in

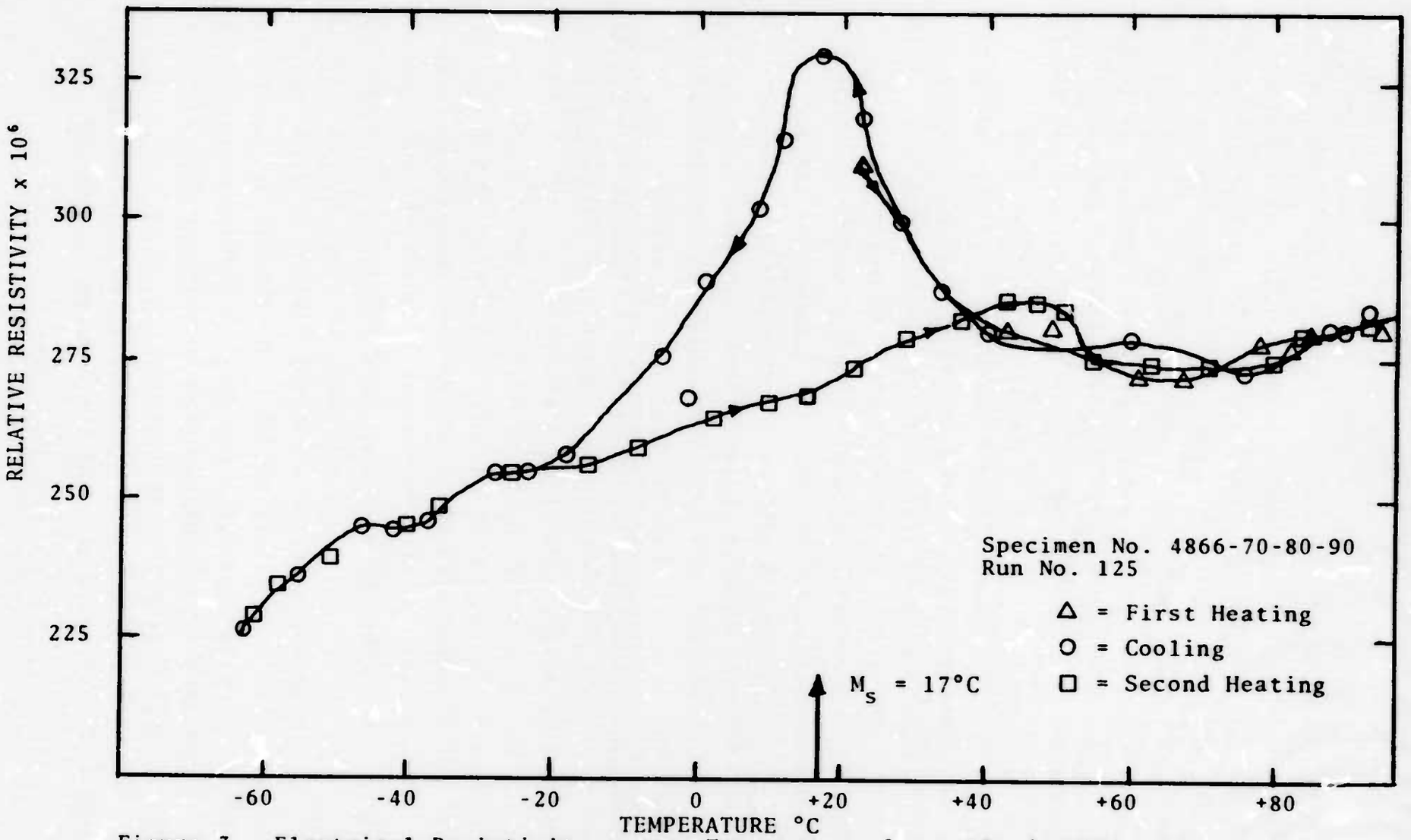

Figure 3. Electrical Resistivity versus Temperature for a 55 w/o NiTi Alloy as a Function of Temperature after 50 cycles between -65°C and +90°C.

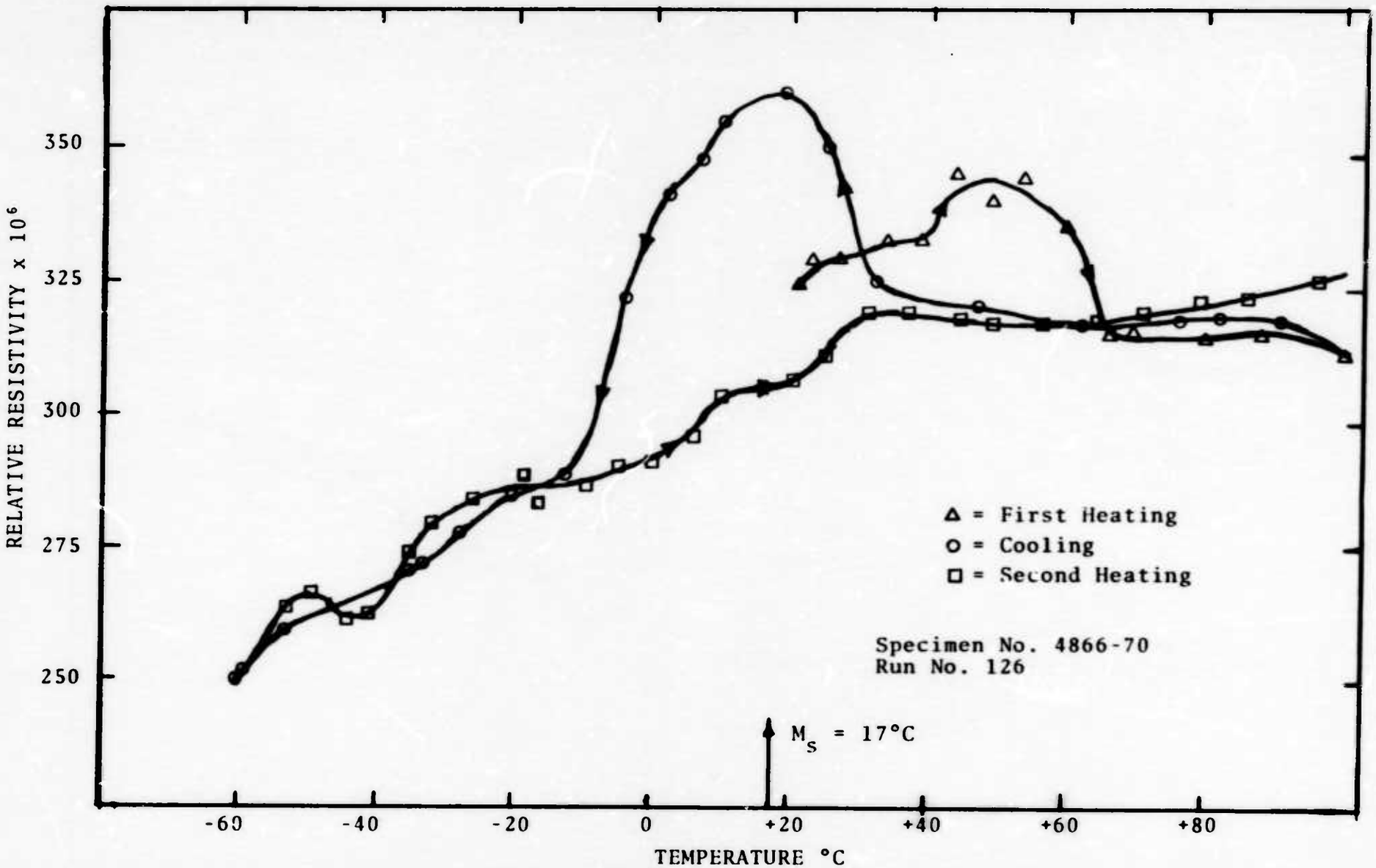

Figure 4. Electrical Resistivity versus Temperature for a 55 w/o NiTi Alloy as a Function of Temperature after 3.2% deformation by rolling followed by 50 cycles between -65°C and +90°C.

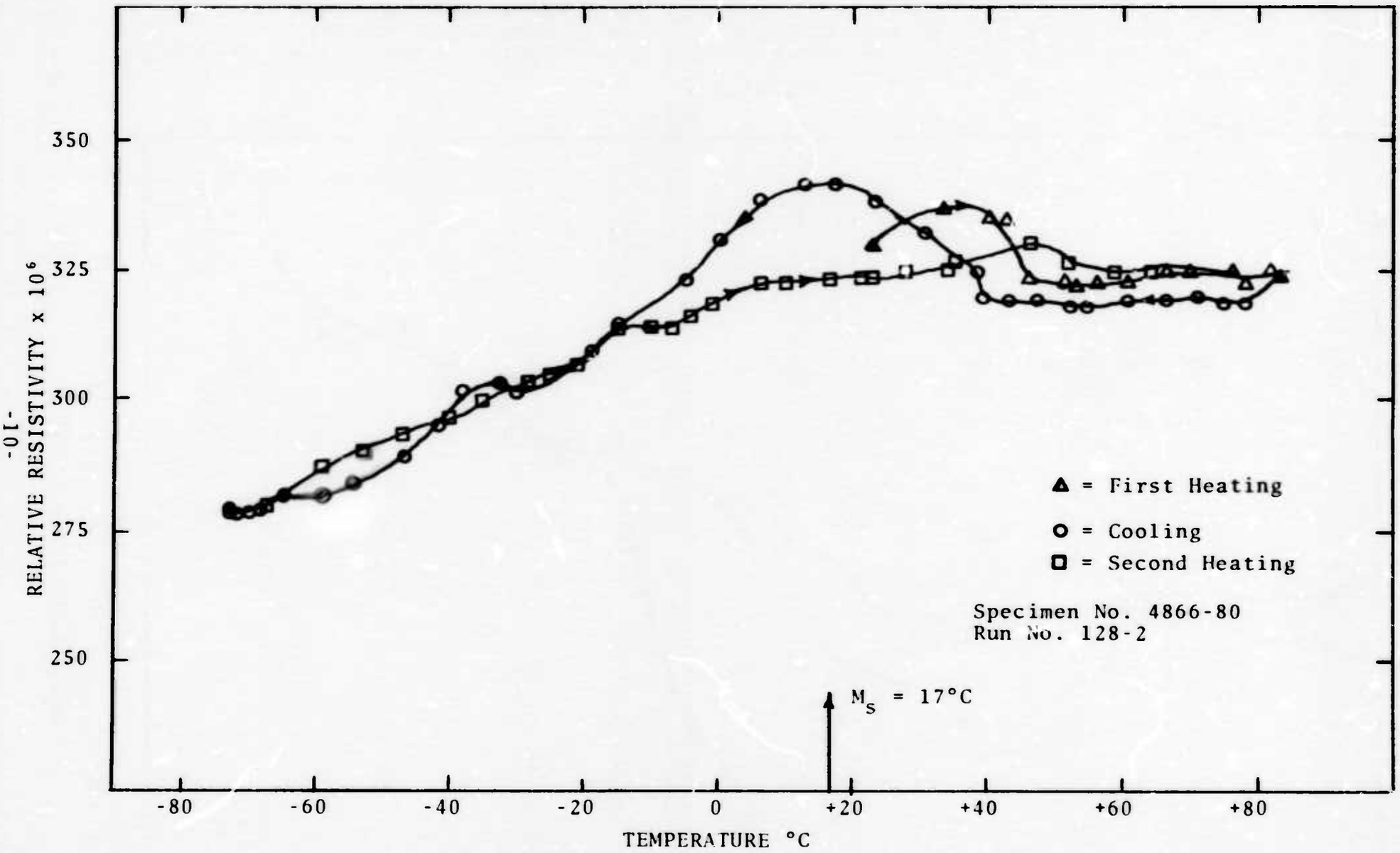

Figure 5. Electrical Resistivity versus Temperature for a 55 w/o NiTi Alloy as a Function of Temperature after 7% deformation by rolling followed by 50 cycles between -65°C and +90°C.

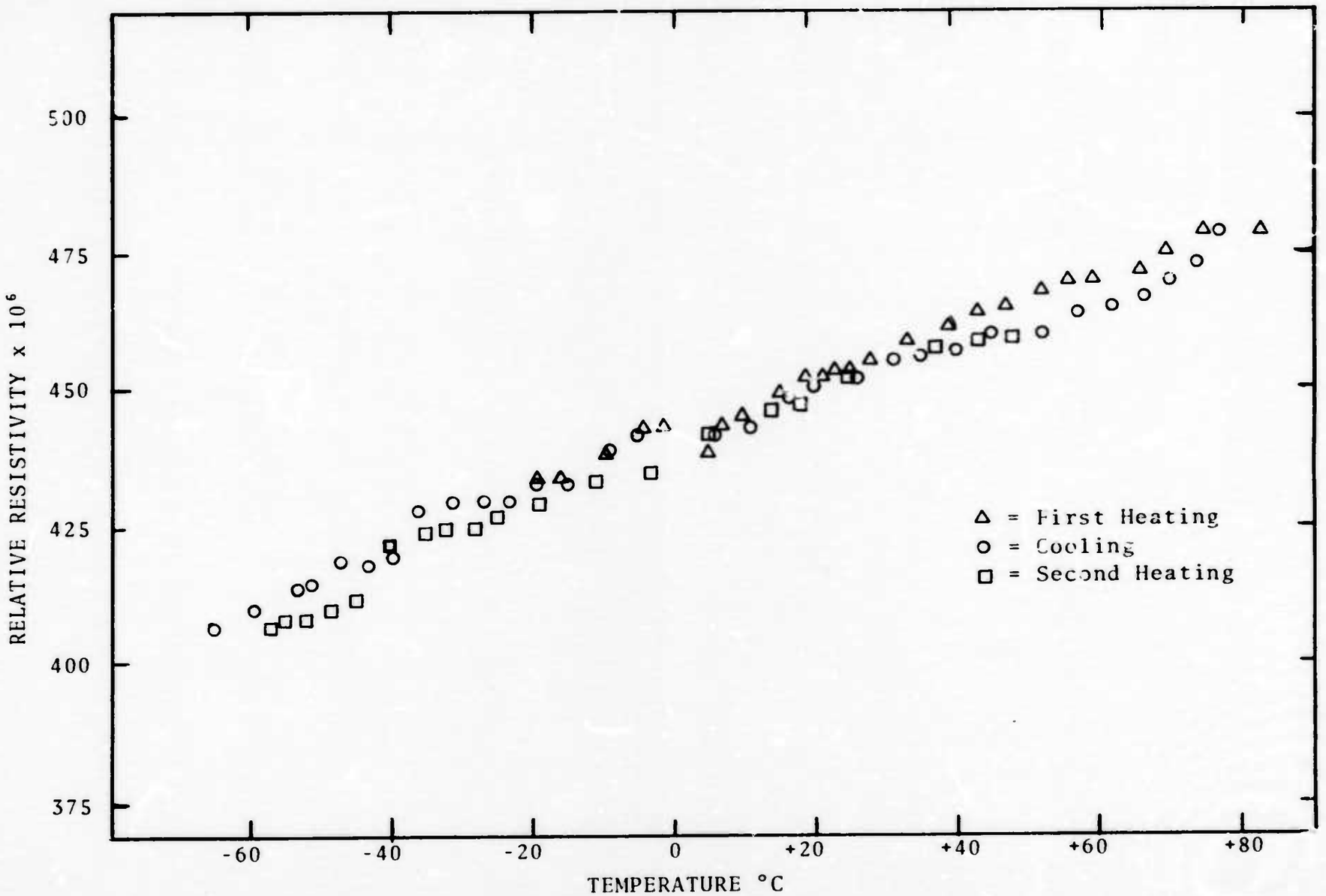

Figure 6. Electrical Resistivity versus Temperature for a 55 w/o NiTi Alloy a a Function of Temperature after 15% deformation by rolling followed by 50 cycles between -65°C and +90°C.

Sections III and IV) describe the behavior at stress levels up to 5000 psi, it is essential to determine if such stresses have an appreciable influence on M_s. Accordingly, the transformation characteristics of the 55 w/o NiTi alloy (i.e. 55 w/o Ni-45 w/o Ti) were redetermined at tensile stresses of 1275 and 5484 respectively. Figures 7 through 9 show the results of runs numbered 124, 130 and 131. Identical samples of the 55 w/o Ni-45 w/o Ti alloy were annealed and run through fifty temperature cycles between -65°C and +90°C. Figure 7 shows the resistivity-temperature curve obtained on a sample with no applied tensile load. The resistivity peak occurs at about +20°C, in good general agreement with the results obtained for samples of this alloy which were run earlier as shown in Figures 2 and 3. Figures 8 and 9 show the resistivity-temperature curves obtained on the companion samples while tensile loads corresponding to stress levels of 1275 and 5484 psi respectively were applied. No appreciable shift in M_s was observed.

A series of experiments were carried out to evaluate the strength levels attainable in the 55 w/o NiTi alloy in the temperature range where high damping levels could be achieved. As a first step, annealed samples were exposed to fifty temperature cycles between -65°C and +90°C and then tested at +83°C, +20°C, 0°C and -74°C in tension. Figures 10-13 show the stress-strain curves obtained from these tests. The 0.2 percent offset strain yield strength is indicated in each case. This heat of the 55 w/o Ni-45 w/o Ti alloy (4866) exhibits an M_s at +17°C after multiple cycling as can be seen in Figures 2, 3, 7, 8 and 9. Thus the +83°C and +20°C tensile tests correspond to temperatures above M_s while the 0°C and -74°C tests correspond to temperatures below M_s. The latter give low yield strengths near 20,000 psi. However, the 20°C yield strengths in the 47000-55000 psi range are attained. The stress-strain curves shown in Figures 10-13 were obtained on samples which were cycled fifty times between -65°C and +90°C. In each case, the final step was heating from -65°C to room temperature before tensile testing. Figures 14 and 15 show the results obtained when the final cycle consists of cooling from 100°C to

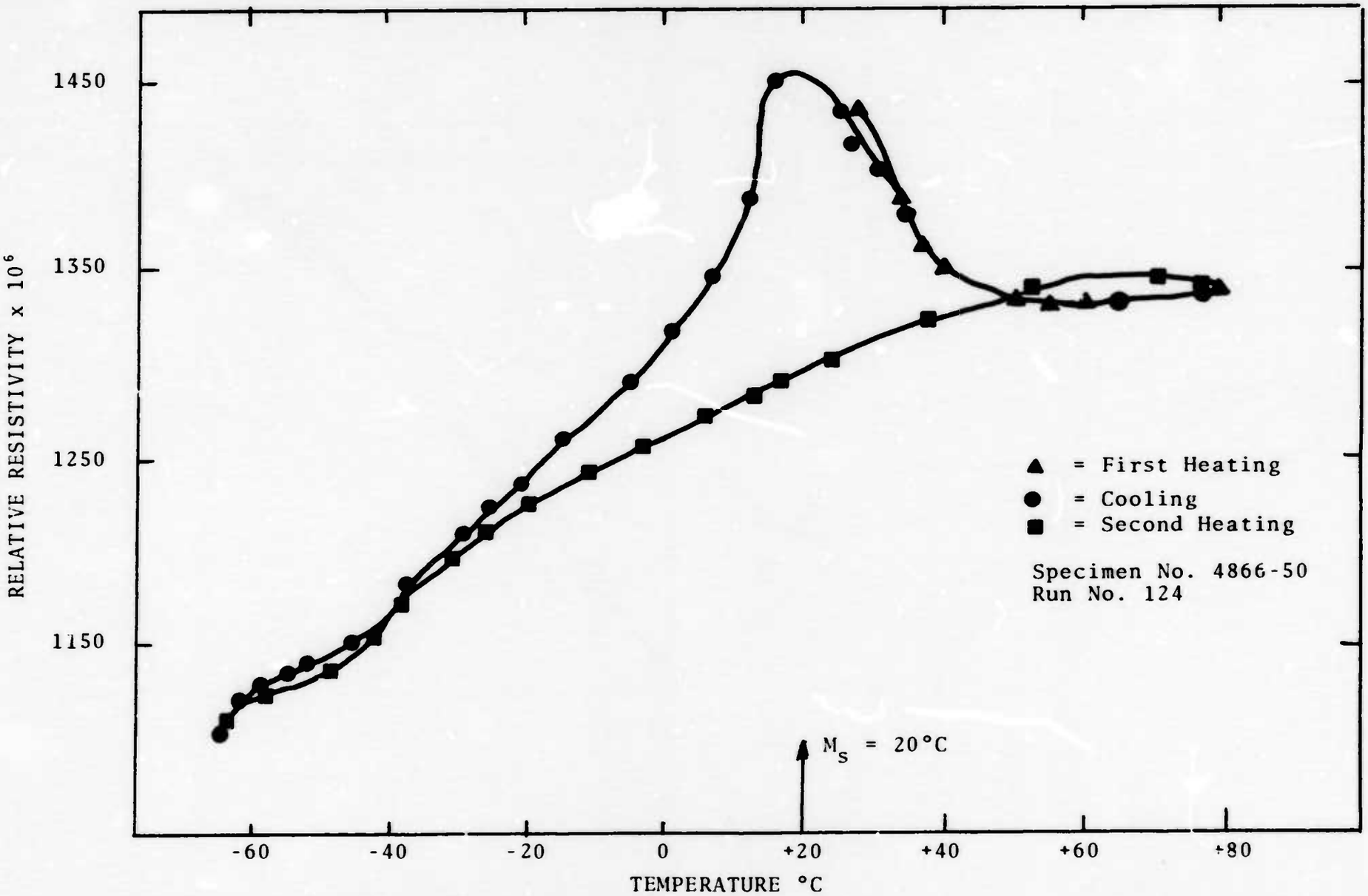

Figure 7. Electrical Resistivity versus Temperature for a 55 w/o Ni-45 w/o Ti Alloy after 50 cycles between -65°C and +90°C.

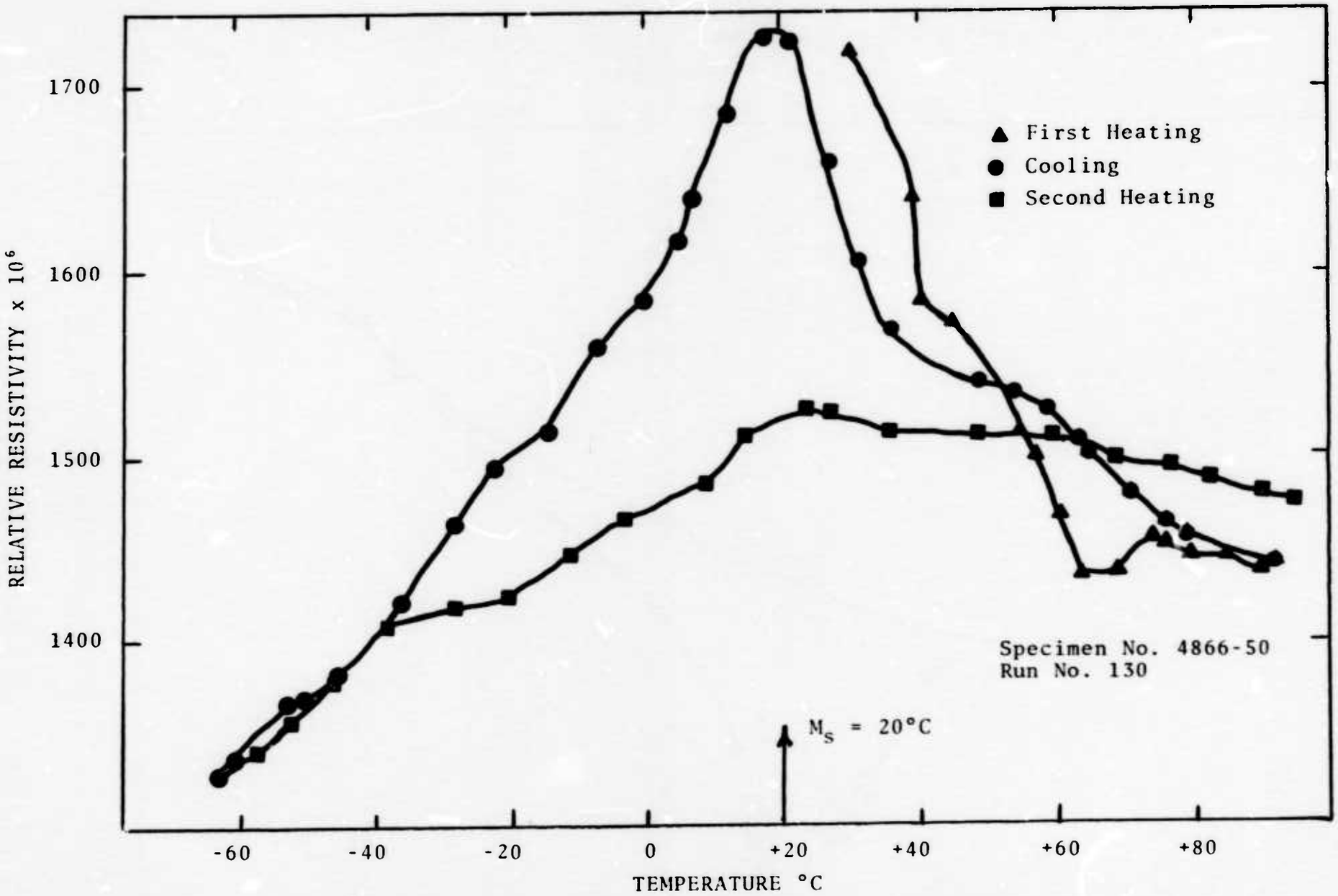

Figure 8. Electrical Resistivity versus Temperature for a 55 w/o Ni-45 w/o Ti Alloy after 50 cycles between -65°C and +90°C. Tensile Stress of 1275 psi Applied during Measurement.

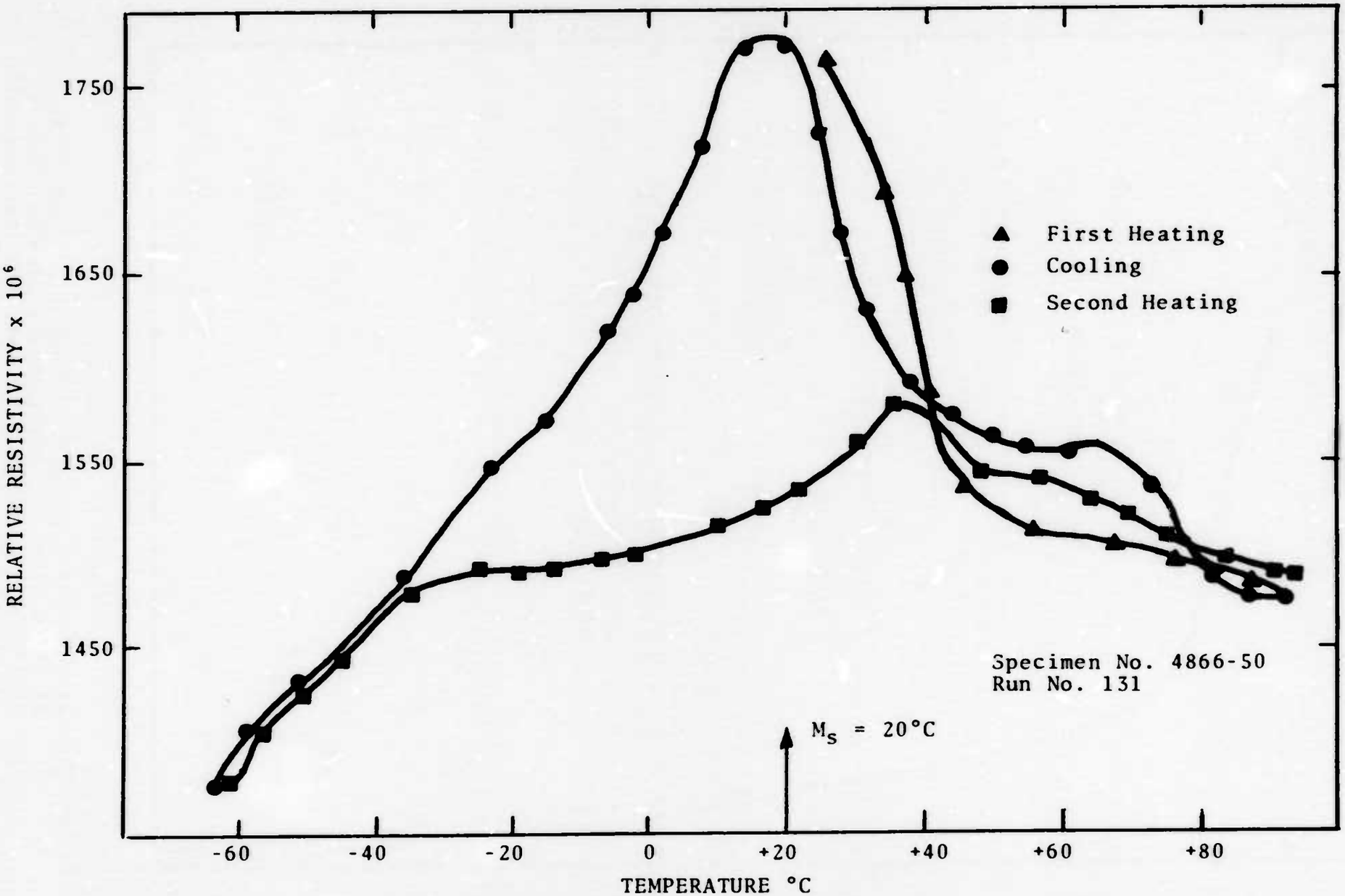

Figure 9. Electrical Resistivity versus Temperature for a 55 w/o Ni-45 w/o Ti Alloy after 50 cycles between -65°C and +90°C. Tensile Stress of 5484 psi Applied during Measurement.

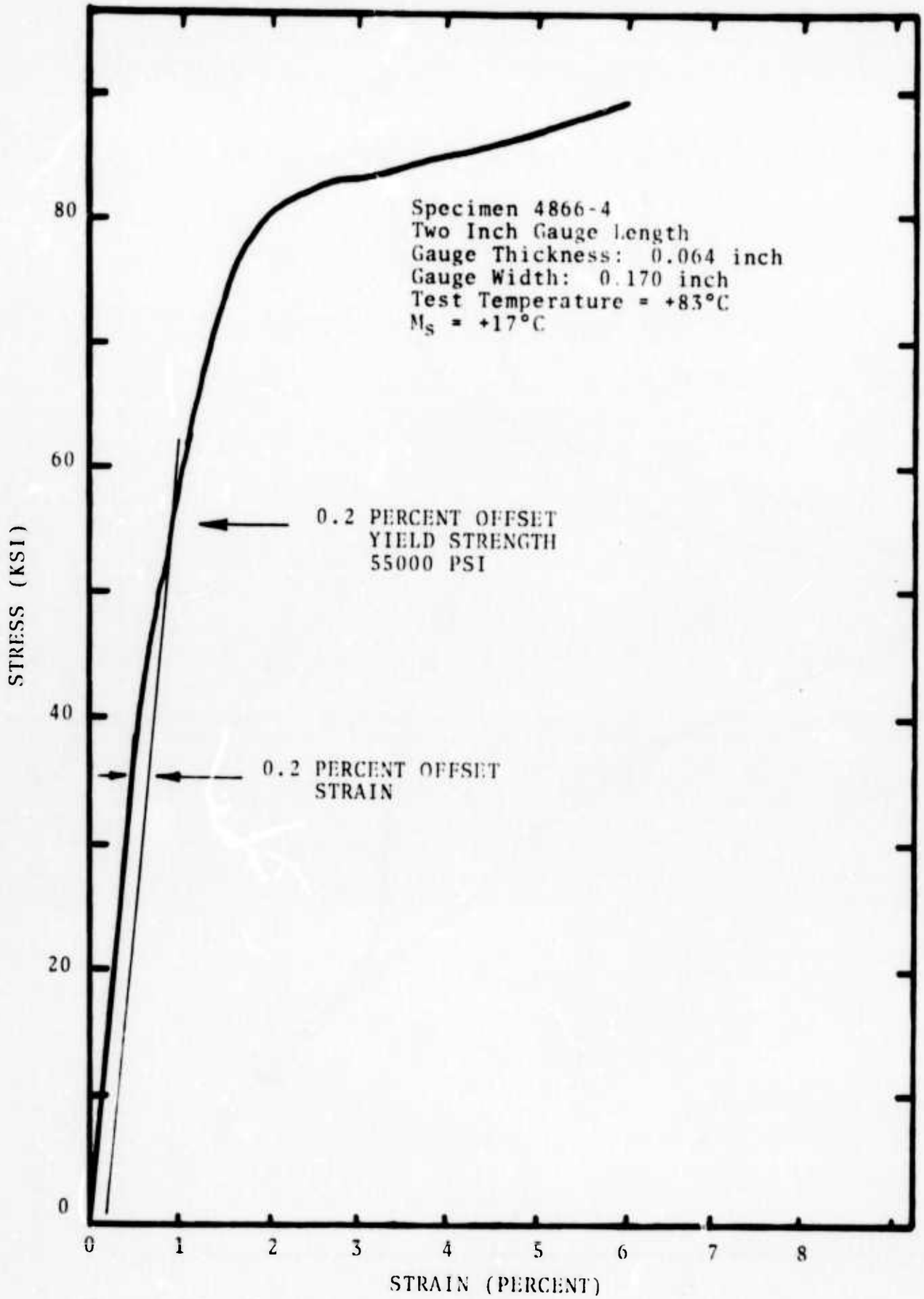

Figure 10. Stress-strain curve for 55 w/o Ni-45 w/o Ti Alloy at +83°C after 50 temperature cycles between -65°C and +90°C. The final step was heating from -65°C to 25°C.

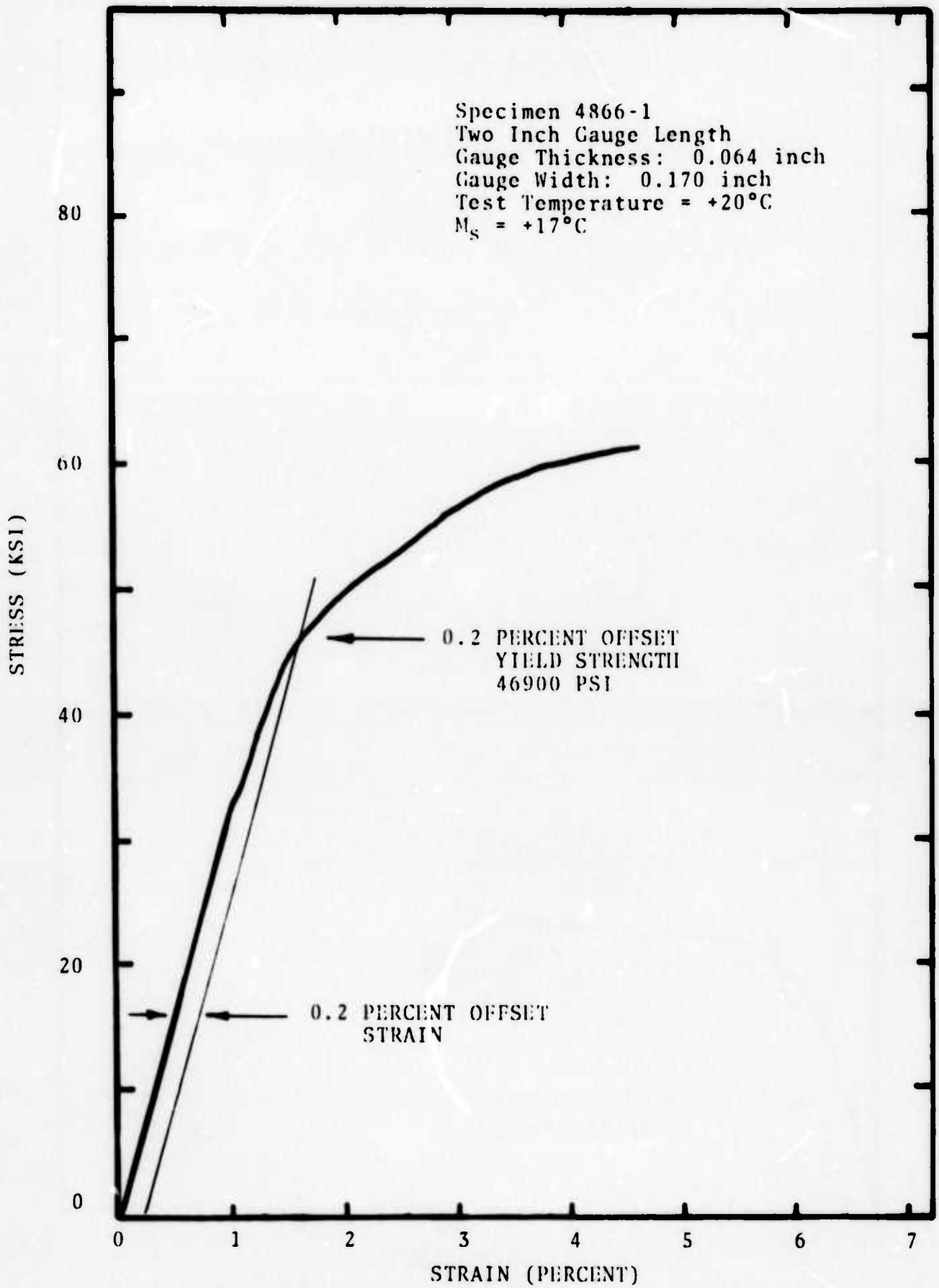

Figure 11. Stress-strain curve for 55 w/o Ni-45 w/o TI Alloy at +20°C after 50 temperature cycles between -65°C and +90°C. The final step was heating from -65°C to 25°C.

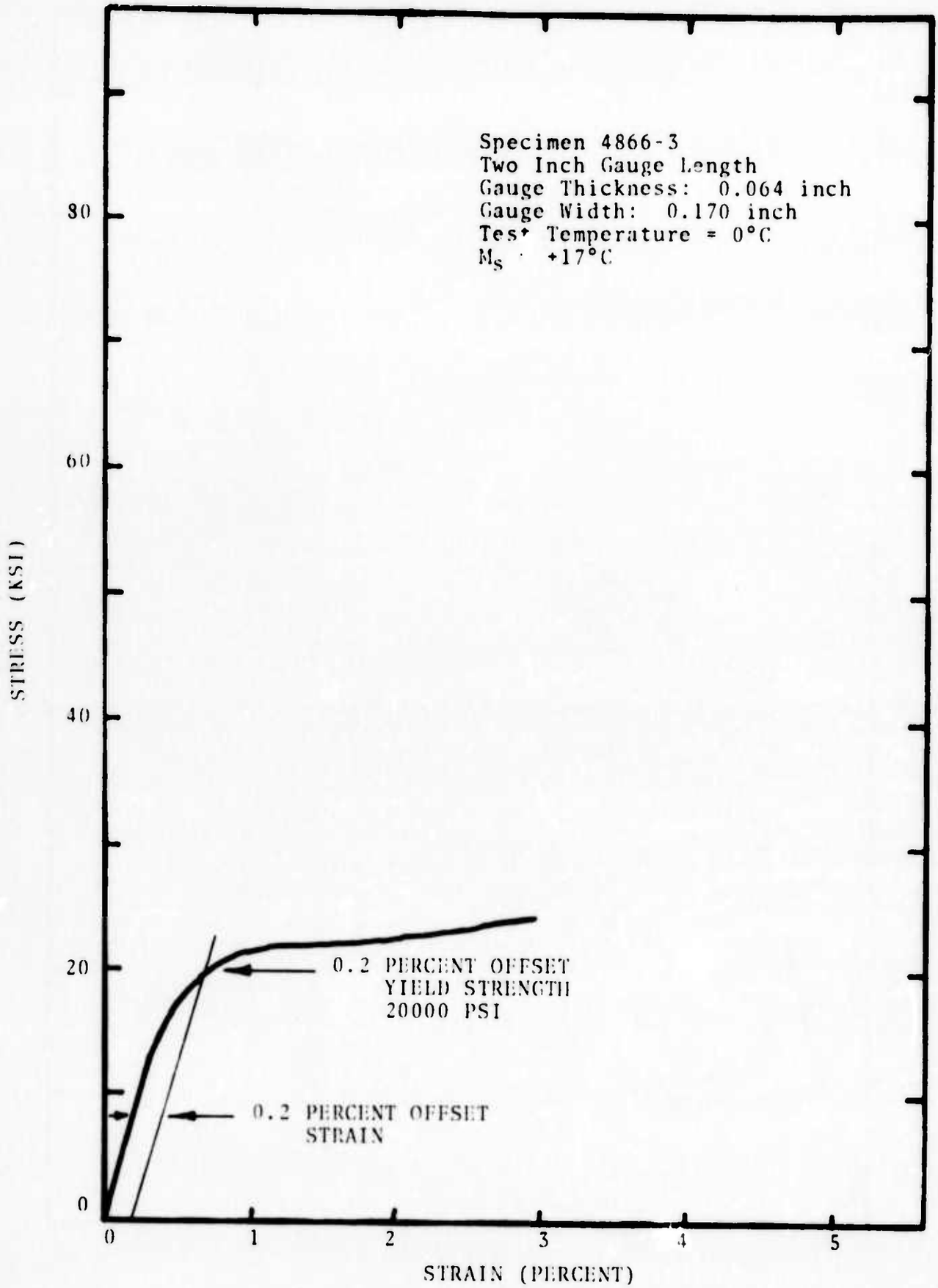

Figure 12. Stress-strain curve for 55 w/o Ni-45 w/o Ti Alloy at 0°C after 50 temperature cycles between -65°C and +90°C. The final step was heating from -65°C to 25°C.

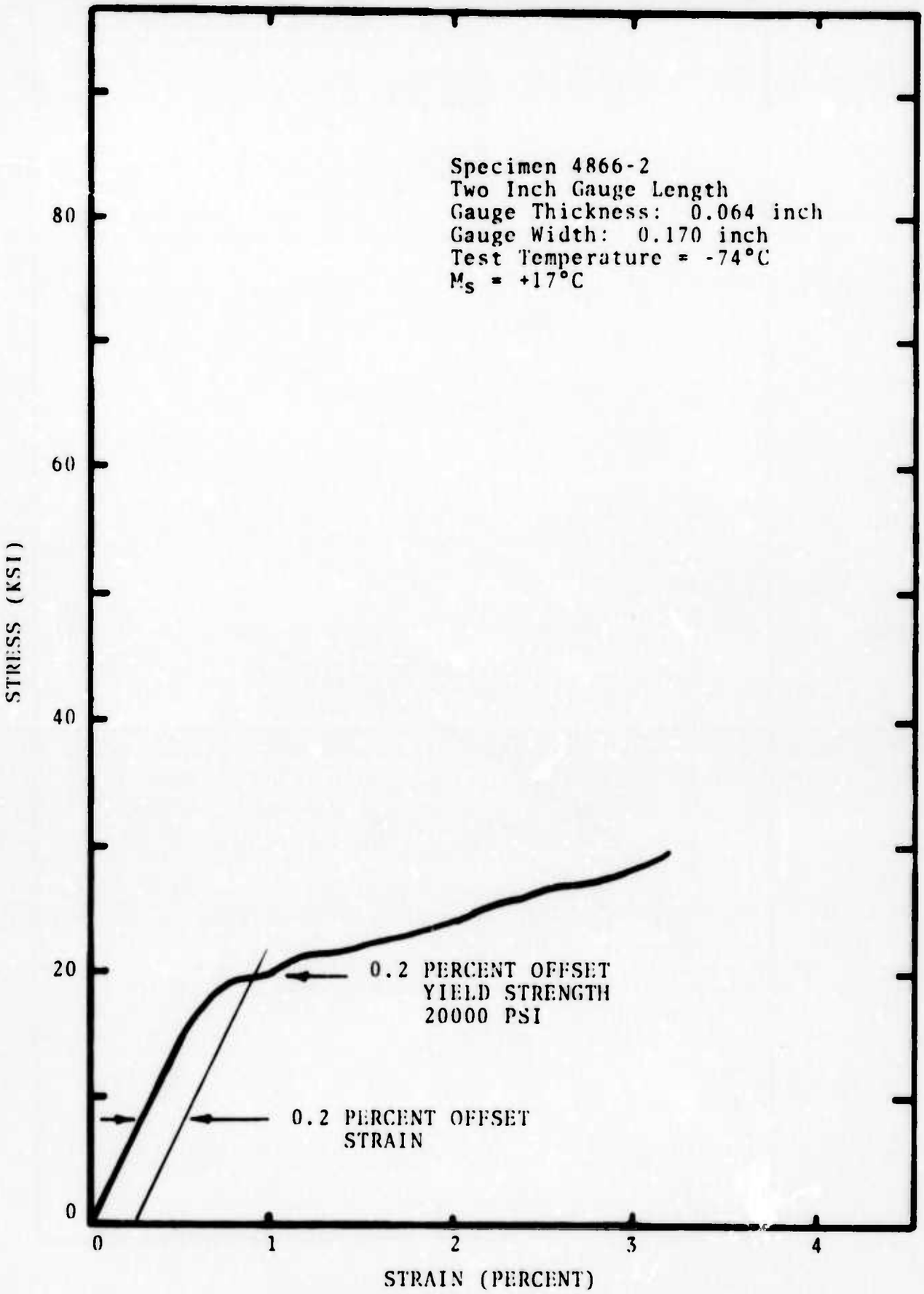

Figure 13. Stress-strain curve for 55 w/o Ni-45 w/o Ti Alloy at -74°C after 50 temperature cycles between -65°C and +90°C. The final step was heating from -65°C to 25°C.

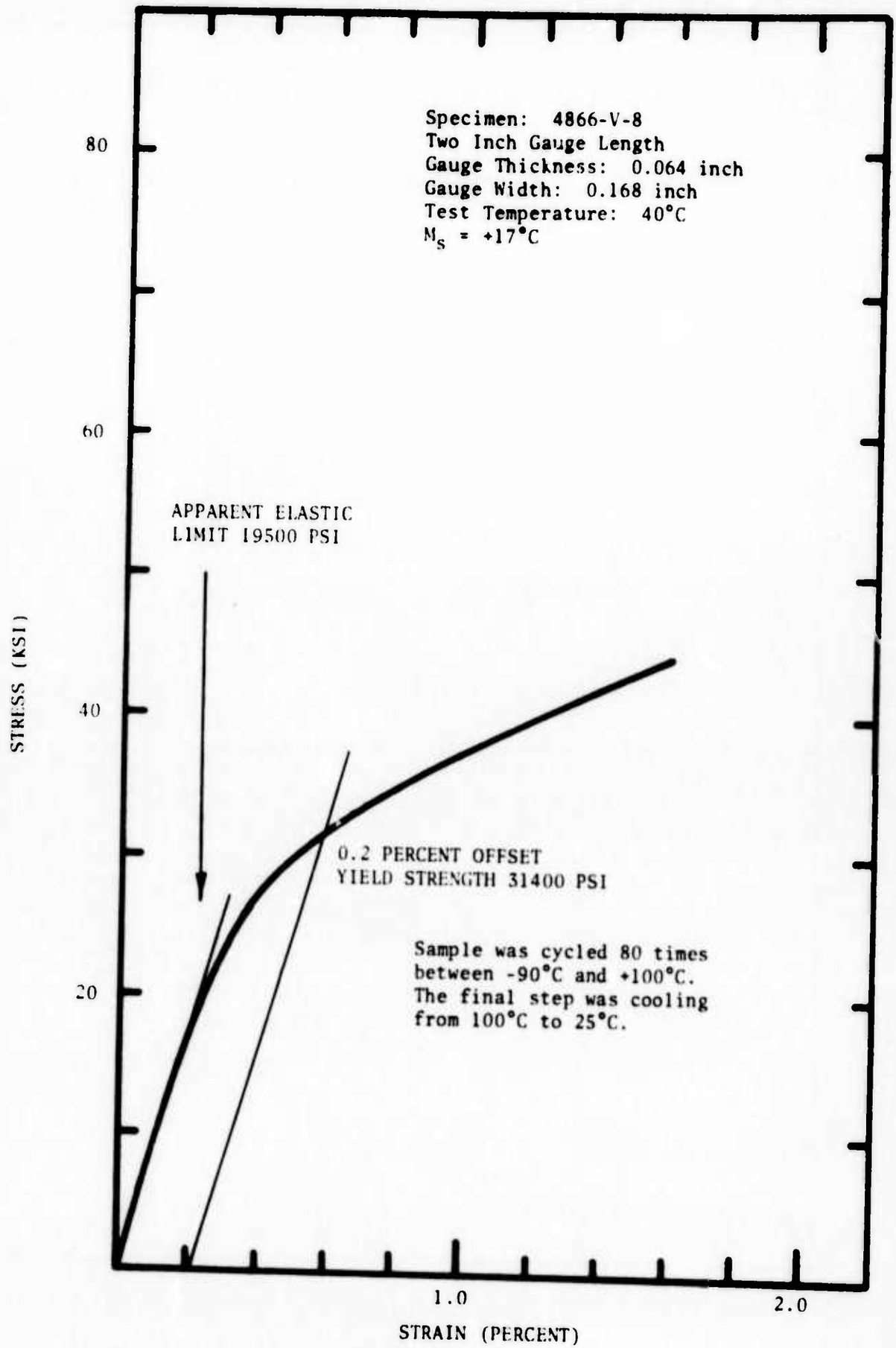

Figure 14. Stress-Strain Curve for 55 w/o Ni-45 w/o Ti at 40°C after Cycling.

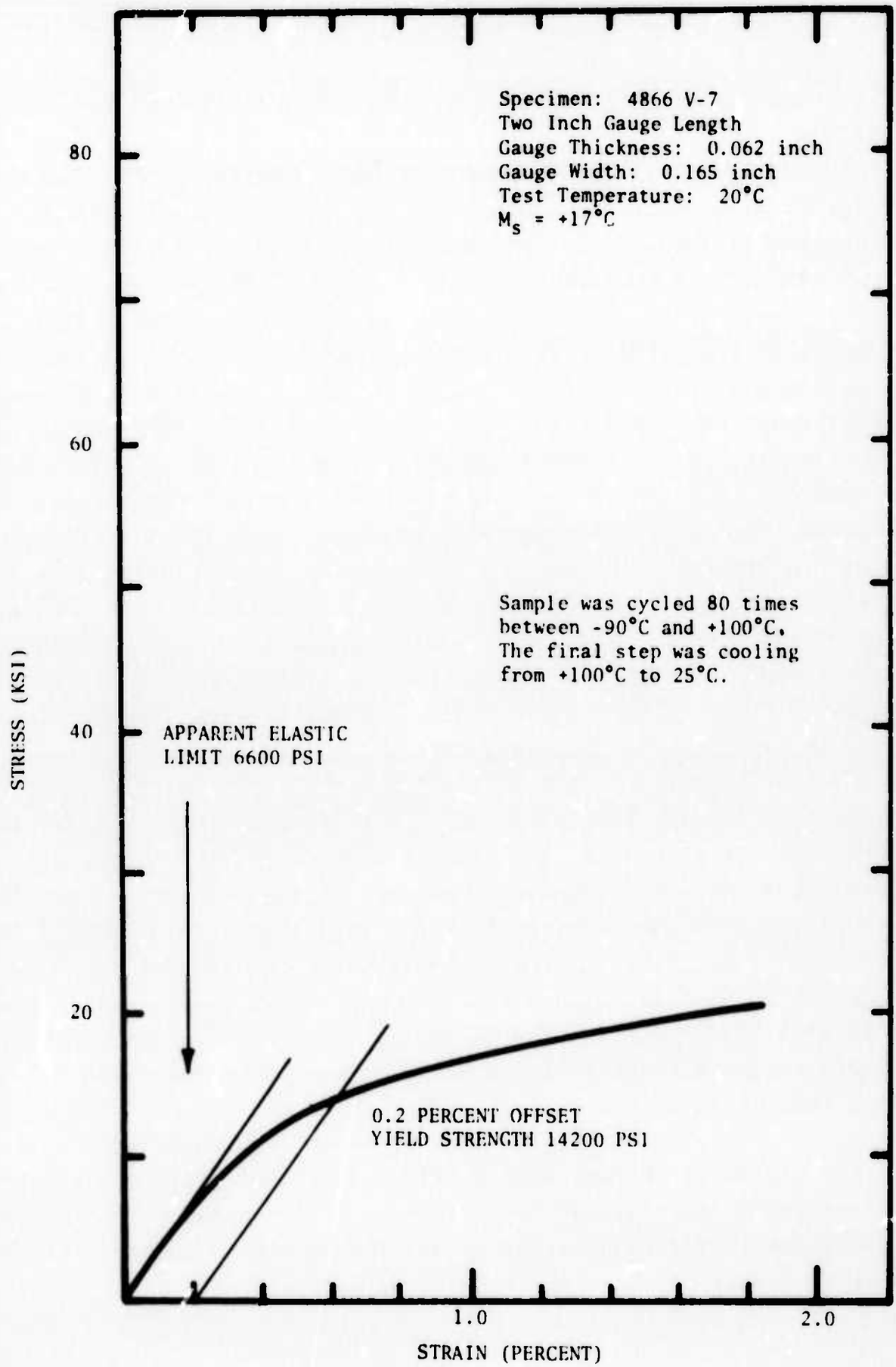

Figure 15. Stress-Strain Curve for 55 w/o Ni-45 w/o Ti at 20°C after Cycling.

room temperature. In this case, lower strength levels are obtained.

Figure 16 is a composite representation of the damping, electrical resistivity and 0.2% offset yield strength data as a function of temperature. Although heats 4609 and 4866 are both 55Ni-45Ti the M_S temperatures are slightly different being 7°C and 17°C respectively. As a consequence, the yield strength data (taken on heat 4866) have been displaced by -10°C. Nevertheless, the composite data shown in Figure 16 shows that in the temperature range above M_S, high damping values near 5×10^{-3} and strengths in the vicinity of 47000-55000 psi can be obtained simultaneously. Since the effect of plastic deformation is to broaden the transformation range (i.e. see Figures 4 and 5) it is quite likely that the temperature range where high strength and high damping factors can be obtained simultaneously will be increased by deformation. Moreover, the strength levels will undoubtedly be higher than those shown in Figure 16. Measurements of the damping behavior and yield strength of plastically deformed samples were carried out in order to test this hypothesis.

Figures 17 through 26 show the results which were obtained on tensile testing the 55 w/o Ni-45 w/o Ti alloy after cold working. In all cases, the samples were cycled and tested after heating to room temperature. The results for the samples obtained by 3% and 7% cold reduction in thickness, which are displayed in Figures 17-22, show a decrease in strength as compared to the samples which were not cold worked. However, the samples which received a 15% cold reduction in thickness were considerably stronger, exhibiting 0.2 percent offset yield strengths in the 60000-70000 psi range between 0°C and 83°C.

In view of the low modulus of the 55 w/o Ni-45 w/o Ti alloy disclosed by the tensile tests, an attempt was made to observe anelastic behavior by performing "load-unload tests" which were interrupted to observed relaxation or "elastic memory behavior." Figure 27 shows the results of such a test where a sample

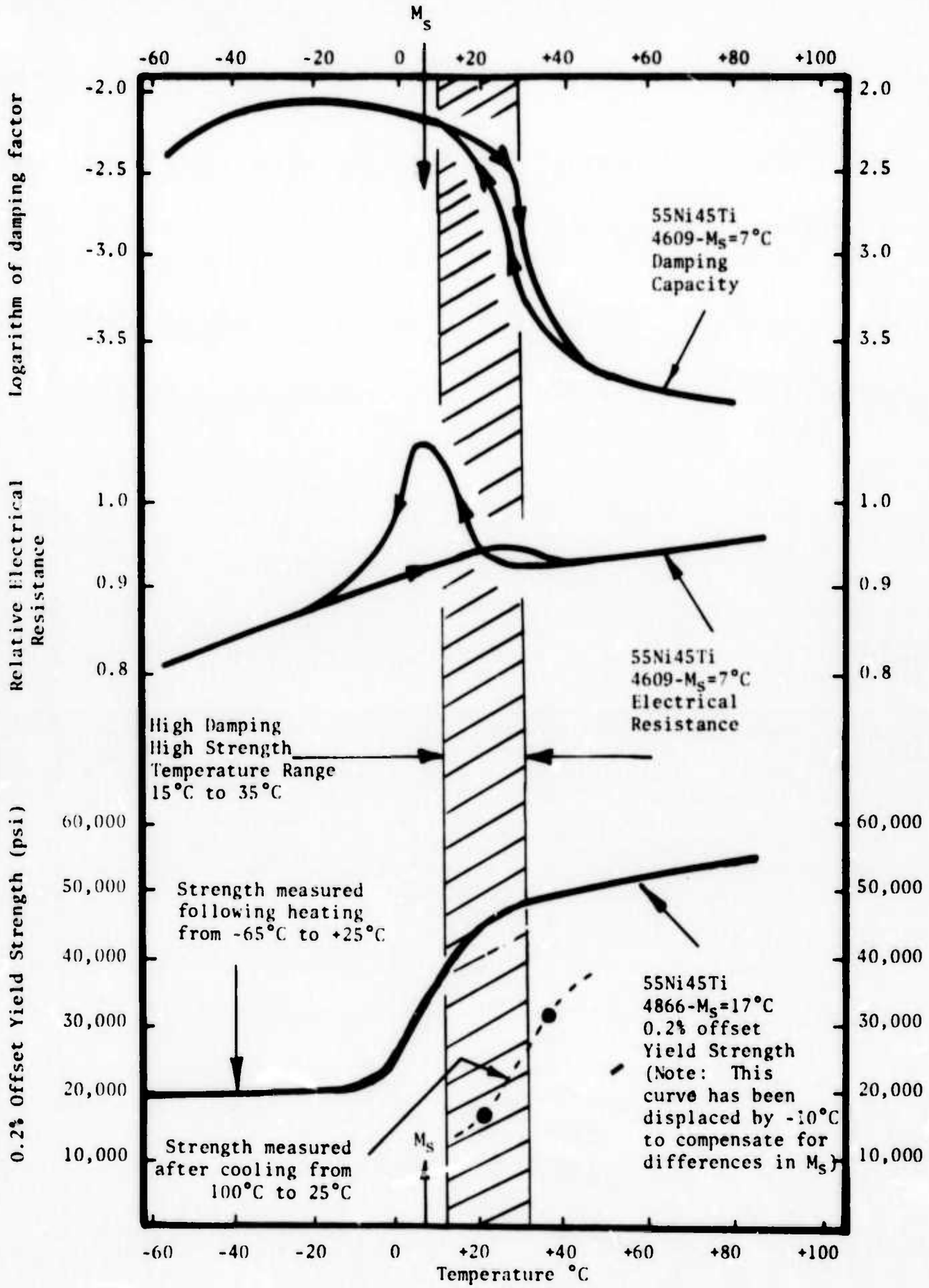

Figure 16. Damping Capacity, Electrical Resistance and 0.2% Offset Yield Strength for 55Ni45Ti as a function of temperature after Multiple Cycling Treatment.

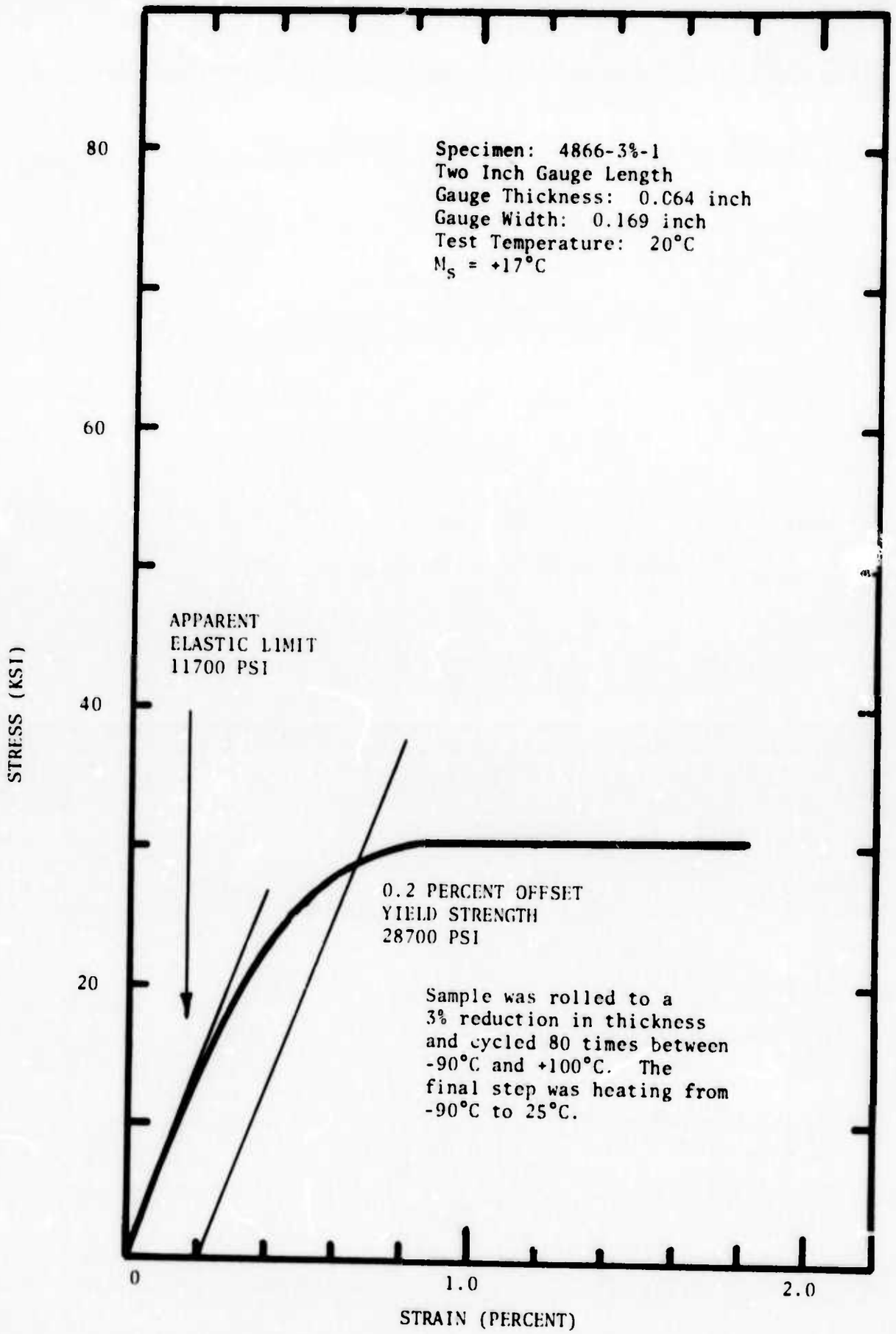

Figure 17. Stress-Strain Curve for 55 w/o Ni-45 w/o Ti at 20°C after Cold Work and Cycling.

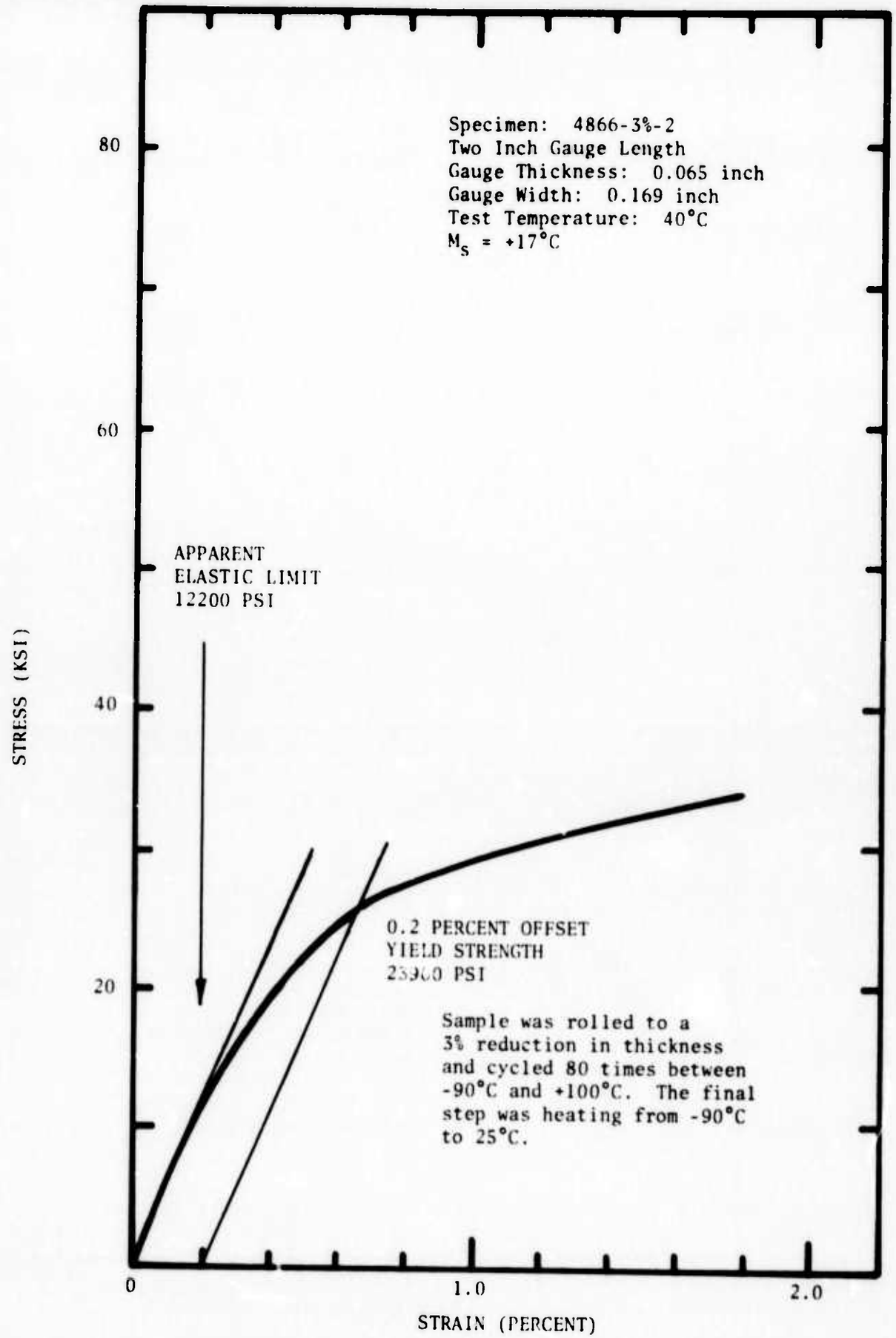

Figure 18. Stress-Strain Curve for 55 w/o Ni-45 w/o Ti at 40°C after Cold Work and Cycling.

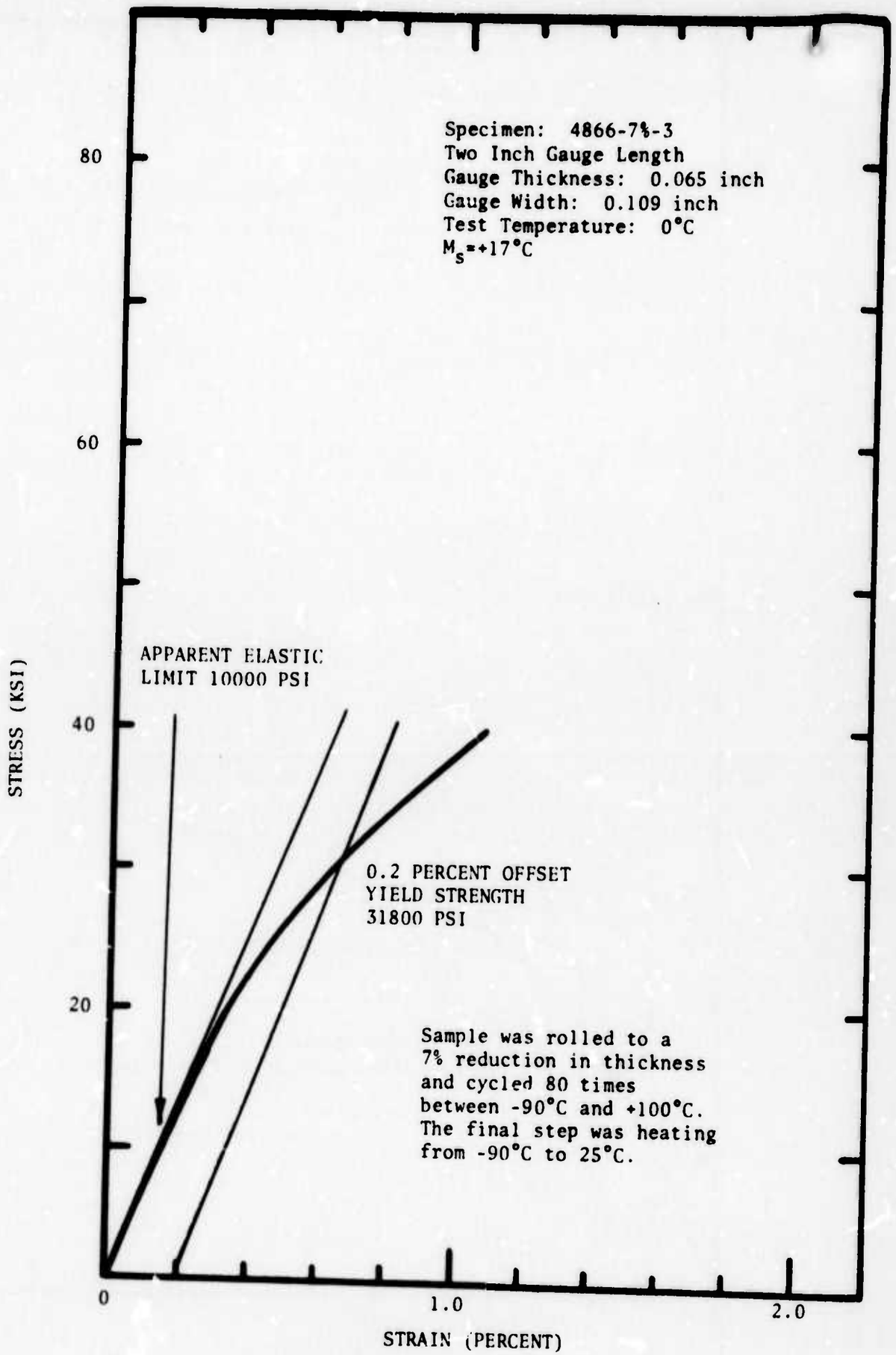

Figure 19. Stress-Strain Curve for 55 w/o Ni-45 w/o Ti at 0°C after Cold Work and Cycling.

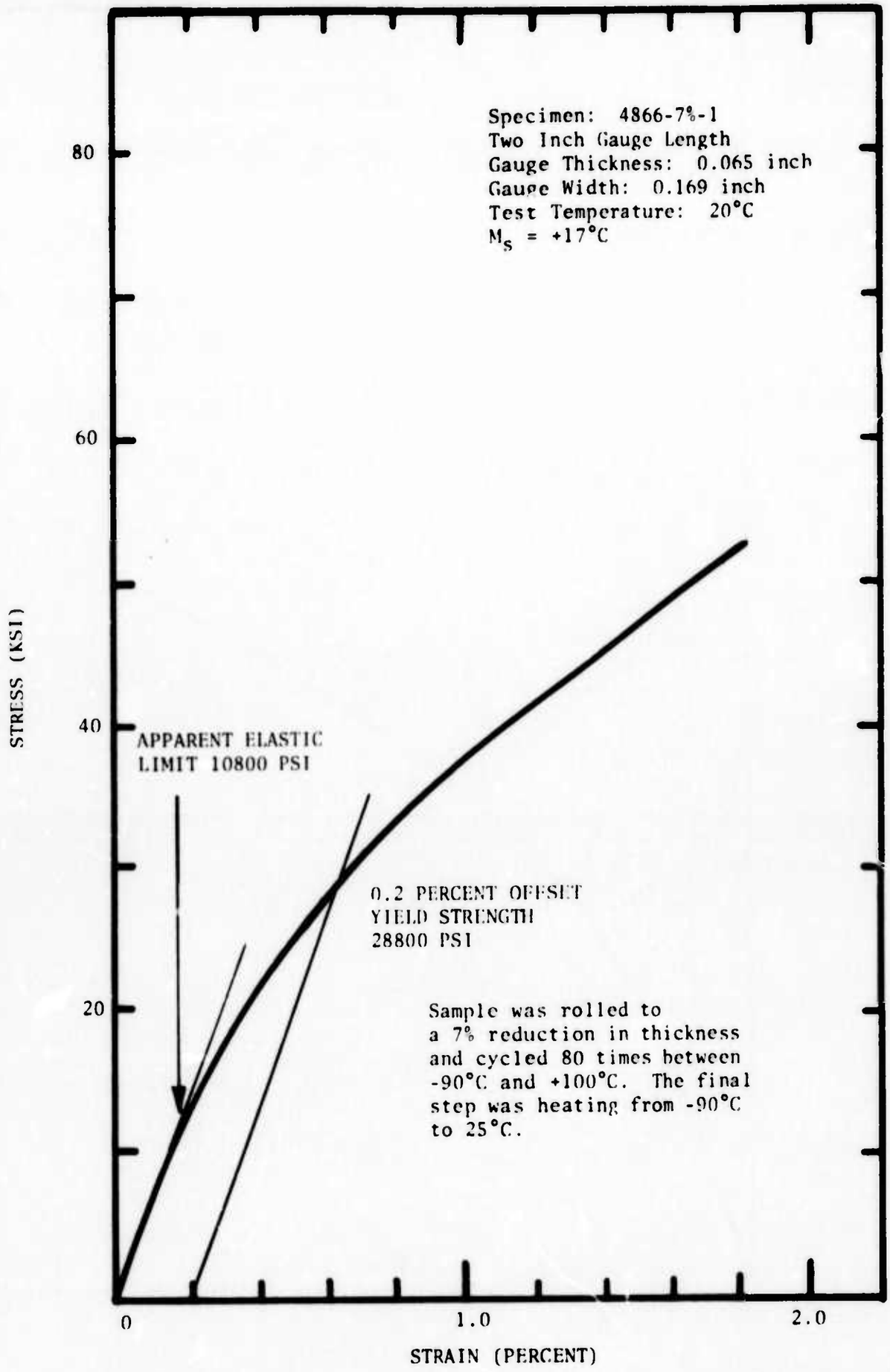

Figure 20. Stress-Strain Curve for 55 w/o Ni-45 w/o Ti at 20°C after cold work and cycling.

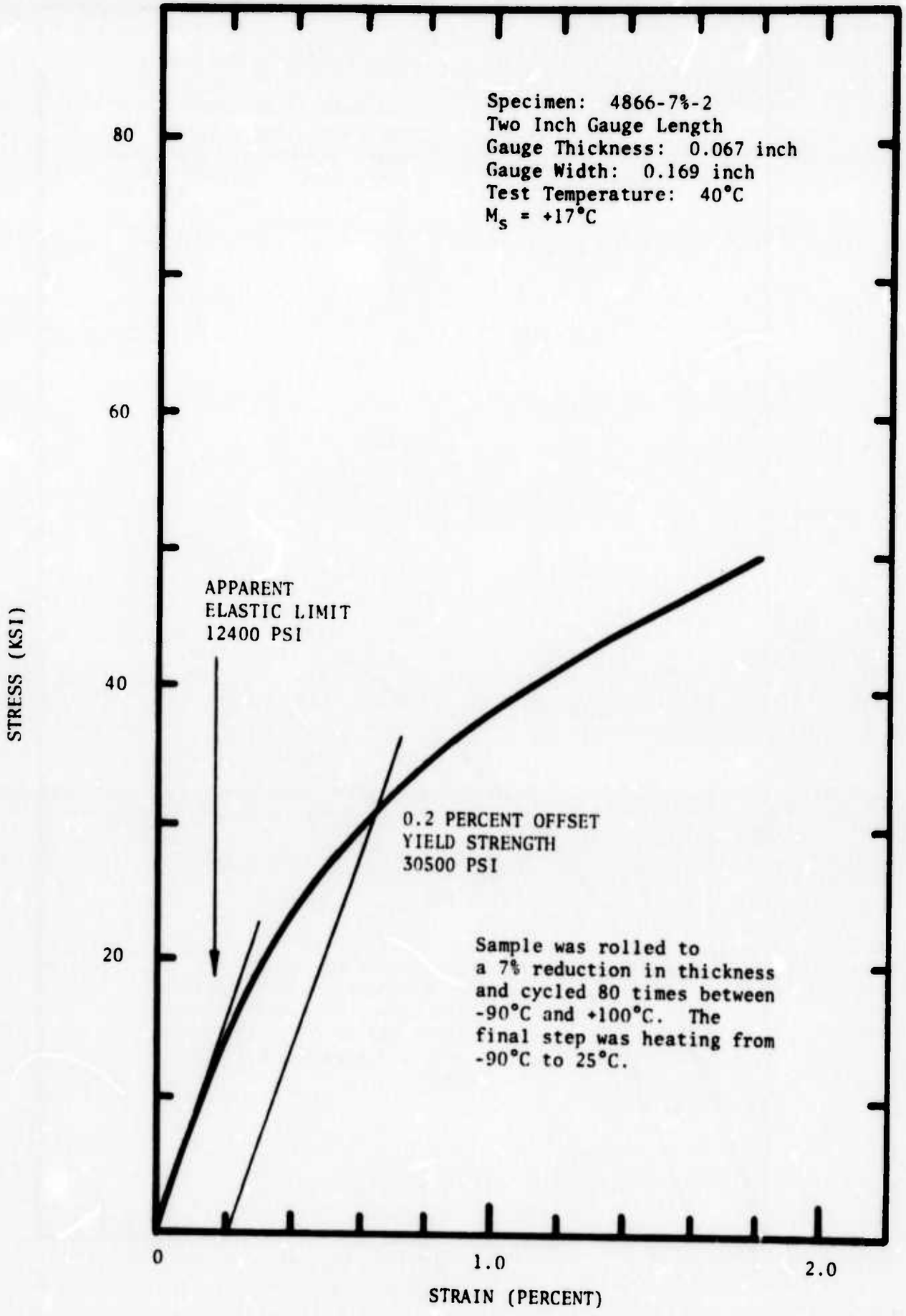

Figure 21. Stress-Strain Curve for 55 w/o Ni-45 w/o Ti at 40°C after cold work and cycling.

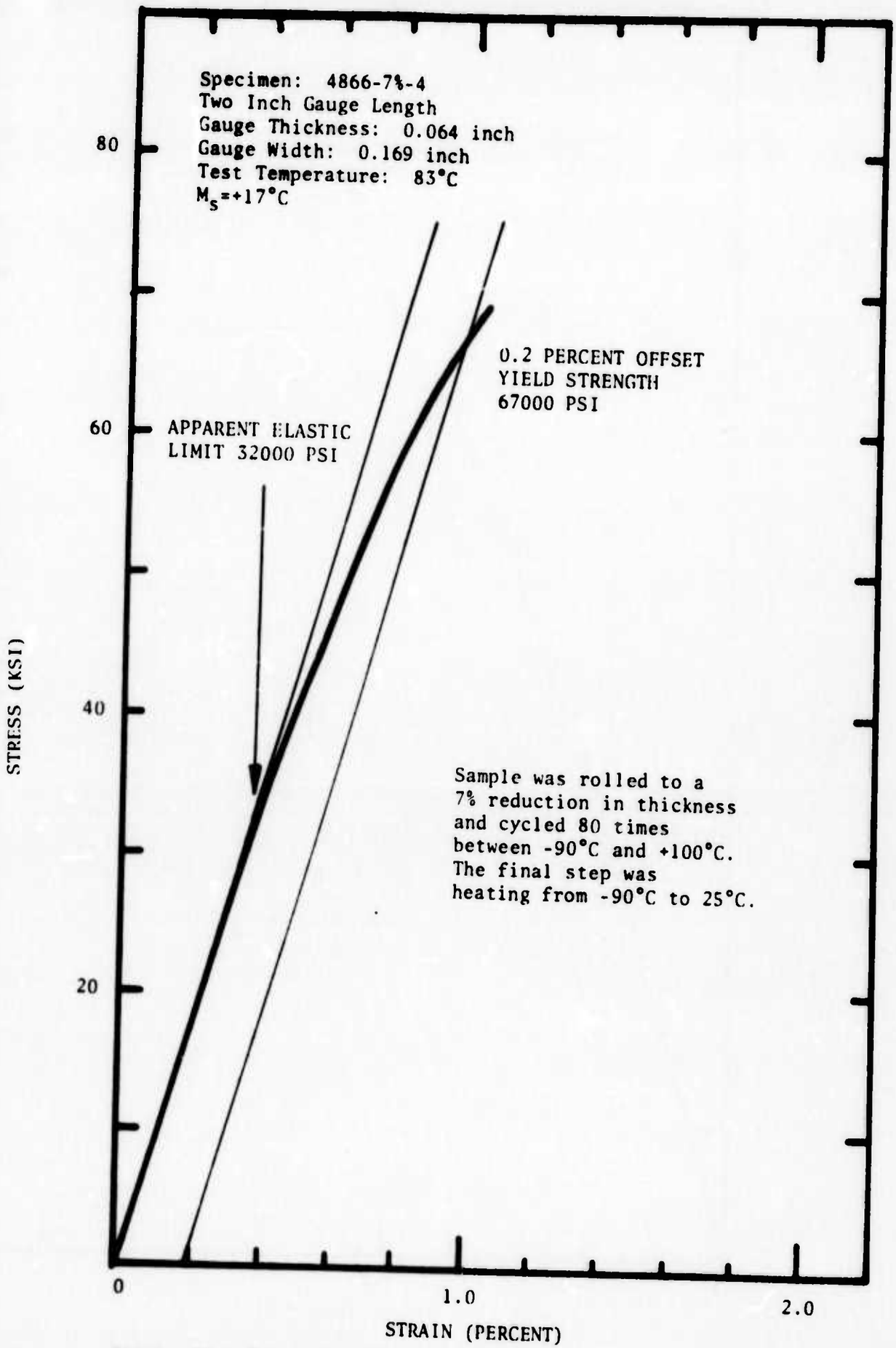

Figure 22. Stress-Strain Curve for 55 w/o Ni-45 w/o Ti at 83°C after Cold Work and Cycling.

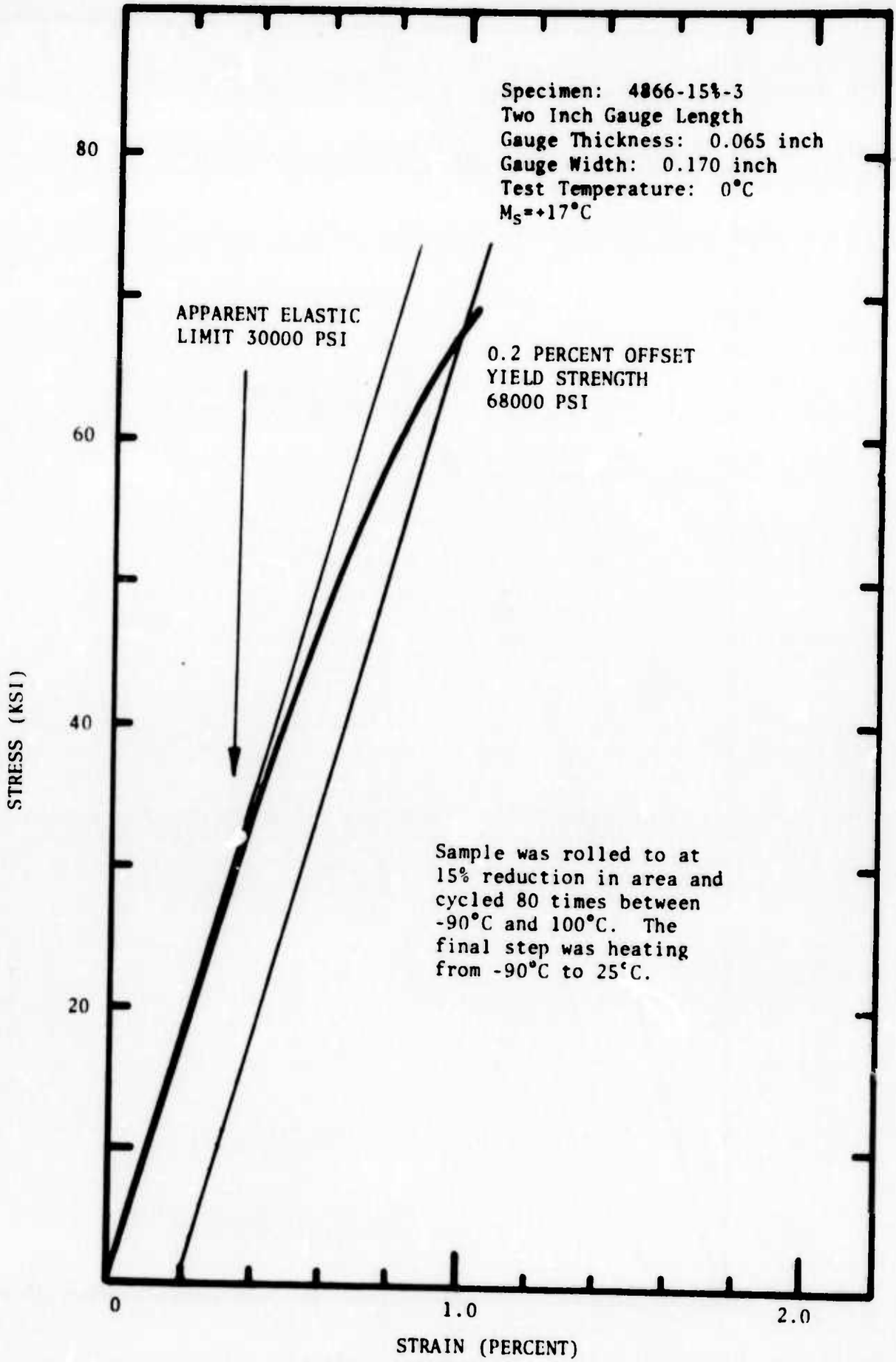

Figure 23. Stress-Strain Curve for 55 w/o Ni-45 w/o Ti at 0°C after Cold Work and Cycling.

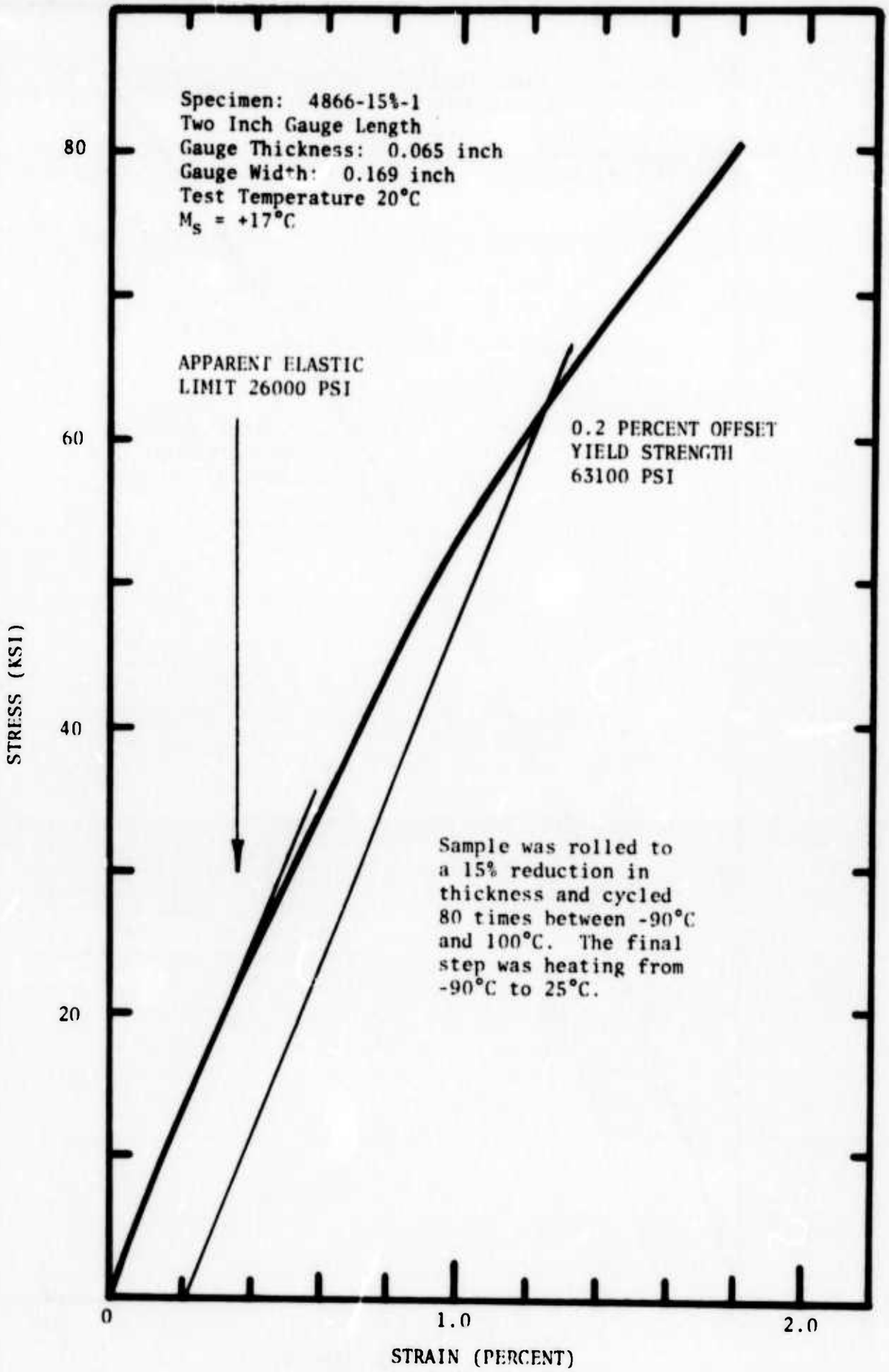

Figure 24. Stress-Strain Curve for 55 w/o Ni-45 w/o Ti at 20°C after Cold Work and Cycling.

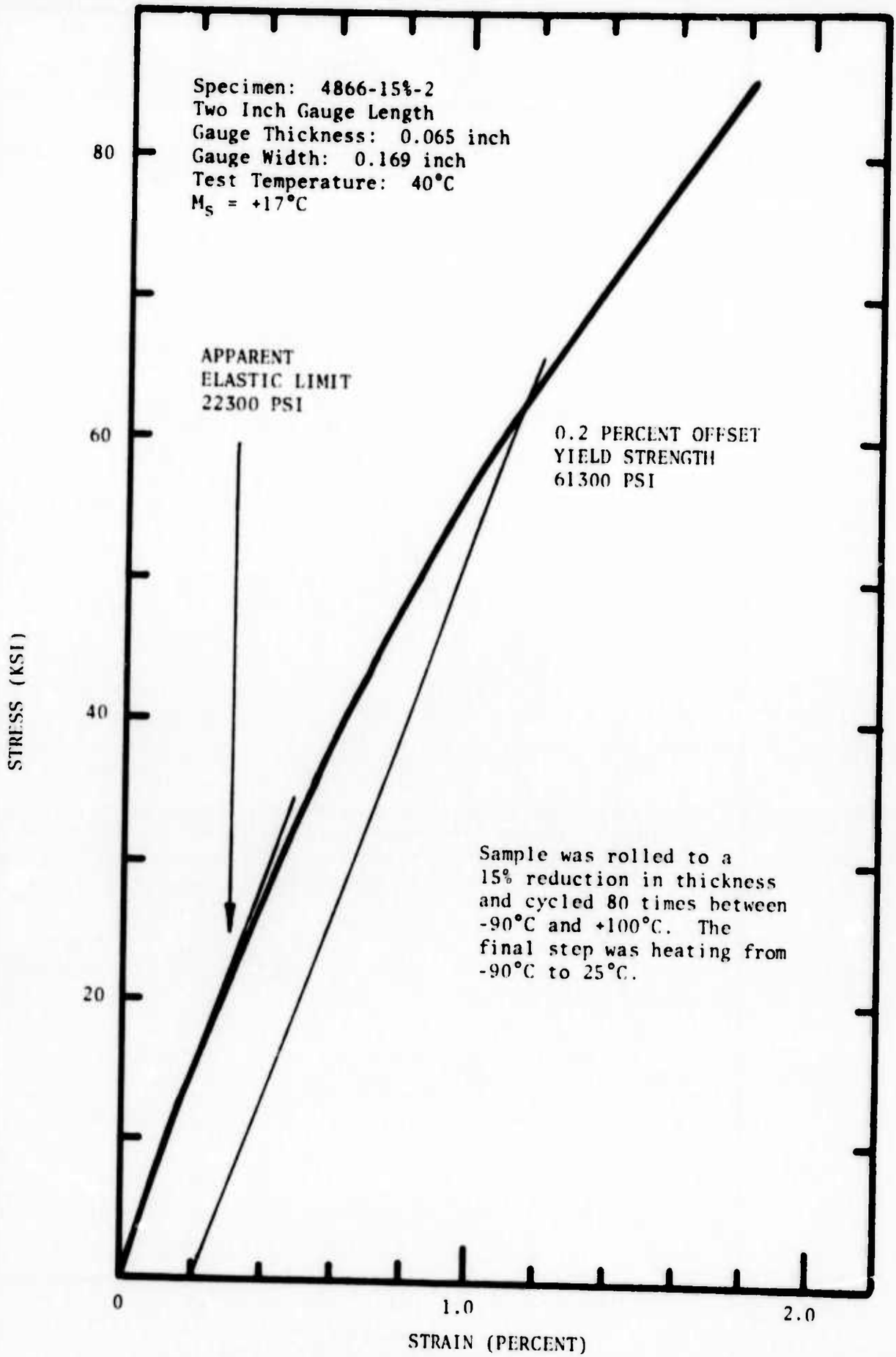

Figure 25. Stress-Strain Curve for 55 w/o Ni-45 w/o Ti at 40°C after Cold Work and Cycling.

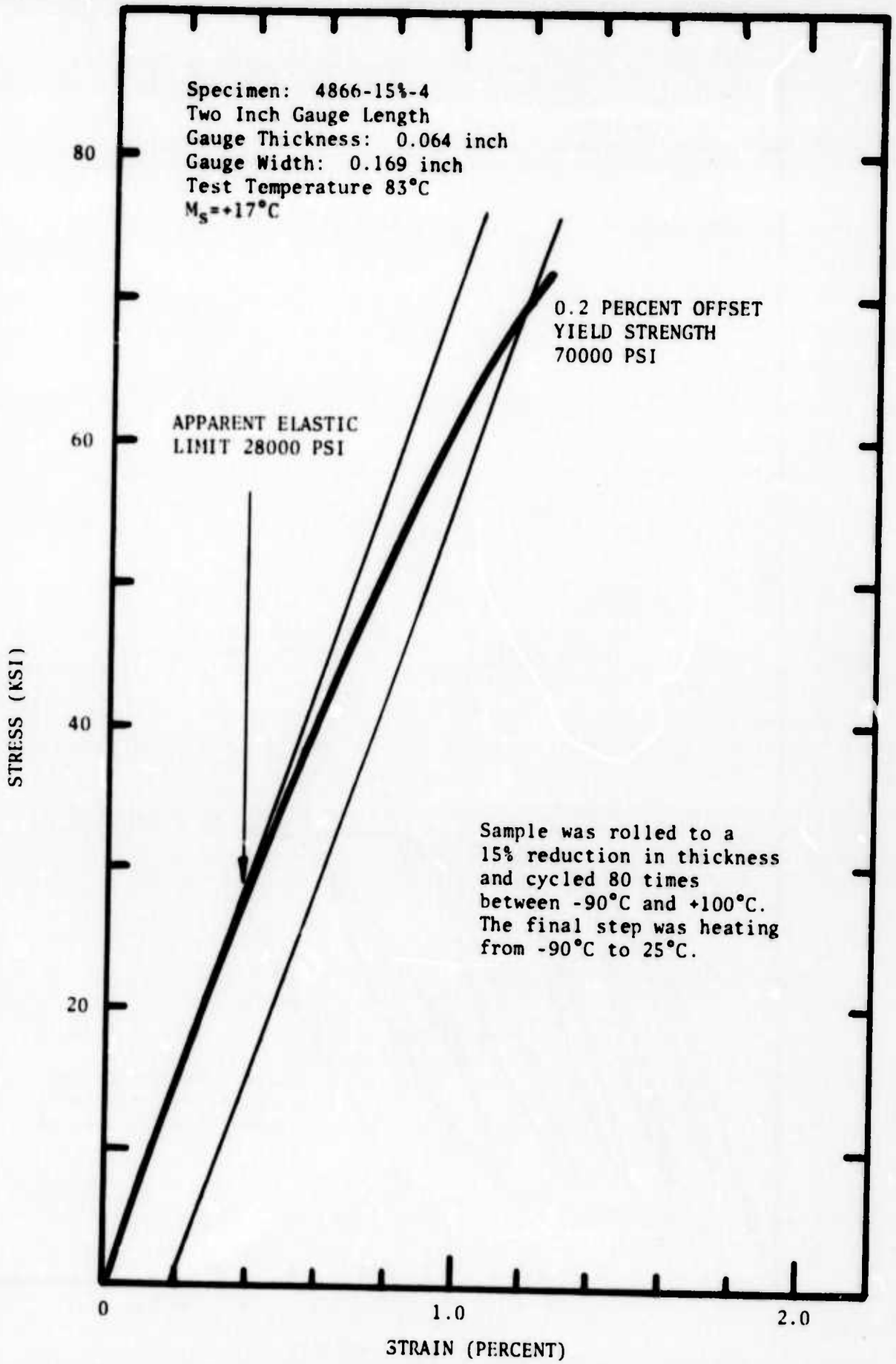

Figure 26. Stress-Strain Curve for a 55 w/o Ni-45 w/o Ti at 83°C after Cold Work and Cycling.

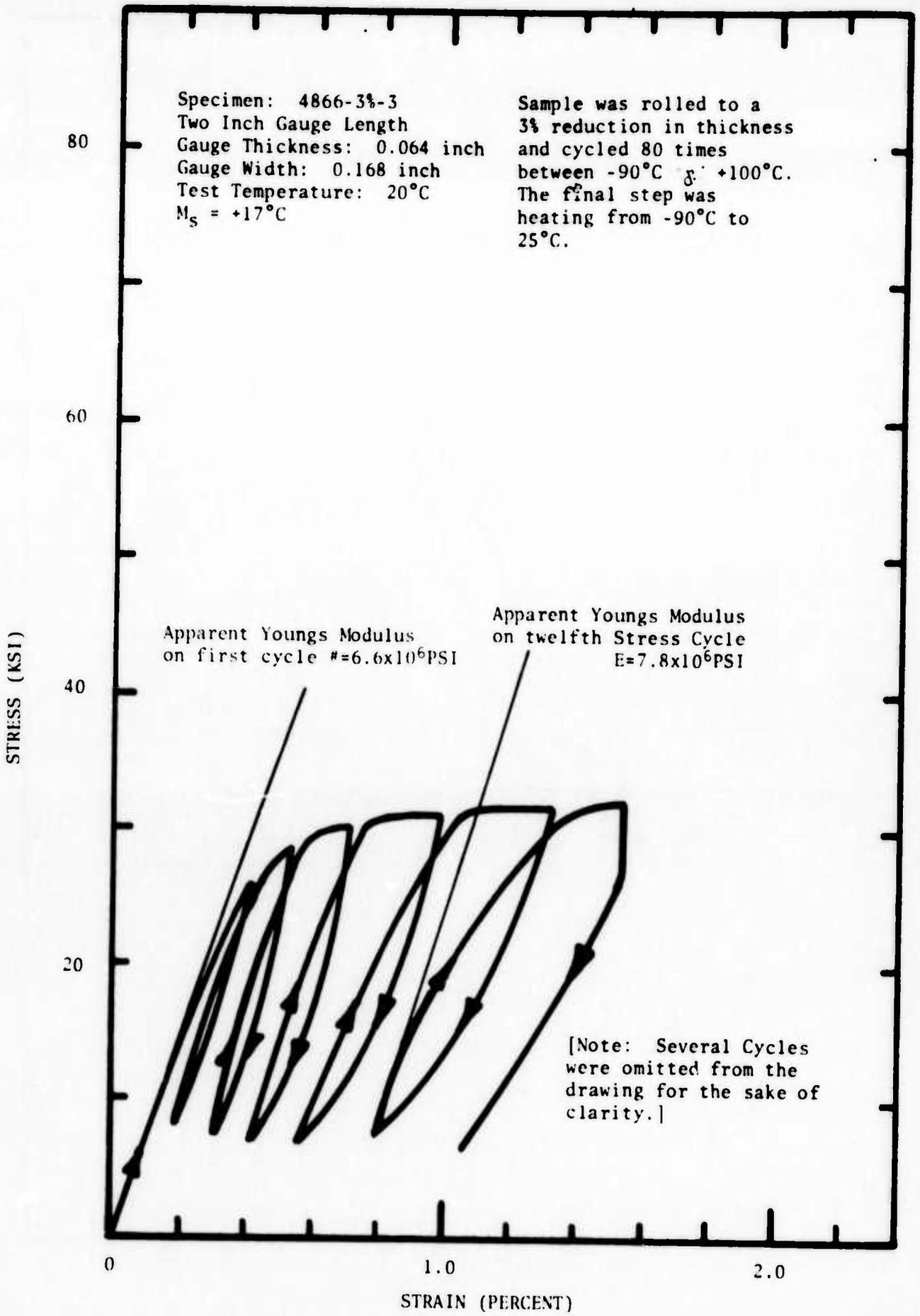

Figure 27. Stress-Strain Curve for 55 w/o Ni-45 w/o Ti at 20°C after Cold Work and Cycling.

of the material which had received a 3% cold reduction was mechanically cycled. The observed stress-strain curve follows the envelope shown in Figure 17 where no load cycling was applied. The results indicate an increase in elastic modulus on loading with increasing number of stress cycles. Thus the modulus increases by 20% in the twelfth cycle as compared to the initial cycle. There is an appreciable increase in mechanical hysteresis with increasing plastic strain. Upon unloading to a low stress level and holding for thirty minutes the amount of anelastic strain recovery was approximately 0.02%.

The foregoing data on yield strength and electrical resistance are combined with data on damping capacity (reported in Section III) for the 55 w/o Ni-45 w/o Ti alloy with 3%, 7% and 15% cold reduction. The results, shown in Figures 28-30, are counterparts to the overall comparison displayed in Figure 16. These results indicate that the best combination of properties can be achieved by a 15% cold reduction which generates yield strengths in the 60000-70000 psi range over the 0°C-80°C temperature range in combination with loss factors of Q^{-1} equal to 100×10^{-4} at 25°C and at temperatures down to -60°C. At 60°C the loss factor drops to 30×10^{-4}.

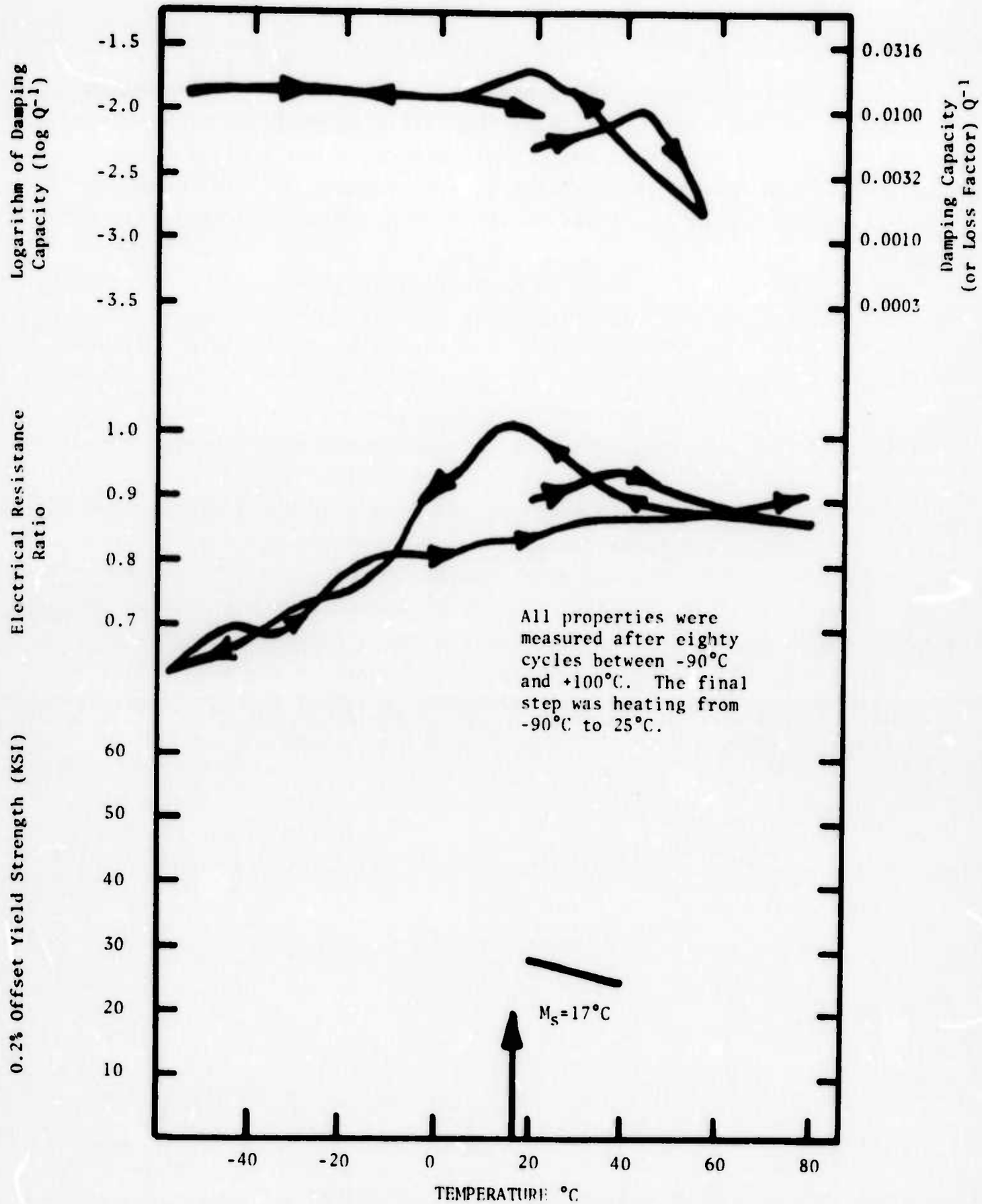

Figure 28. Damping Capacity, Electrical Resistance and 0.2% Offset Yield Strength for 55 w/o Ni-45 w/o Ti versus Temperature after 3% Cold Reduction and Cycling Treatment.

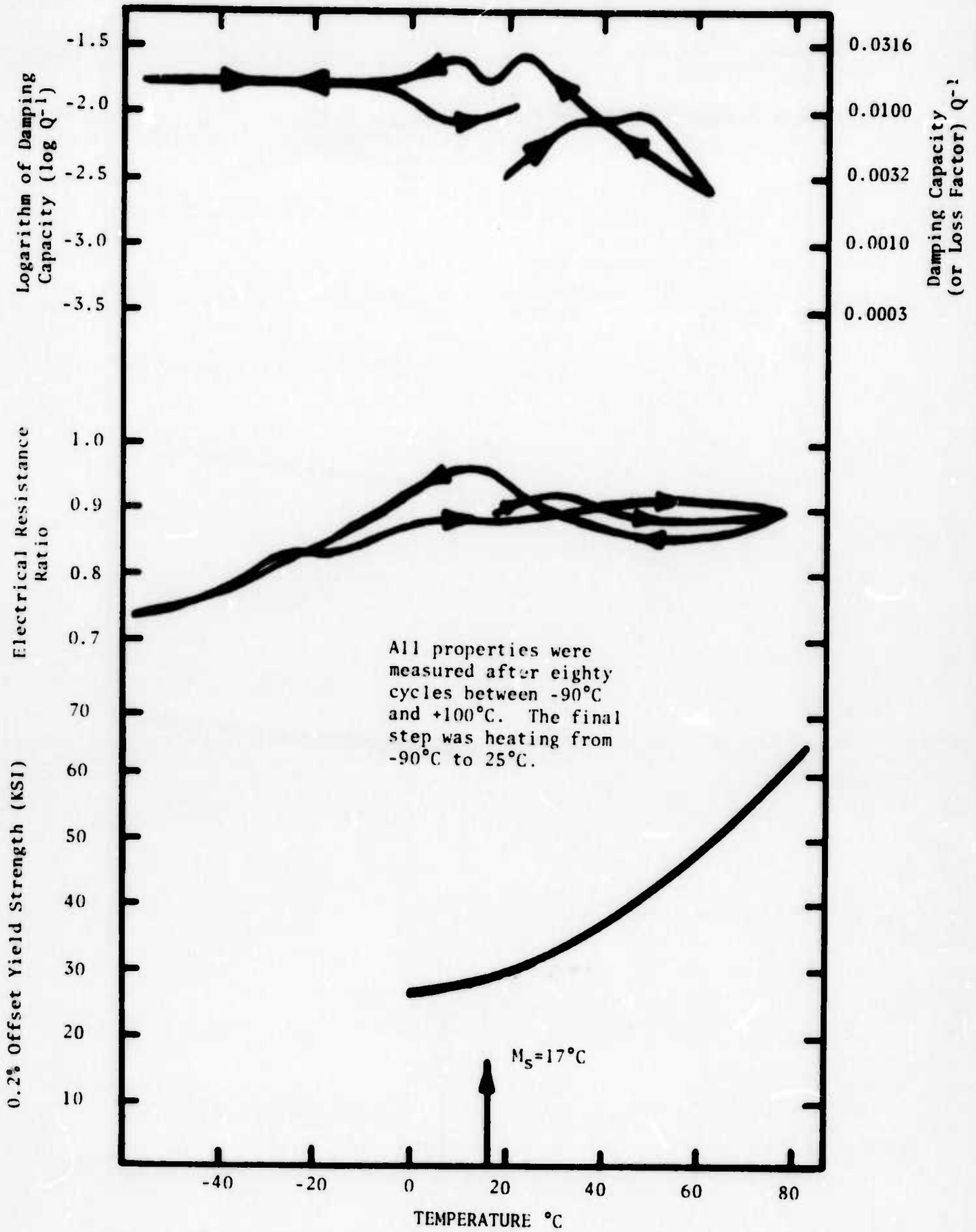

Figure 29. Damping Capacity, Electrical Resistance and 0.2% Offset Yield Strength for 55 w/o Ni-45 w/o Ti versus Temperature after 7% Cold Reduction and Cycling Treatment.

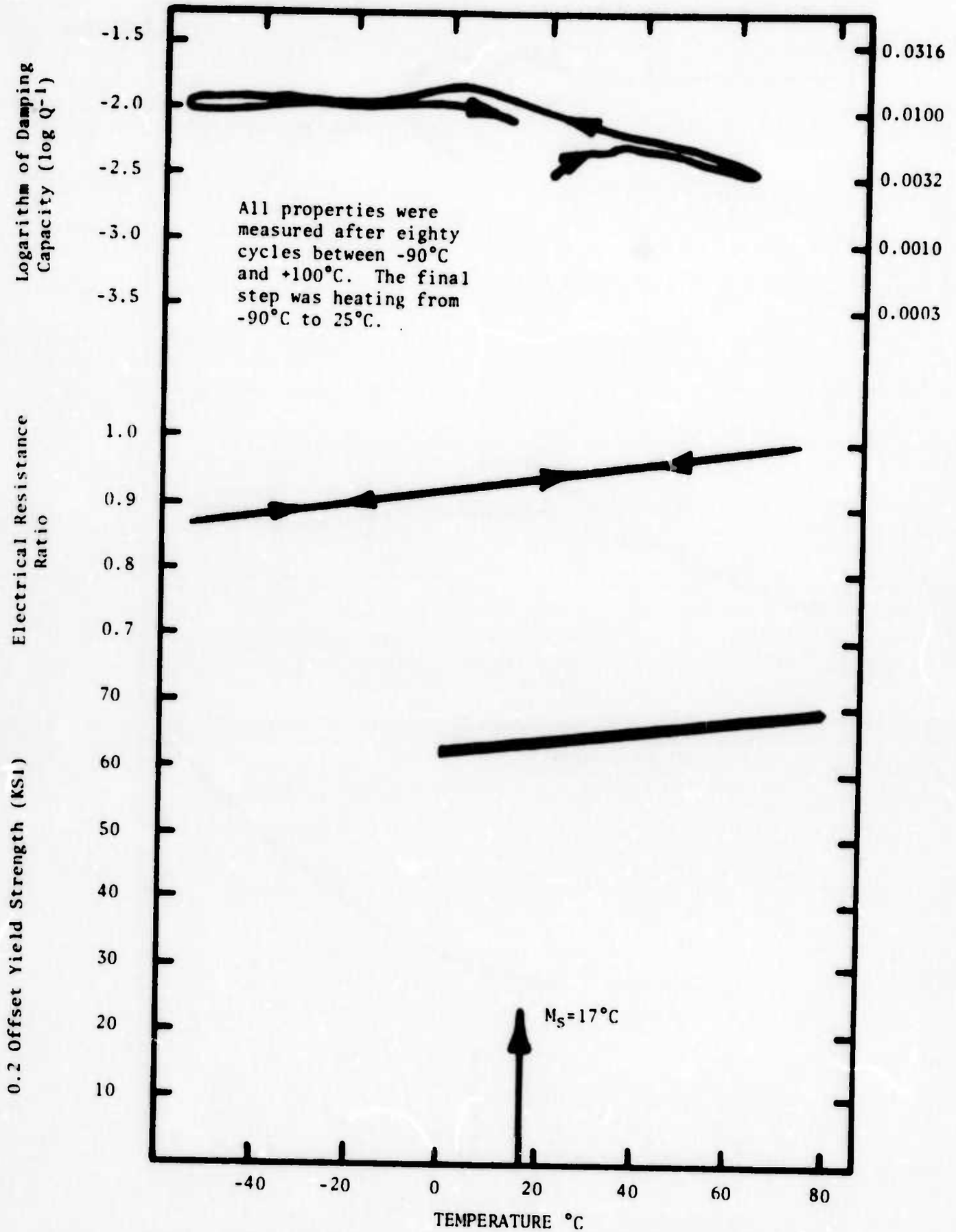

Figure 30. Damping Capacity, Electrical Resistance and 0.2% Offset Yield Strength for 55 w/o Ni-45 w/o Ti versus Temperature after 15% Cold Reduction and Cycling Treatment.

III. MEASUREMENT OF THE DAMPING CAPACITY AND DYNAMIC ELASTIC MODULUS OF Ni-Ti AND Cu-Al-Ni ALLOYS

Development of potential structural materials which are capable of high internal damping requires the simultaneous evaluation of the strength and acoustic absorption. In particular, the present study is directed toward development of materials with high damping capacity in the audible range. Thus, frequencies in the 150 to 200 cycle/sec (i.e. Hertz) range are of greatest interest. In this frequency range, loss factors (Q^{-1}) of one percent or more are considered to be quite high. Since the loss factor is a function of frequency it is important to specify the frequency range at which the loss factor is measured. Section V of the present report describes the "resonant dwell" method currently being employed to measure the loss factor. A substantial literature on damping behavior and internal friction of metals and alloys exists. However, a large part of this literature is related to torsional pendulum measurements which are conducted at very low frequencies (i.e. Hertz). Although high damping materials will show good loss factors over the entire range of frequencies, the loss factors measured at 1 cycle/sec are generally much higher than those measured at 200 cycles/sec.

Torsional pendulum studies conducted on Cu-14 w/o Al-3 w/o Ni alloys and indium-thallium alloys in the vicinity of low energy martensitic transformation temperatures indicate that high damping factors can be attained. The Cu-Al-Ni alloys can develop loss factors up to 1500×10^{-4} at 20°C when properly heat treated (5,6). Similarly In-Tl alloys transforming in the vicinity of room temperature exhibit loss factors near 3000×10^{-4} (7,8). Although In-Tl cannot be considered to be a structural material the Cu-14 w/o Al-3 w/o Ni alloy might prove to be a suitable candidate.

The above mentioned results for Cu-14 w/o Al-3 w/o Ni and In-Tl have been reinforced by the finding that Fe_3Pt can be heat treated to produce a low energy thermoelastic martensitic

transformation which exhibits substantially higher damping than the disordered form.

High damping ferromagnetic alloys based on combinations of iron, nickel, cobalt and chromium in binary and ternary combinations have been known for some time (9). These alloys were developed specifically for high temperature steam turbine applications and are thought to develop their damping capacity from the interaction of magnetic domains (9). Interestingly enough, the binary alloys which exhibit the greatest damping capacity are Co-35 Ni and Co-20 Fe. These alloys lie extremely close to compositions where the free energy differences between the high temperature and low temperature phases vanish (10). In the first case of the Co-35 Ni alloy which exhibits a loss factor of 1800×10^{-4} at a stress level near 1500 psi in a torsional pendulum experiment (at 25°C), the phase transformation in question is a fcc (high temperature phase)/hcp (low temperature phase) transition with a very small enthalpy difference of the order of 50 cal/g.at. (10). Thus the transformation may provide an important component of the damping capacity. Moreover it may be possible to improve the damping behavior by proper heat treatment.

The second most effective alloy is Co-20 Fe (9) which exhibits a loss factor of 1100×10^{-4} at 1500 psi. This composition is near the T_o-concentration curve at room temperature for the fcc/bcc reaction (10). Thus, this alloy may also be susceptible to improvement by heat treatment. The third best alloy uncovered by Cochardt was Co-28 Fe-7 Ni. This alloy showed a loss factor of 800×10^{-4} at 8000 psi. Curiously the alloy lies along the locus of $\Delta F(fcc/bcc)=0$ for the Co-Fe-Ni system at room temperature (10).

In order to evaluate the Cu-14Al-3Ni alloy and the cobalt base alloys cited above as potential damping materials samples of these materials have been melted, cast and machined into the standard reed configuration. In addition to the Cu-14Al-3Ni composition, 77 w/o Co-23 w/o Ni, 70Co-30Ni, 68Co-32Ni, 78Co-22Fe, 80Co-20Fe, 82Co-18Fe, 90Co-10Fe, 65Co-28Fe-7Ni and 70Fe-20Co-10Cr al-

loys have been prepared and characterized. The present section deals with results of measurements conducted on the Cu-Al-Ni and Ni-Ti alloys while Section IV deals with the cobalt base materials.

As indicated above, torsional pendulum studies of Cu_3Al (5,6) in the frequency range near 1 cycle/sec have yielded loss factors as high as 1500×10^{-4}. These loss factors can be altered by appropriate temperature cycling. They also seem to exhibit peaks as a function of temperature as shown schematically in Figure 31. In these cases it is not clear whether the peak is directly associated with M_s. However, the present study should clear up this matter. It should be pointed out that the figure shows Q^{-1} versus T as determined in a torsional pendulum at low frequency and stress levels.

Preliminary experiments indicated that the acoustical absorption of Fe_3Pt is increased greatly by ordering the parent phase before transformation. All the other known high-damping-capacity martensitic alloys are also ordered. Thus we are studying ordering in Fe_3Pt, the effect this has on the kinetics of the nucleation and growth of martensitic plates and on the physical properties of the two-phase product, and the ways in which these order-induced changes in structure and physical properties affect acoustical absorption. It is known from earlier work that stoichiometric Fe_3Pt undergoes a paramagnetic-ferromagnetic transition in the austenitic state, the Curie temperature increasing with the degree of order (11). This alloy exhibits a large Invar dilation on passing through the Curie temperature. It also has a sharp internal friction peak in the vicinity of the Curie temperature and the martensite formed from ferromagnetic austenite is thermoelastic (12). It is possible, of course, that all these changes in physical properties induced by changing the order in the γ-phase are interrelated, but details of the interactions are not known. In particular, although it is conceivable that in order to achieve high damping the martensite must be capable of reversible thermoelastic growth, this has not been demonstrated experimentally and the structural factors promoting thermoelastic growth are not under-

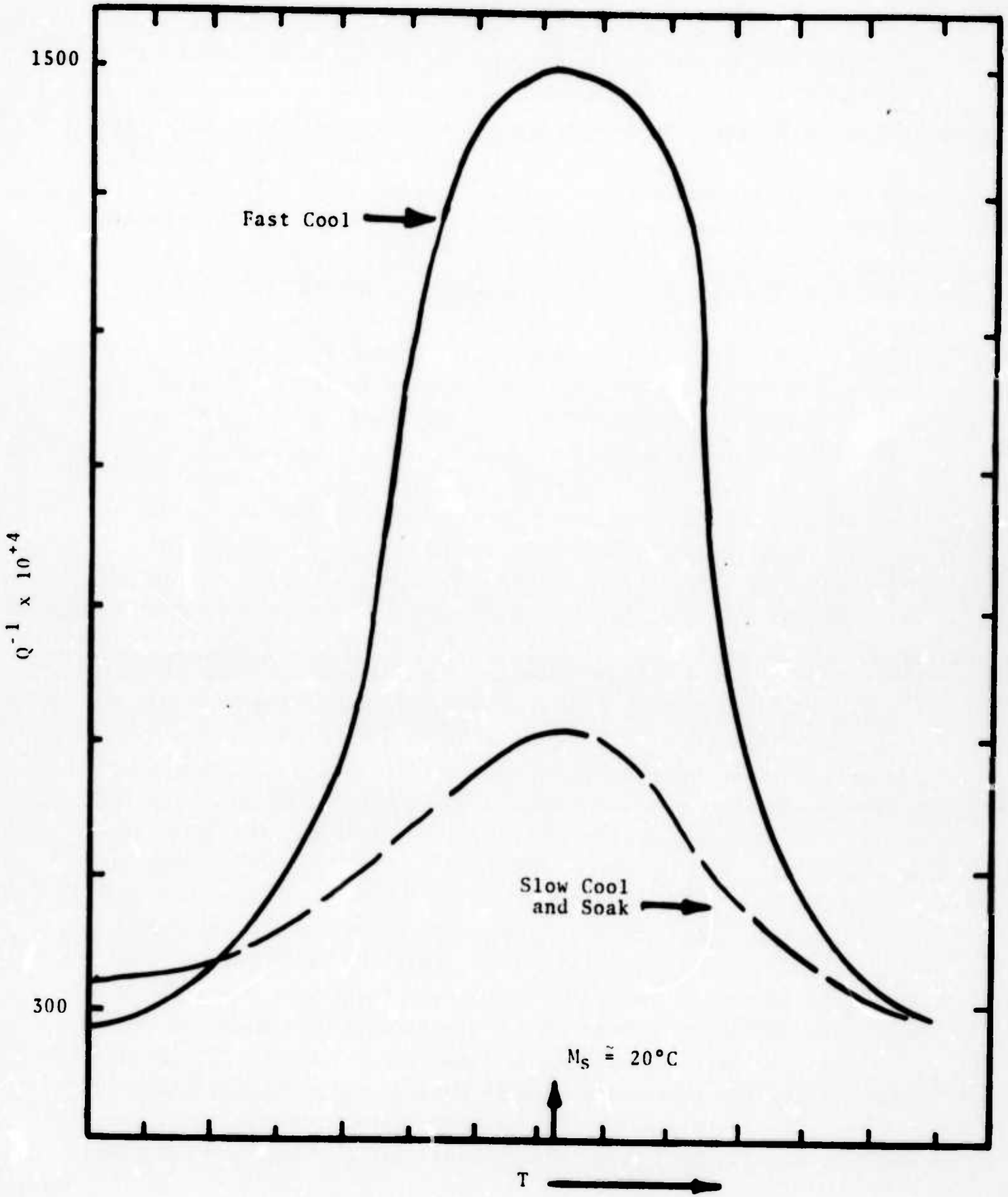

Figure 31. Schematic Diagram of Damping Factor versus Temperature for a Cu-Al-Ni Alloy.

stood sufficiently to provide a basis for the design of high damping-capacity alloys.

The initial evaluation of Fe_3Pt carried out under the present contract was designed to examine the ordering process in Fe_3Pt by X-ray diffraction and transmission electron microscopy to determine the influence of the degree of order of the γ-phase on the martensitic transformation by measuring the enthalpy of transformation in a differential calorimeter and calculating the free energy driving the process, and to determine the influence of the degree of order on the damping properties and on the mechanical strength of the alloy.

The first experiments have been done on an iron-25.2 a/o platinum alloy. In order to achieve a completely disordered structure, various quenching procedures were tried, but in all instances a certain degree of order remained in the specimens. It seems that the ordering reaction is very fast and cannot be suppressed by applied quenching rates.

The ordering process of this alloy is complex. After short annealing times, besides the superlattice lines of the ordered Fe_3Pt phase, some other diffraction lines appear. They at first become stronger with increasing annealing time, but eventually disappear, leaving only the lines of the ordered Fe_3Pt phase. It was possible to index the new lines as belonging to a tetragonal face-centered cubic lattice, corresponding to the FePt structure.

A series of samples ordered various times at 625°C were examined in a scanning differential calorimeter in order to evaluate the enthalpy of martensitic transformation. It was also possible to determine the M_S temperature by the same method. The results show that the M_S temperature decreases with ordering time, dropping to about 100°K after four hours at 625°C. Since this was the lower limit of the calorimeter, the samples with higher degrees of order could not be measured.

Detailed X-ray and metallographic work has shown that on quenching from above 900°C an ordered tetragonal phase based on

FePt is nucleated at austenitic grain boundaries. On subsequent annealing at 625°C, this phase grows simultaneously with the ordering of the Fe_3Pt cubic phase within the grains. At an intermediate stage of annealing the tetragonal phase, based on a CuAu I-type structure, spreads over the whole specimen. This phase is metastable, however, and on prolonged annealing at 625°C it disappears, being replaced by cubic, ordered Fe_3Pt. The sequence in which the tetragonal FePt and cubic Fe_3Pt phases appear on annealing is the same in the 25 and 27 a/o Pt alloys, but both ordering processes are slower in the latter alloy.

The metastable tetragonal phase in both alloys has the same lattice parameter ($a = 3.850\text{Å}$, $c = 3.715\text{Å}$) which does not change with time of annealing. These cell dimensions are the same as for the stable ordered FePt phase found in alloys with between 32 and 62 a/o Pt. The lattice parameter of the cubic Fe_3Pt increases gradually during the ordering process (from 3.722Å to 3.734Å in the 25 a/o Pt alloy).

It is now possible to understand some earlier observations on the effect of ordering on the martensitic behavior of the 25 a/o Pt alloy. The thermoelastic and microstructural reversibility are markedly different in specimens quenched after annealing for medium and long times. The present work has shown that martensite formed on quenching specimens after medium annealing times is generated from the metastable, tetragonal AuCu I-type structure, whereas the martensite formed from well-annealed austenite originates from the cubic, ordered Fe_3Pt structure. Simple experiments have indicated that the martensite produced from the cubic phase has a high damping capacity. The relative magnitude of the damping effect in martensite formed from the metastable tetragonal phase is unknown as yet.

Several attempts have been made to fabricate suitable samples of the 75 a/o Fe-25 a/o Pt alloy which can be used for damping measurements. However, while the compositions have been melted and cast successfully, it has not been possible to generate

the ordered and disordered phases successively in the same sample thus far. Consequently, while measurements of the loss factor in the disordered phase have been made (these are reported in Section IV) no measurements on the ordered 75 a/o Fe-25 a/o Pt have been made to date.

Extensive measurements of the damping capacity of 55 w/o Ni-45 w/o Ti samples have been made using the Resonant Dwell Apparatus designed by Bolt, Beranek and Newman. Section V details the characteristics of this apparatus.

The BBN resonant dwell apparatus generates damping (Q^{-1}) versus temperature curves. The applied bending stress is between 1 and 10 ksi, and the frequency is between 100 and 1000 Hz. Experimentally, it was found that the damping varies with the cycling of the temperature-control unit, but the quality of the measurements could be improved significantly by determining the damping isothermally versus strain amplitude (tip deflection). This involves measuring the resonant frequency and the accelerometer output as a function of controlled tip displacement. Over the range of tip displacement, y_t, employed, the acceleration, a_o, and the resonant frequency, f_n, of the sample are each nearly linear functions of y_t which increases confidence in the values of a_o and f_n as shown in Figure 32. The damping, Q^{-1}, is nearly independent of y_t at low values of Q^{-1}, but increases with y_t at larger values as illustrated in Figure 33.

"Isothermal" curves of f_n and a_o versus y_t were taken on both cooling and heating; values of f_n and a_o were selected for y_t = 0.040 in. and used to calculate Q^{-1}. All specimens were first heated to well above M_s, held for 15-30 minutes, then slowly cooled to the temperature at which the measurement was to be made, and held for 15 to 20 minutes to insure thermal equilibrium. The f_n versus y_t and a_o versus y_t data were taken by increasing y_t in a stepwise fashion at the given temperature. Each of these "isothermal" curves yields one point on the damping versus temperature plots, and since only comparatively few of these measurements can be made each day, compatibility of measurements taken on different

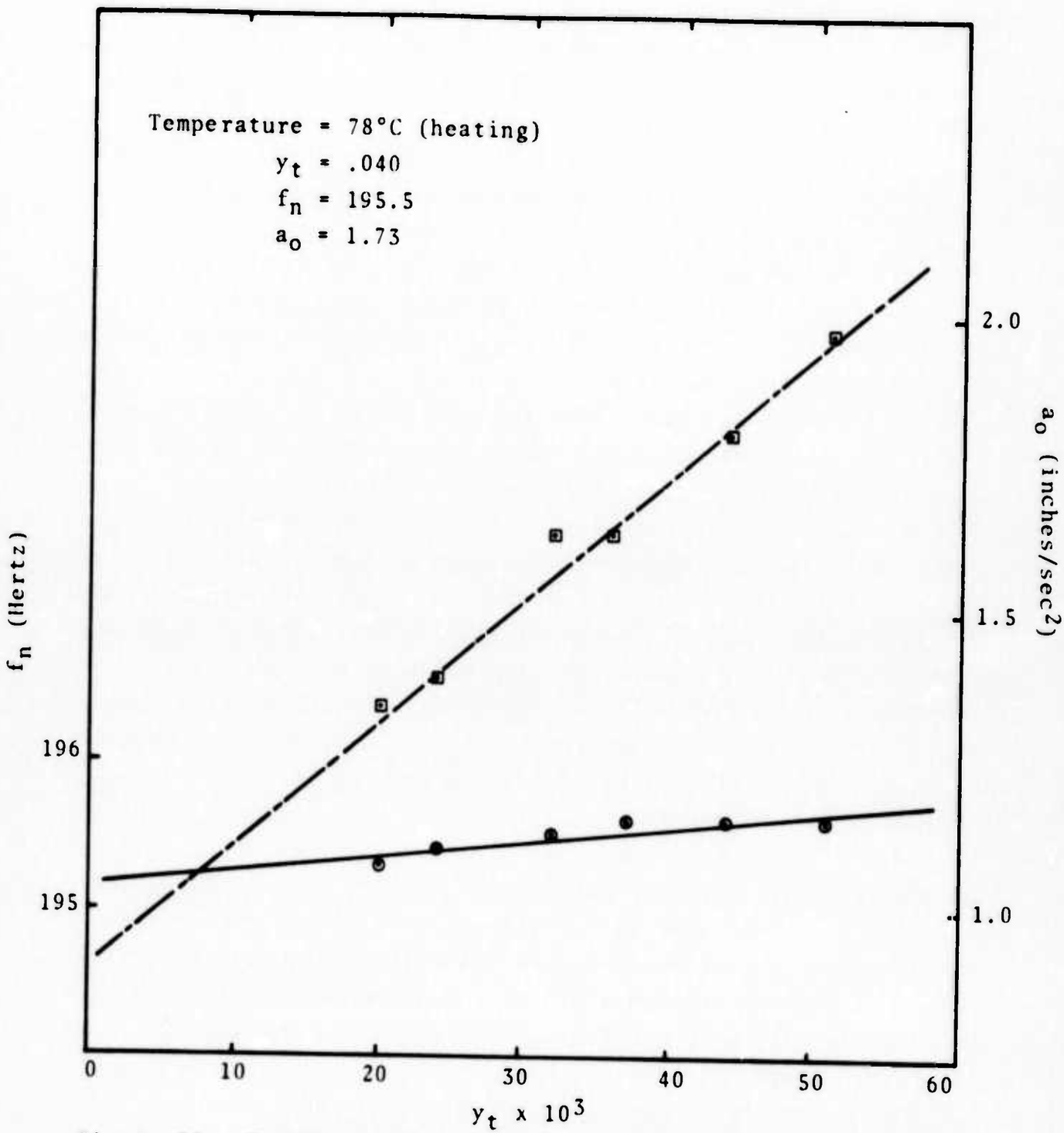

Figure 32. Sample resonant frequency (f_n) and acceleration (a_o) as a function of tip deflection (y_t) at a temperature of 78°C for a sample of 55w/oNi-45w/oTi.

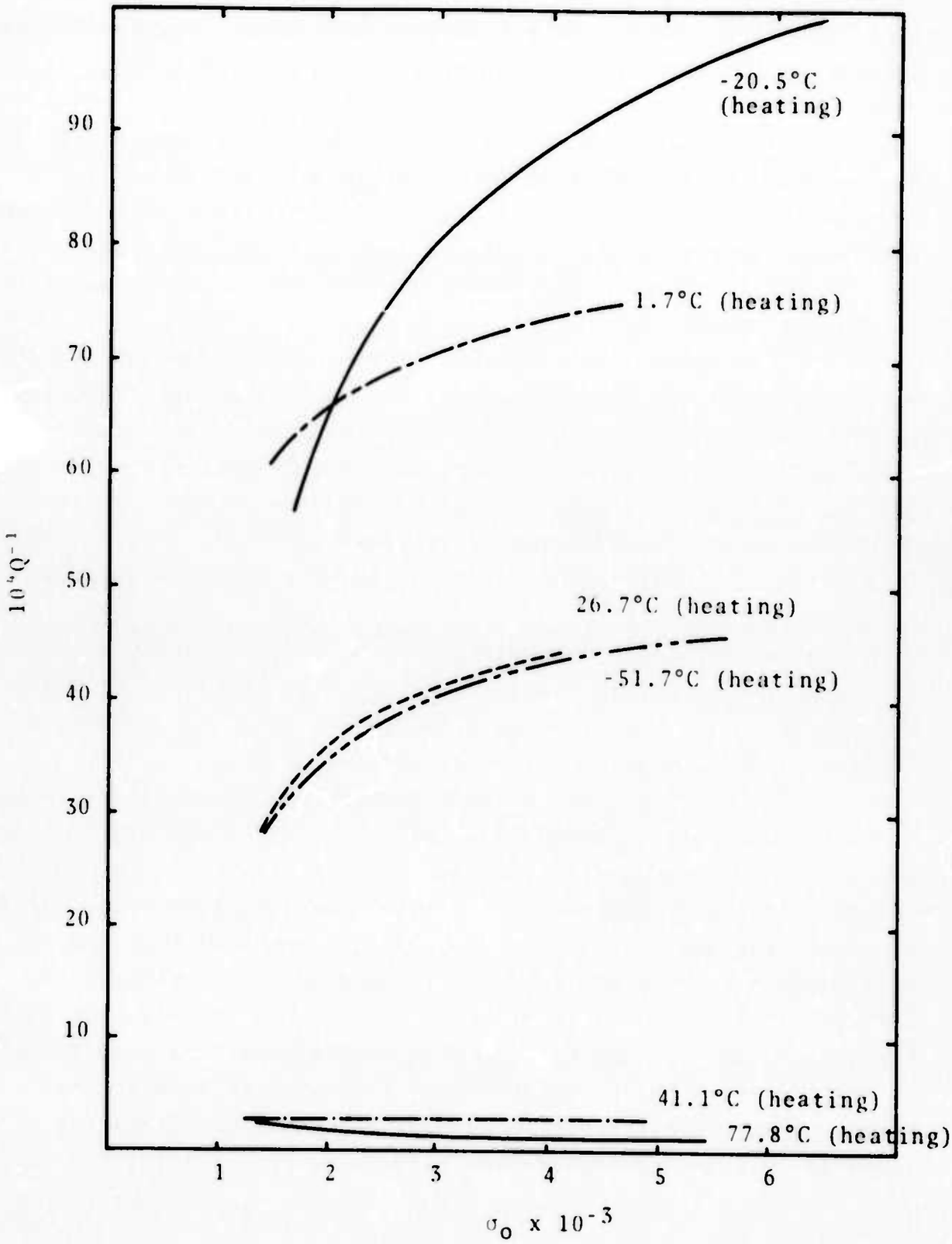

Figure 33. Specimen damping factor (g_s) as a function of maximum bending stress (σ_o) at various temperatures for a sample of 55w/oNi-45w/oTi.

days had to be determined. The agreement was found to be good. Figure 34 is a plot of damping versus temperature data for specimens with different stress and thermal histories. Figure 35 shows the curves for specimens during heating and cooling. There is a small hysteresis.

The dynamic Young's modulus of NiTi, measured at 180Hz, was determined as a function of temperature by noting the variation in resonant frequency. These results, together with data on the change in electrical resistance and heat capacity, measured in a differential thermal calorimeter, are shown as a function of temperature in Figure 36.

On cooling, the marked increase in the damping capacity and the decrease in Young's modulus set in at the same temperature (approximately 45°C). The increases in electrical resistance and heat capacity also start together, but at a temperature (approximately 25°C) which is some 20°C lower than the temperature at which the modulus and damping start their increase. The M_s of this alloy is, however, indicated by the peak in the resistivity curve on cooling, and this occurs at about 5°C. The damping thus seems to increase significantly before M_s is reached (in the unstressed sample) and this may result from (1) stress-induced martensite (i.e. the stress-induced raising of M_s), (2) premartensitic effects in the alloy, or (3) a combination of both.

In initial tests of NiTi alloys, the cantilever beam portion of the sample deformed (i.e. it both twisted and bent) during testing. The cause of this deformation was believed to be connected with the "shape memory" of this material, more specifically, the machining and heat treating operations combined to cause the NiTi samples to bend and twist as the sample transformed as the temperature was lowered to affect a martensitic (or reverse) transformation. The bending and twisting of the sample is deleterious to testing using the resonance dwell apparatus because of the change in stress distribution associated with the deformation. In order to avoid macro-deformation associated with the transformation,

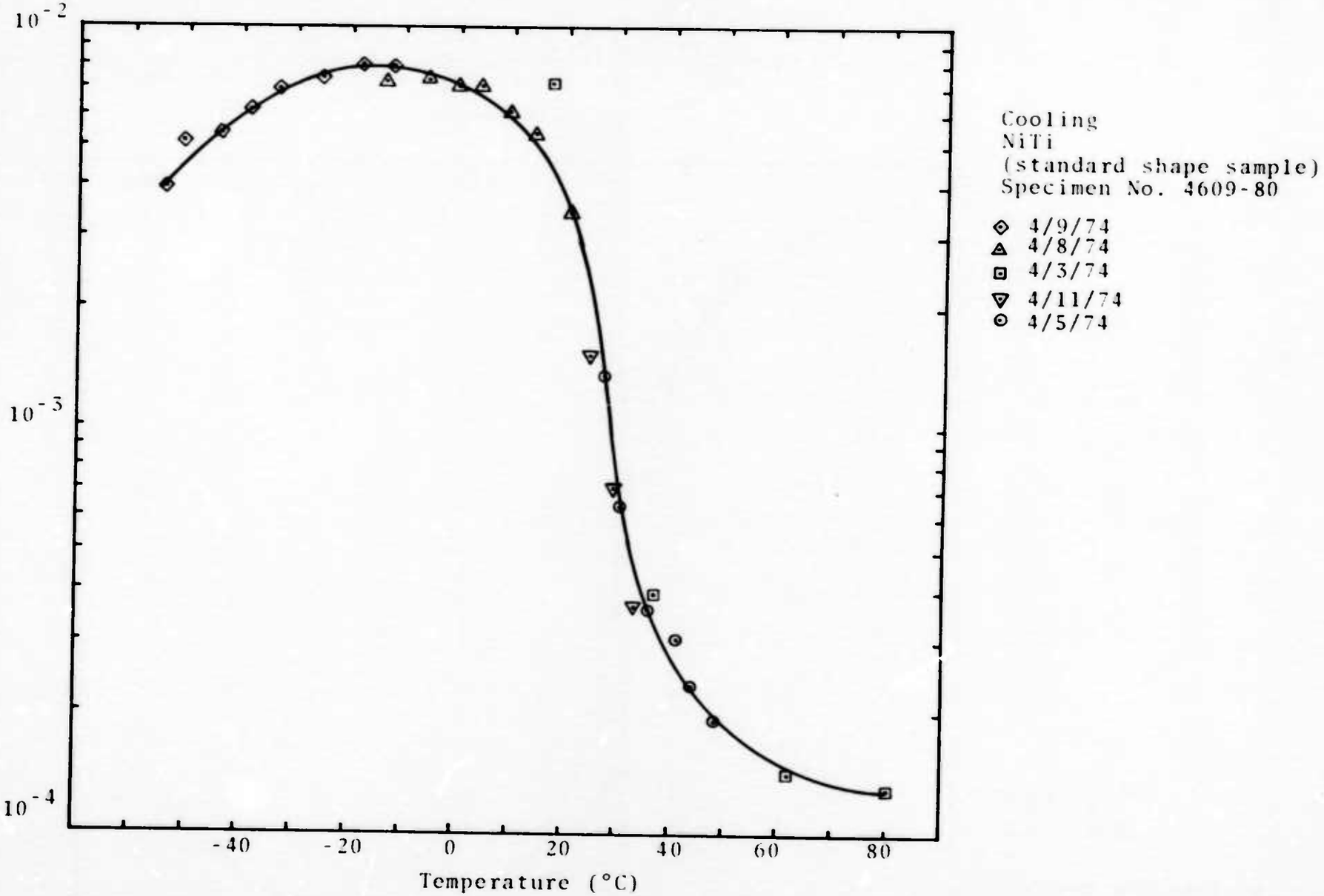

Figure 34. Specimen damping factor (g_s) as a function of temperature on cooling (for a constant y = 0.040 in.) for a sample of 55 w/o Ni-45 w/o Ti.

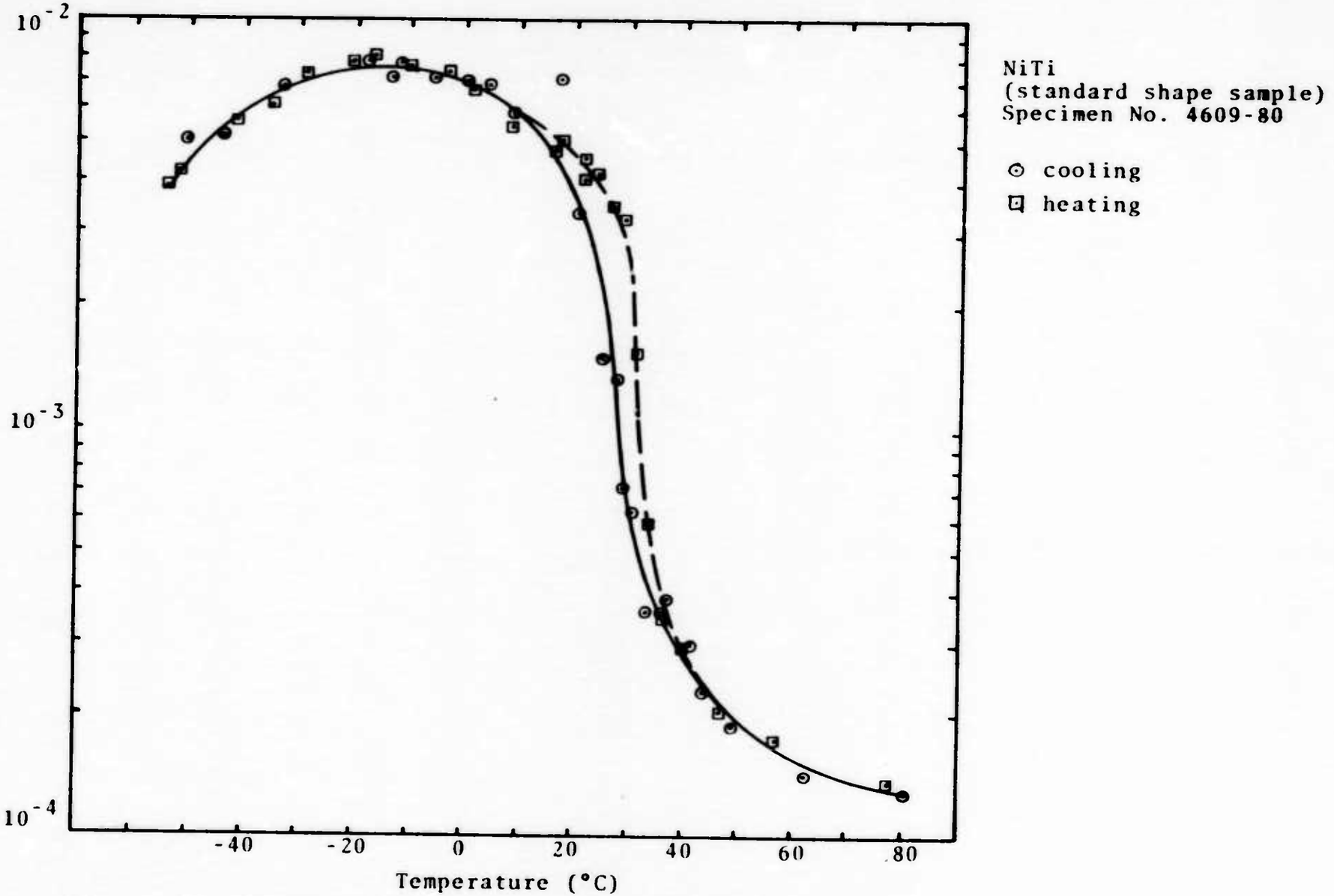

Figure 35. Specimen damping factor (g_s) as a function of temperature on both heating and cooling for a sample of 55 w/o Ni-45 w/o Ti.

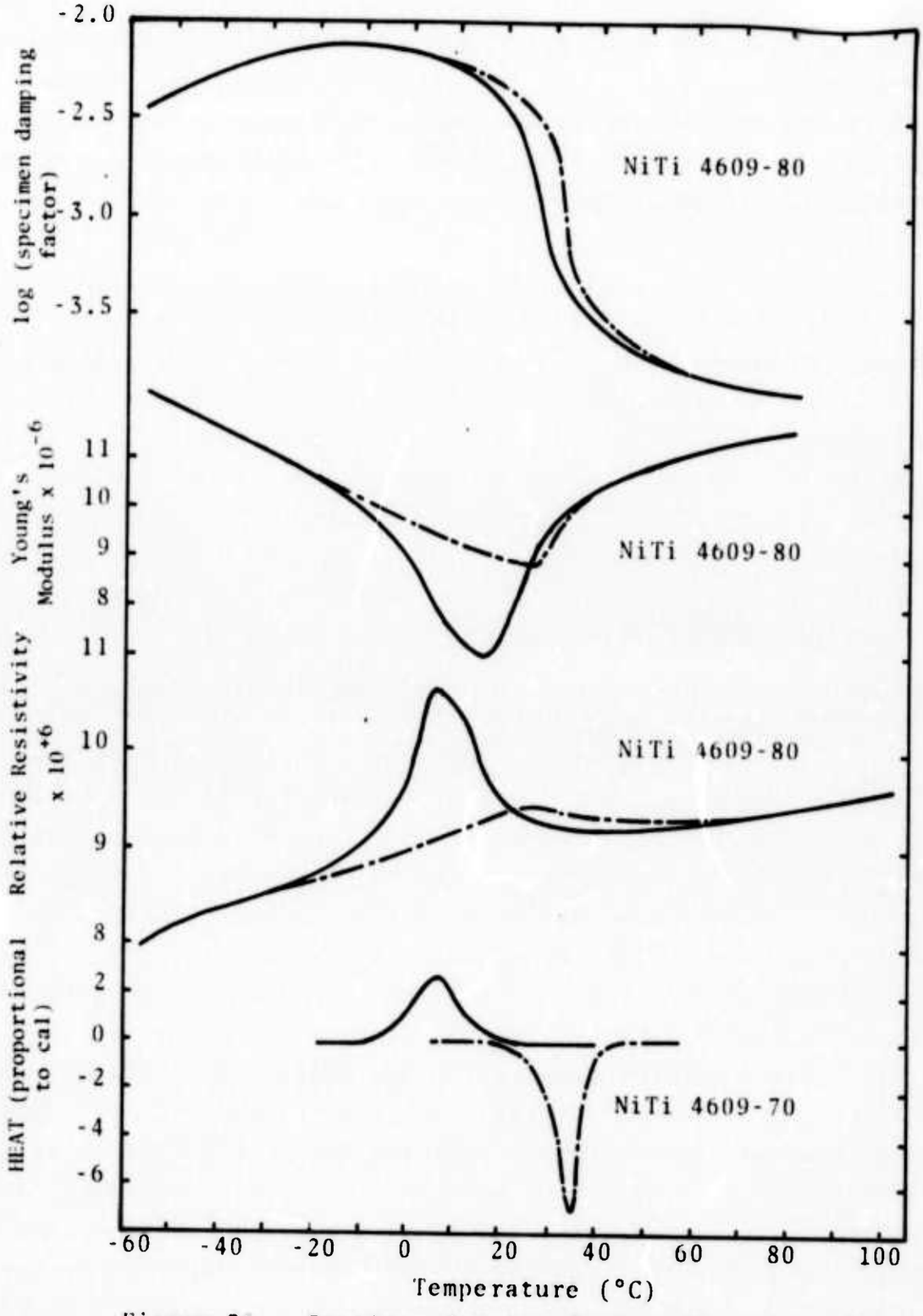

Figure 36. Specimen damping factor, Young's modulus, relative resistivity and heat evolved as a function of temperature for the same series (4609) of 55w/oNi-45w/oTi.

the samples were heat treated with the intention of putting a straight untwisted beam into the "memory" of the sample. To do this, the NiTi specimen was fixed in an appropriately shaped steel clamping device, put into a furnace at 800°C, allowed to come to equilibrium and then water quenched. The quenched samples were then thermally cycled (through their M_s temperatures) approximately seventy-five times before damping tests were performed on these samples.

The damping tests on samples V-4866-40 and V-4866-60 (55 w/o Ni-45 w/o Ti) are shown in Figures 37 and 38. The cooling curves are shown as solid lines and the dashed lines indicate the heating curves. The two figures show curves which are similar to each other. Upon cooling both of the samples showed a significant increase in damping by 40°C, the damping continued to rise to a maximum at about 22°C. The damping then more or less levels to an approximately constant value. On heating, the damping curve basically follows the same path as the cooling curve except that the maximum is reduced and there is a hysteresis effect. That is, the damping remains high to a temperature above that where the damping first increased on cooling.

During the tests on samples V-4866-40 and -60, the beams deformed slightly so that the memory was not entirely "straight." Figures 37 and 38 can be compared with Figure 39 which shows the damping curve of sample 4866-40 before the effort to straighten the beam. In this test the beam deformed significantly, but as shown in the figure, the basic shape and position (with respect to temperature) of the curve is the same as the curves from the "straight memory" samples.

An important point which was necessary to clarify was the location of the martensite start temperature (M_s) in relation to the damping curve. The resistivity curve of a 4866 sample (thermally cycled through M_s seventy-five times) indicates the M_s is at about 20°C. However, there was a question as to how much the (vibratory) stress applied by the resonant dwell apparatus

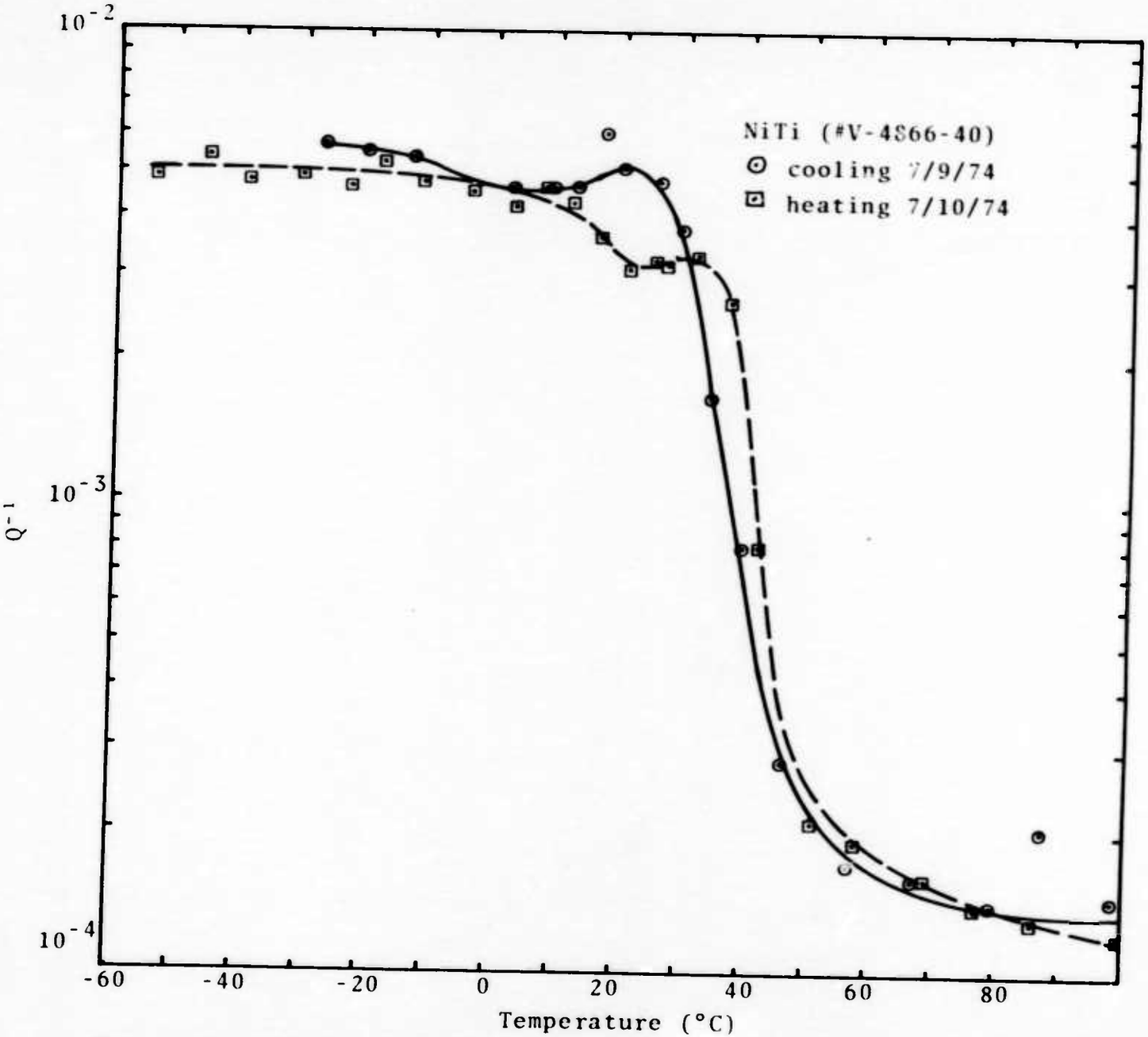

Figure 37. Damping behavior of NiTi alloy 4866 (sample no. 40) heat treated such that cantilever beam sample remains undeformed throughout the test. Composition 55 w/o Ni-45 w/o Ti.

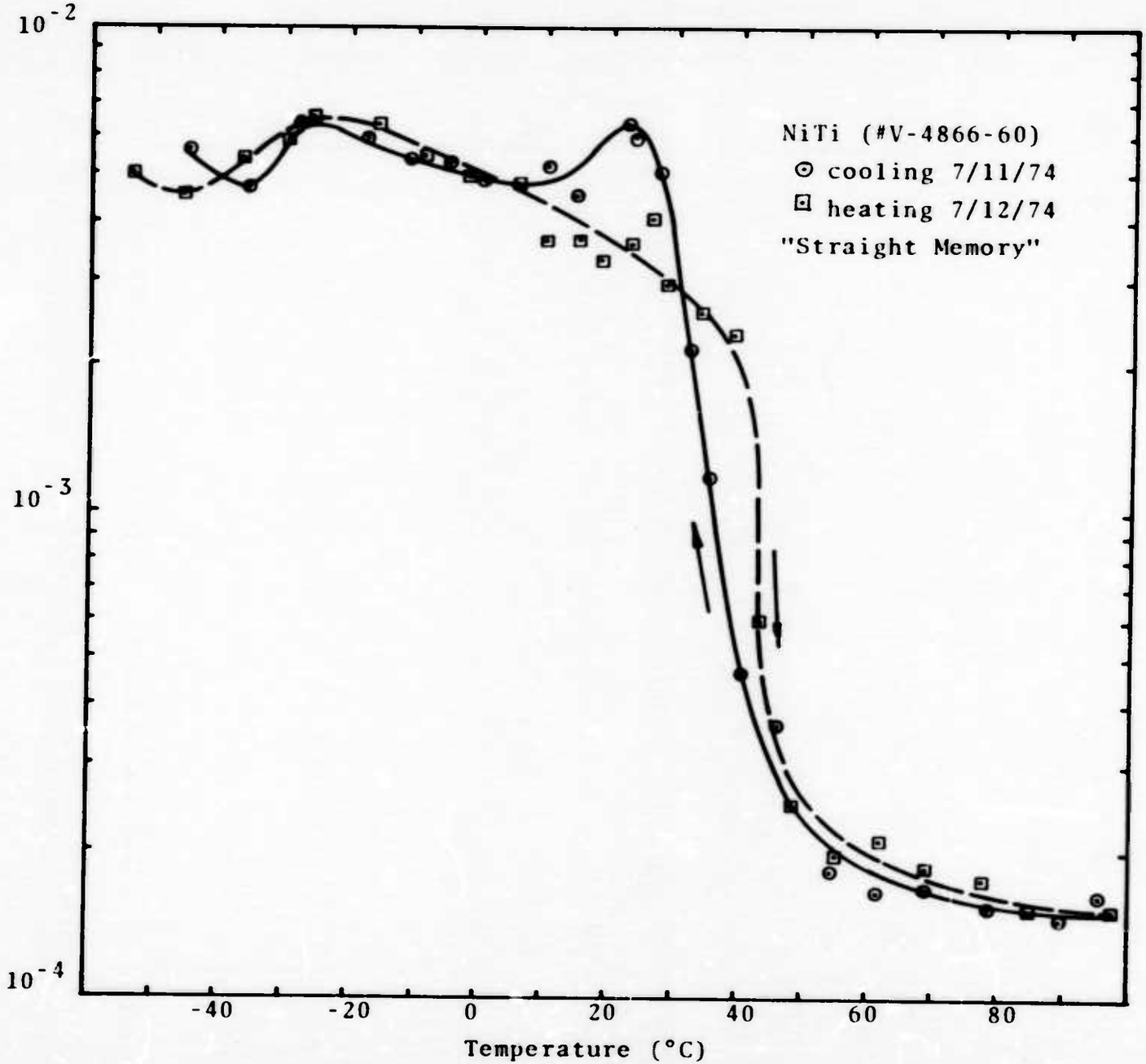

Figure 38. Damping behavior of NiTi alloy 4866 (sample no. 60) heat treated such that the cantilever beam sample remains undeformed throughout the test. Composition 55w/oNi-45w/oTi.

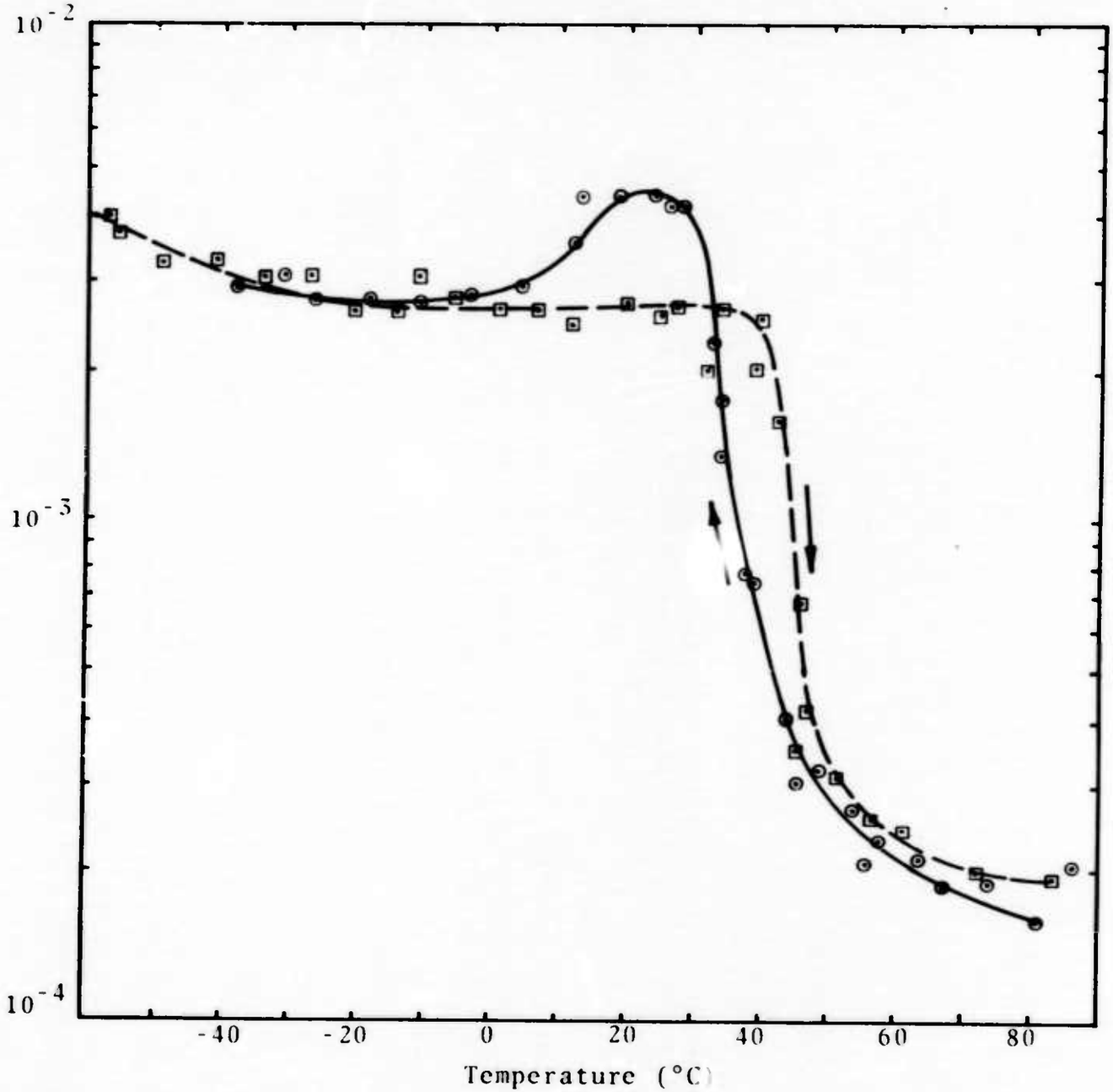

Figure 39. Damping behavior of NiTi alloy 4866 (sample no. 40) prior to straightening heat treatment. Composition 55 w/o Ni-45 w/o Ti.

might raise the M_s temperature. In order to obtain a reasonable estimate of how M_s is affected by the stress (applied by the testing apparatus), the resistivity of a sample of 4866 NiTi material was measured with a dead load of 1275 psi and 5485 psi (the maximum stress applied in the damping test). These tests showed that M_s (indicated by the temperature at the peak in resistivity) was not shifted (see Figures 7-9). The conclusion of the damping and resistivity measurements is that the damping increases significantly (that is, some 20°C) before M_s is reached. This suggests that the damping increase upon cooling is initially (in the 40°C to 20°C range) caused by premartensitic phenomena. It is also of interest to note that the dynamic Young's modulus (i.e. the modulus measured at the resonant frequency of the sample) has a minimum at the same temperature that the damping is at a maximum. (Note also the anomalous positive slope of the modulus above M_s). The curves for damping, Young's modulus, and resistivity versus temperature are shown in Figure 40 for sample 4866-40. The cooling curves (solid lines) of each property have extrema at approximately the same temperature. Also, viewing the heating curves (dashed lines), extrema are again found at about the same temperature.

It is apparent that the damping remains at a high level even after M_f (approximately -10°C) has been reached. Thus the mechanism which causes the high damping (up to 20°C) is probably distinct from the mechanism which causes the high damping from 20°C to -45°C. In order to gain further information about the mechanisms causing damping a thermal-tensile stage for a light microscope has been constructed. The stage has been tested over the temperature range of -50°C to +60°C (with only slight modification this temperature range can be considerably expanded). The stage was constructed in order to observe the behavior of the sample when a stress is applied and subsequently removed at various temperatures. Samples of 4866 NiTi were polished (both mechanically and electrolytically) and observed in the stage (with no applied stress) as the temperature was lowered from 60°C to -50°C.

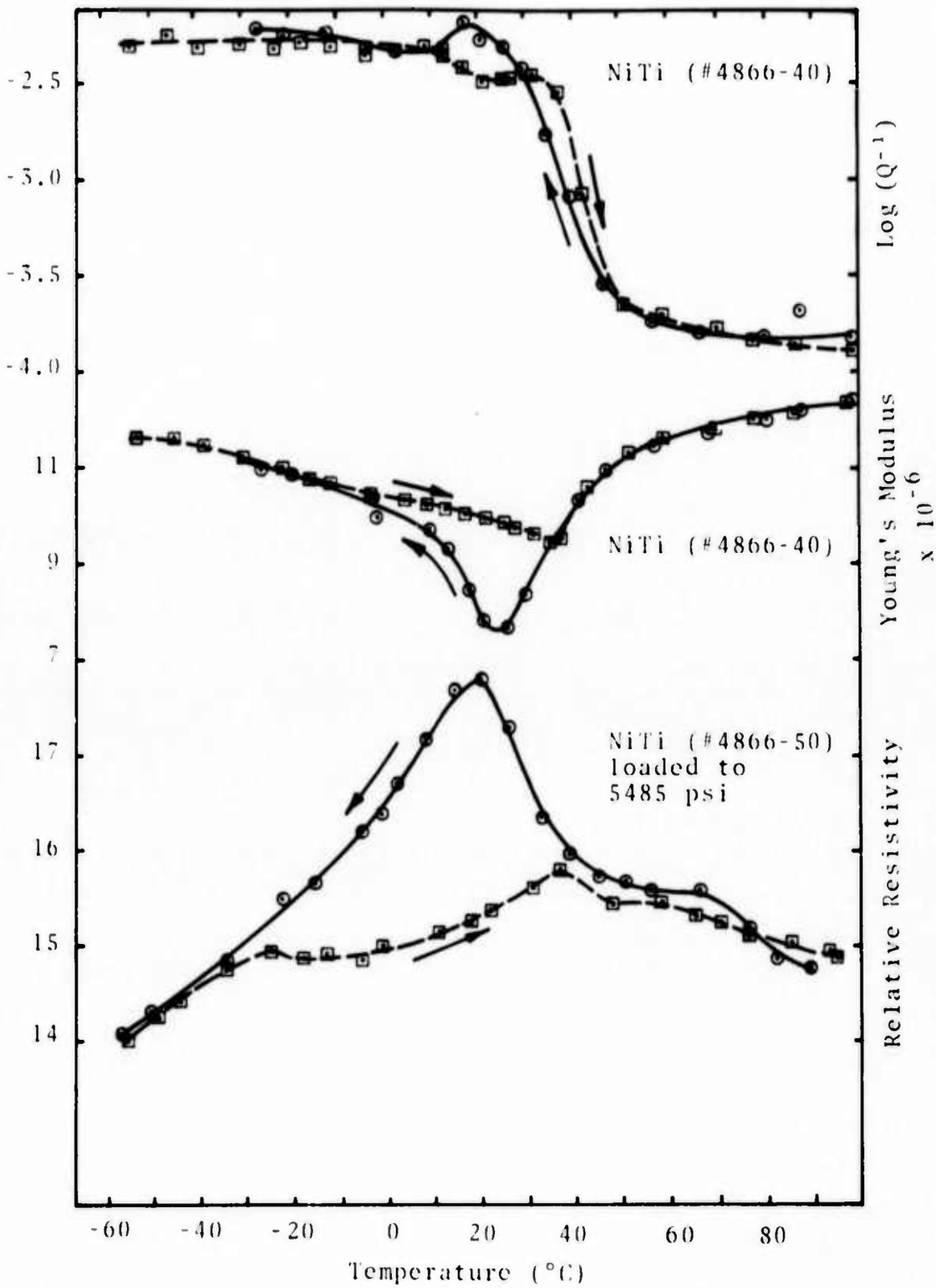

Figure 40. Damping behavior, Young's modulus, and electrical resistivity as a function of temperature for NiTi alloy 4866. (55 w/o Ni-45 w/o Ti)

No surface relief caused by the martensite has yet been noted in these samples. Work is continuing on this problem.

In order to evaluate the effects of cold working on the loss factor, Q^{-1}, a series of samples were cold worked and then machined into reeds. These were subsequently cycled eighty times between -90°C and +100°C and measured over the range -60°C to +80°C. Figures 41-46 show the results for Q^{-1} versus T and the dynamic Young's modulus versus temperature. The general features of these curves are similar to those shown earlier in Figure 36. However, the results obtained for the sample which received 15% reduction do not show the maxima and minima exhibited by the other curves.

The damping behavior of 73 w/o Cu-14 w/o Al-3 w/o Ni has been measured by preparing samples of this alloy in the single crystal and polycrystalline forms. The initial results were obtained on a polycrystalline sample. Figure 47 shows these results disclosing rather high loss factors. However, subsequent examination showed that the sample exhibited some cracks which may have contributed to the damping. Consequently, several single crystals of this material were prepared and the measurements repeated.

Samples of Cu-14.0Al-3.0Ni and Cu-14.1Al-3.0Ni have been run on a differential thermal calorimeter at AMMRC. Critical results indicate that the M_s of the sample can be determined quite well by calorimetry. Small samples (approximately 20mg) indicated that the $\beta_1 \rightarrow \gamma_1$ martensitic reaction occurs in a very narrow temperature range--less than 0.07°C between the M_s and M_f for the samples tested (indicated from measurements made at the slowest rate of temperature change allowed on the machine used). Larger samples (approximately 120mg) showed a difference of approximately 5.0°C between M_s and M_f. This may be the effect that the bulk characteristics of the larger sample have on the thermoelastic transformation. In both large and small samples there is an appreciable difference between A_s and A_f (about 15°C) and the heat liberated versus temperature curve exhibits a significant amount of struc-

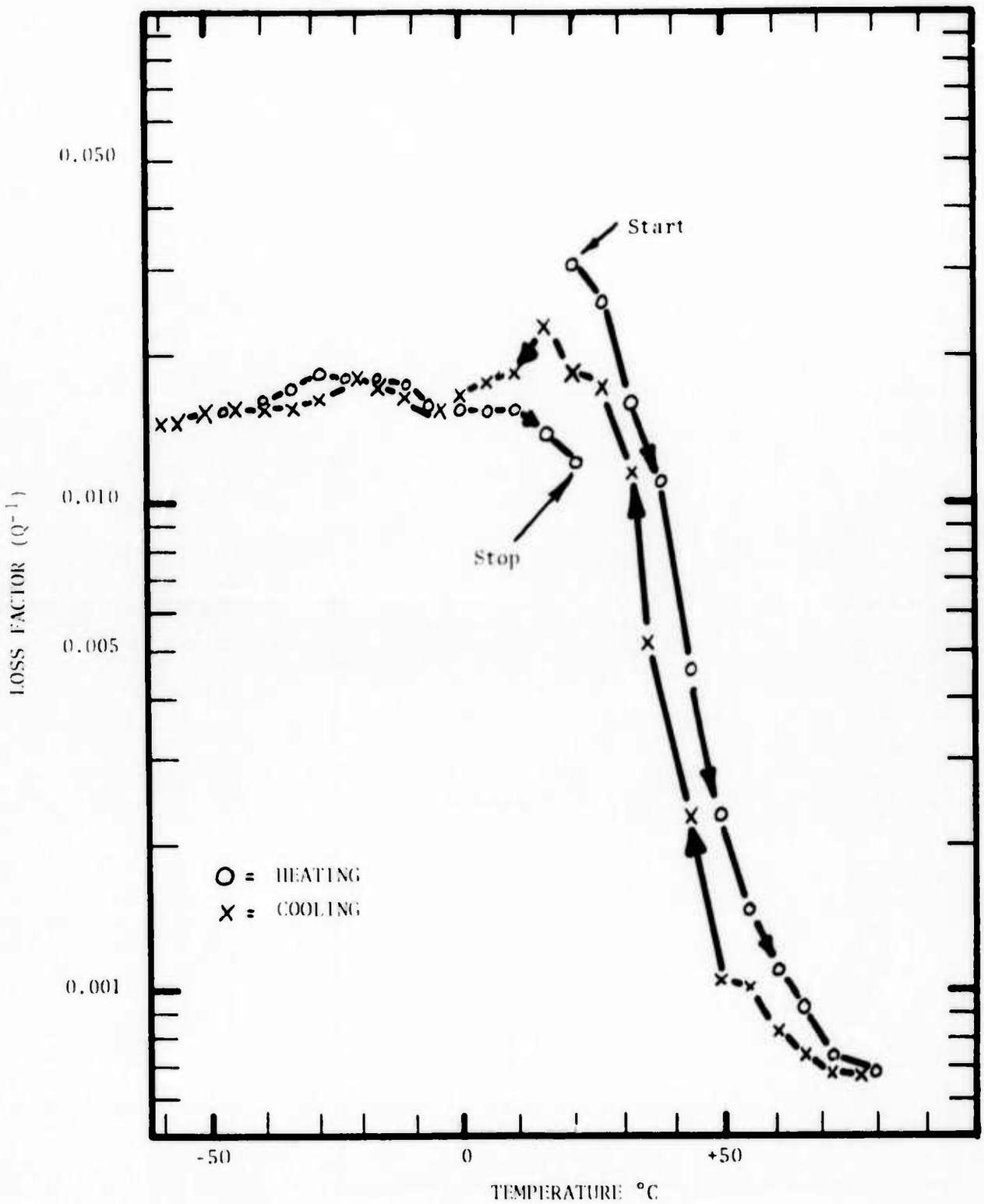

Figure 41. Loss Factor vs. Temperature Curve for a Sample of 55 w/o Ni-45 w/o Ti measured at 160-190 Hertz and a Stress of 2000 psi. The sample was cycled 80 times between -90°C and +100°C prior to testing. The final cycle ended by heating from -90°C to 25°C. The M_s is at +17°C.

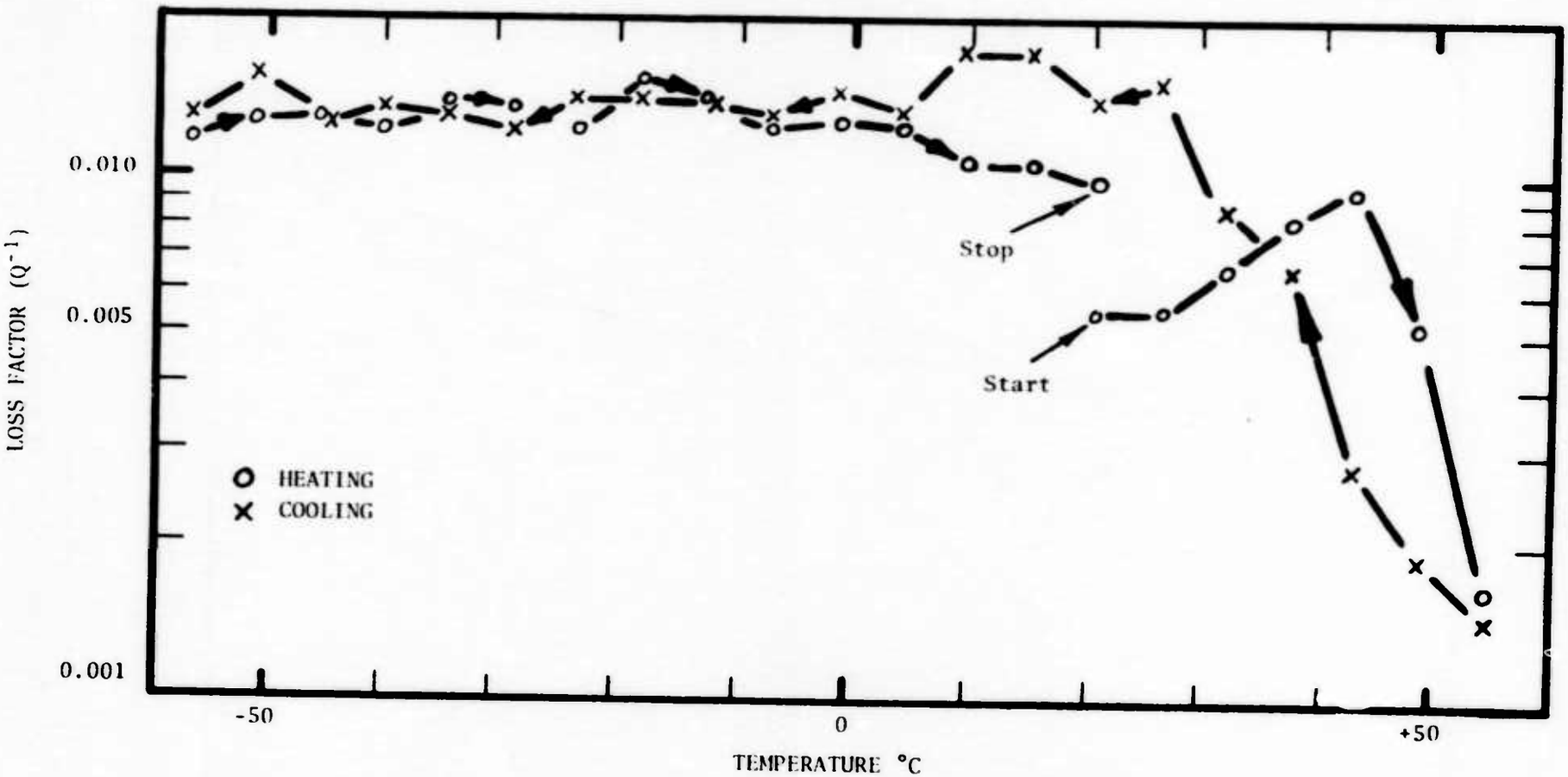

Figure 42. Loss Factor vs. Temperature Curve for a Sample of 55 w/o Ni-45 w/o Ti measured at 145-175 Hertz and a Stress of 2000 psi. The sample was deformed 3.2% by rolling and cycled 80 times between -90°C and +100°C prior to testing. The final cycle ended by heating from -90°C to 25°C. The alloy exhibits an M_s near +17°C in the annealed state.

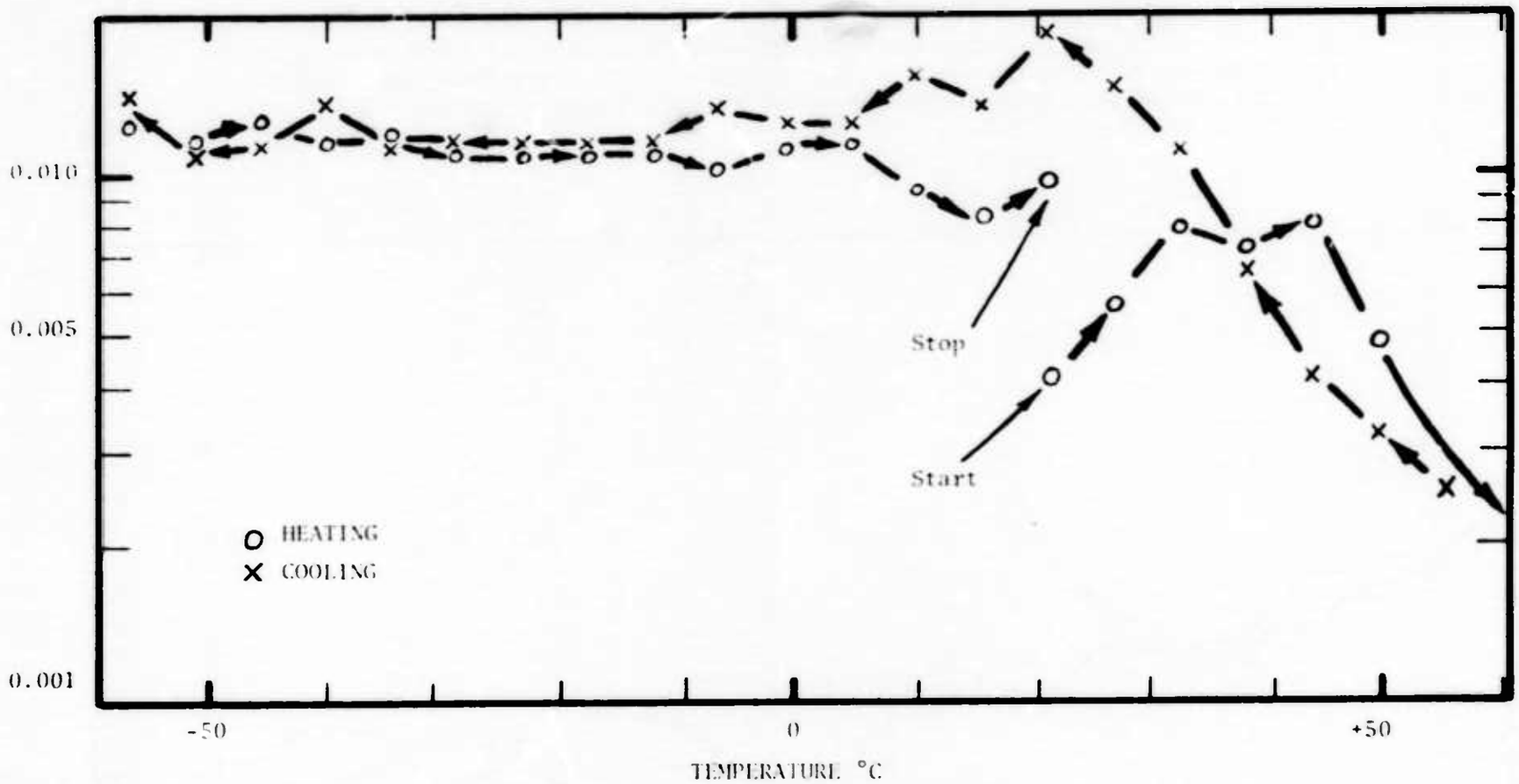

Figure 45. Loss Factor vs. Temperature Curve for a Sample of 55 w/o Ni-45 w/o Ti measured at 170-190 Hertz and a Stress of 2000 psi. The sample was deformed 7% by rolling and cycled 80 times between -90°C and +100°C prior to testing. The final cycle ended by heating from -90°C to 25°C. The alloy exhibits an M_S near +17°C in the annealed state.

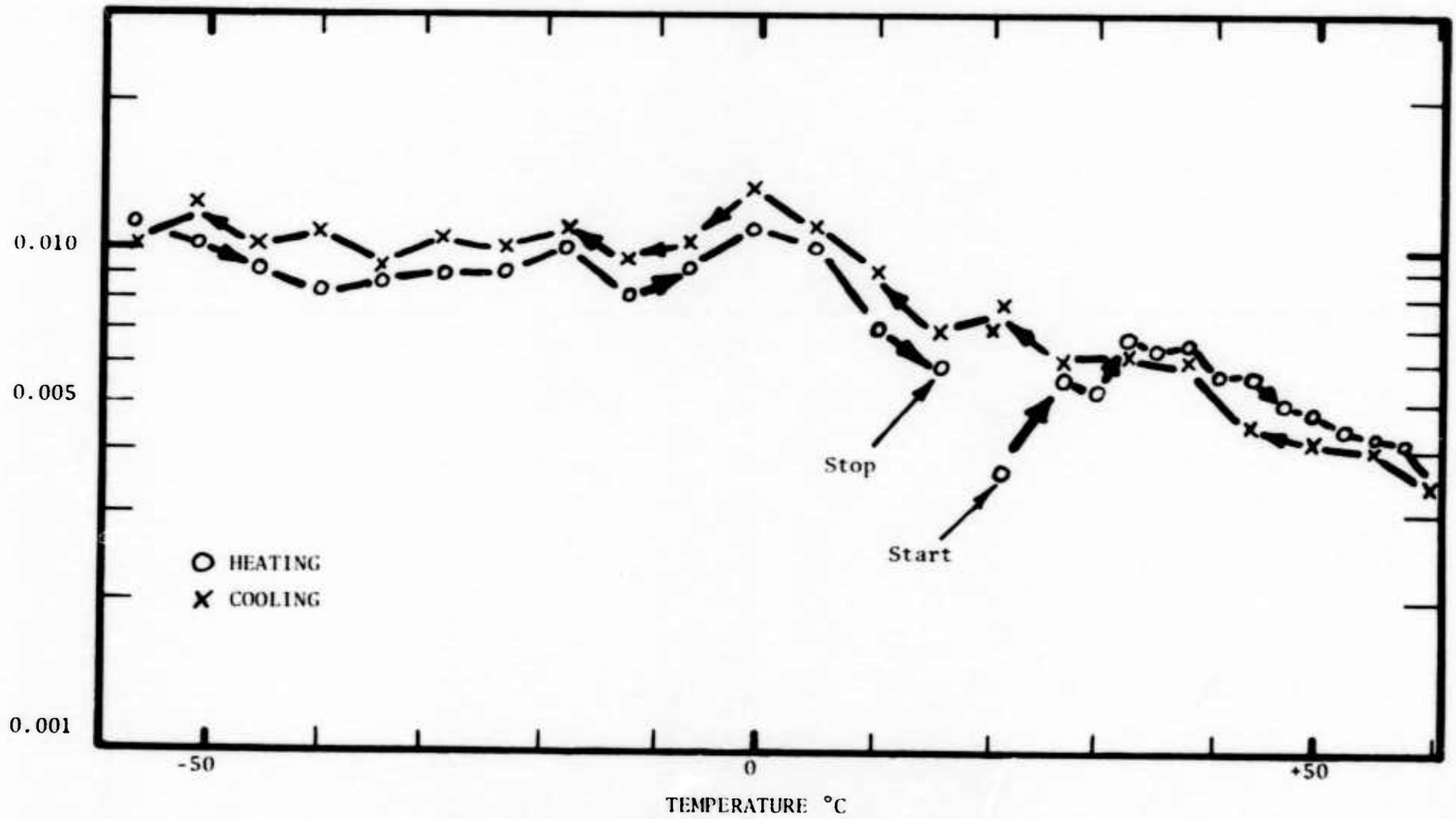

Figure 44. Loss Factor vs. Temperature Curve for a Sample of 55 w/o Ni-45 w/o Ti measured at 155-170 Hertz and a Stress of 2000 psi. The sample was deformed 15% by rolling and cycled 80 times between -90°C and +100°C prior to testing. The final cycle ended by heating from -90°C to 25°C. The alloy exhibits an M_s near +17°C in the annealed state.

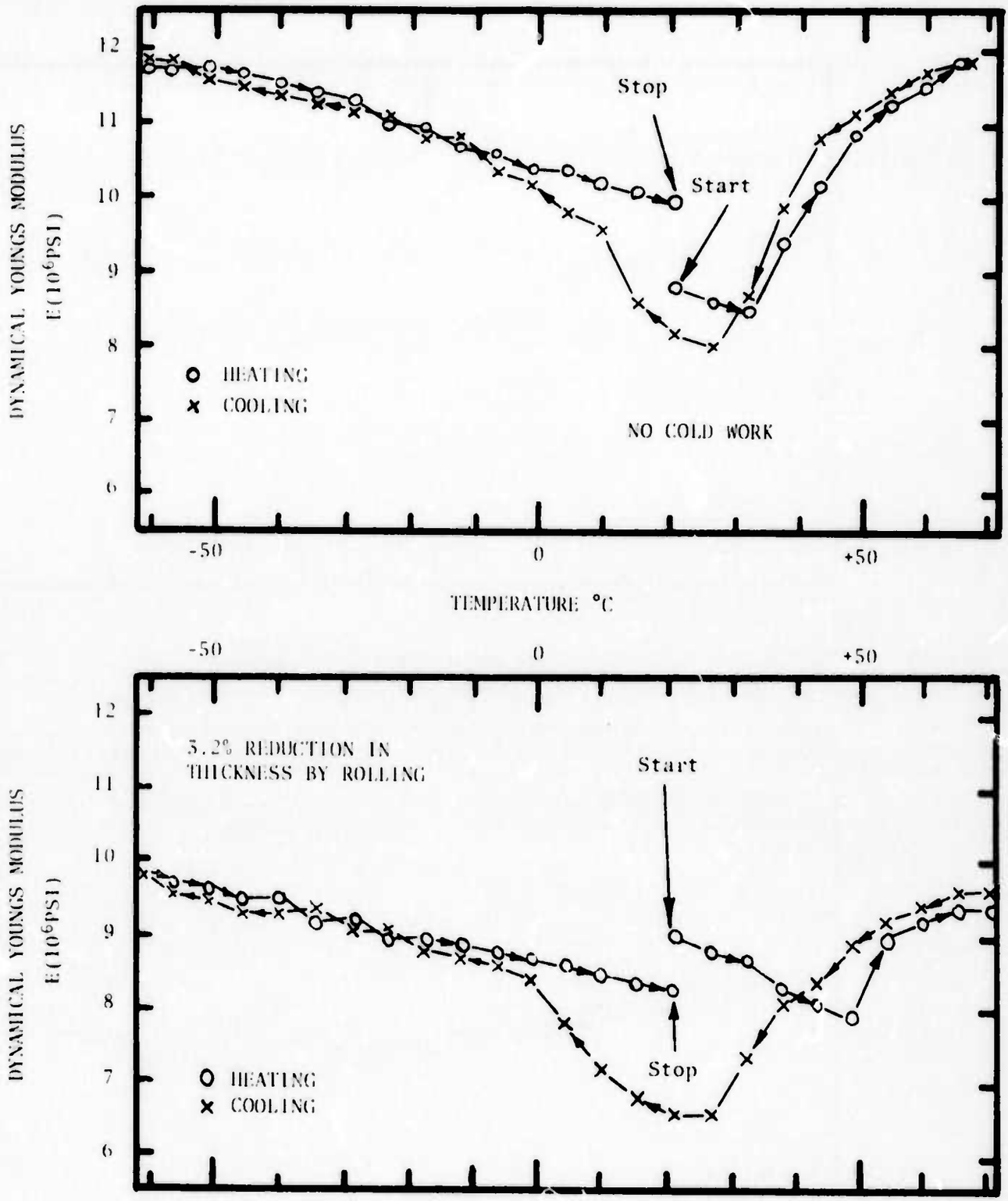

Figure 45. Dynamical Youngs Modulus vs. Temperature for 55 w/o Ni-45 w/oTi measured at 145-190 Hertz at a Stress of 2000 psi. The lower sample was deformed 3.2% by rolling prior to 80 cycles between -90°C and +100°C before testing. The final cycle ended by heating from -90°C to 25°C. The M_s is at +17°C.

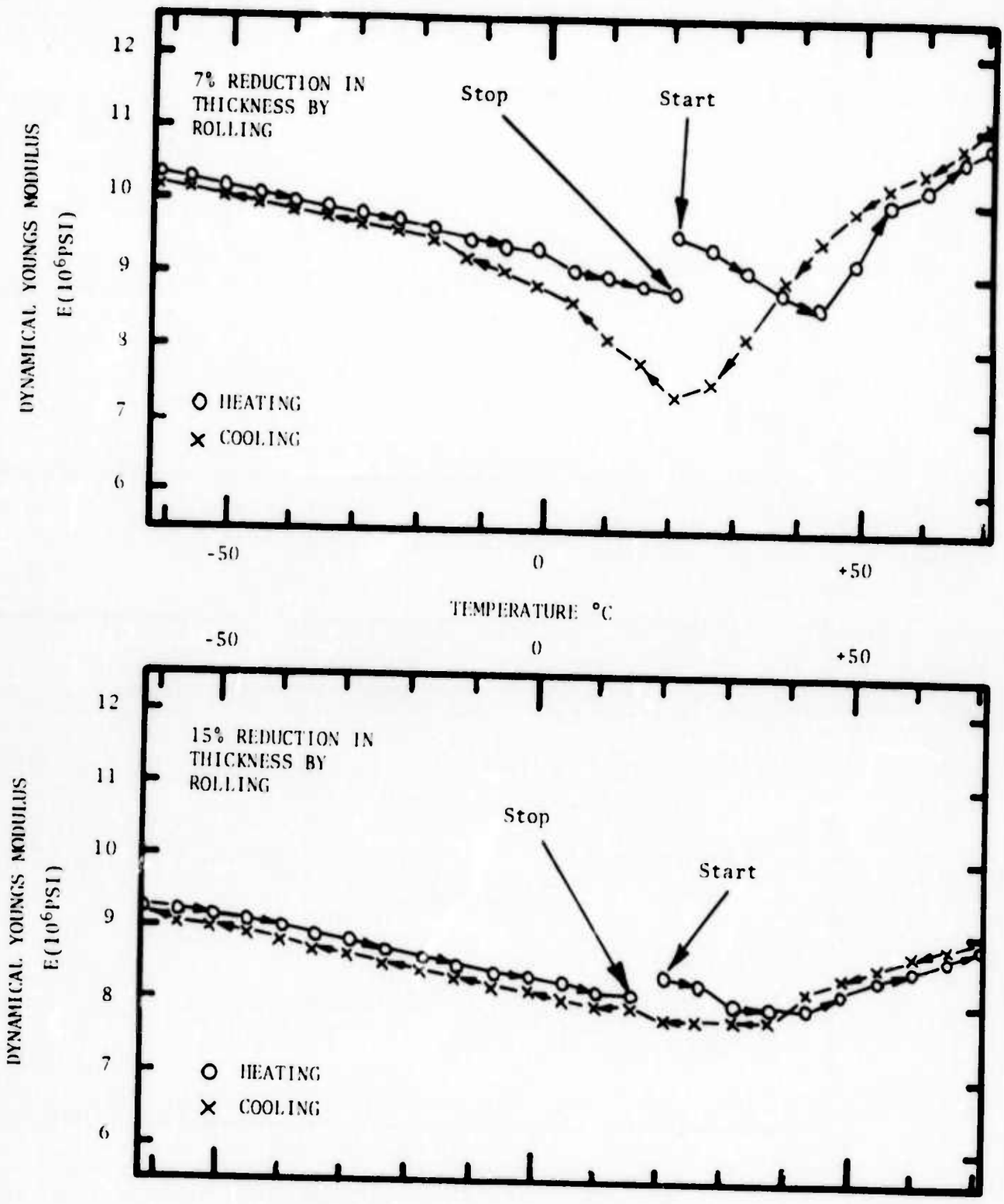

Figure 46. Dynamical Youngs Modulus vs. Temperature for 55 w/o Ni-45 w/o Ti measured at 155-190 Hertz at a Stress of 2000 psi. Both samples were deformed by rolling prior to 80 cycles between -90°C and +100°C before testing. The final cycle ended by heating from -90°C to 20°C. The M_s is at +17°C.

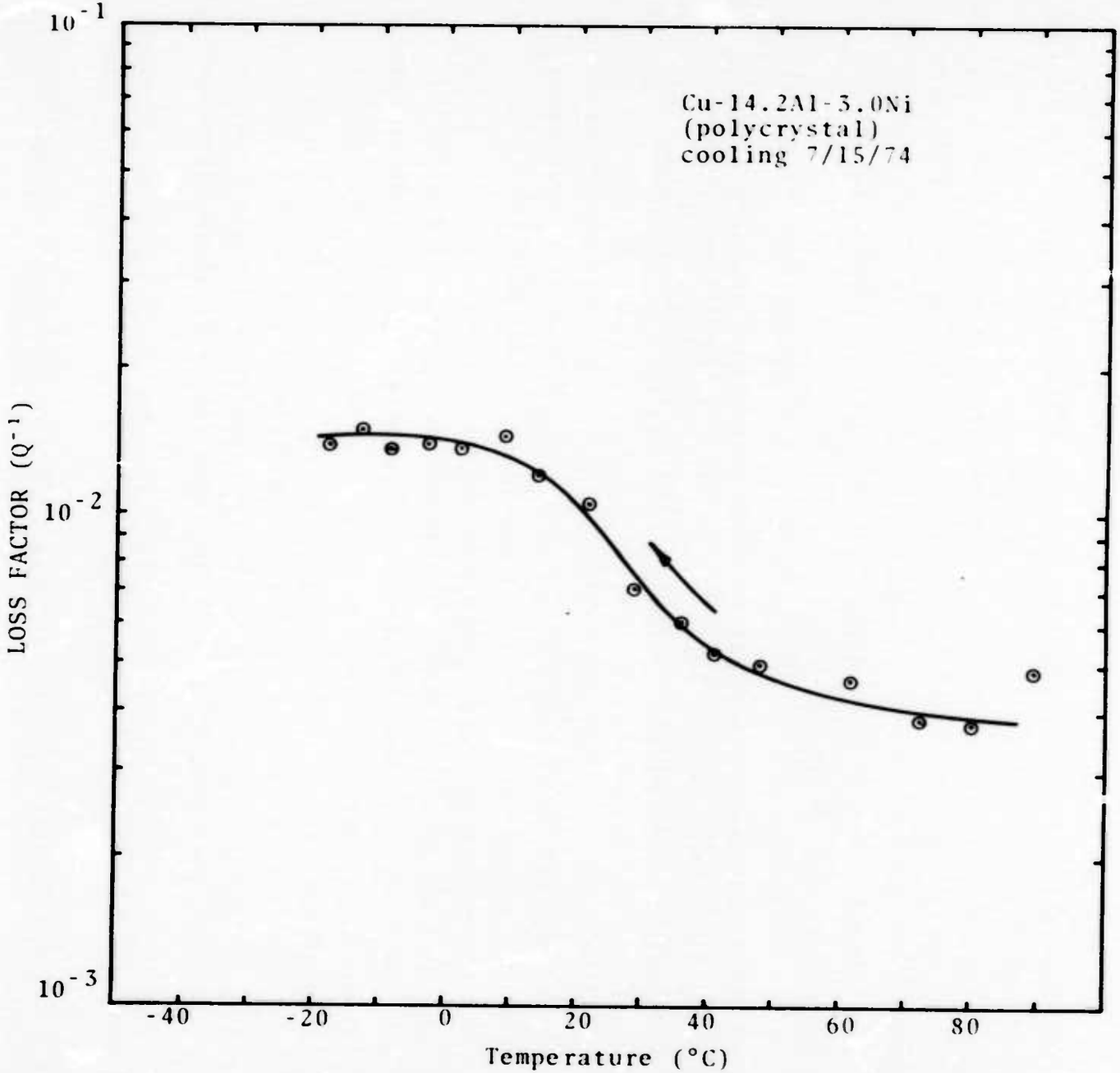

Figure 47. Damping behavior of polycrystalline Cu-14.2 w/o Al-3.0 w/o Ni (thermoelastic alloy).

ture. The complexity of the transformation curves will be better understood after further optical study of the transformations.

Samples of Cu-14.0Al-3.0Ni single crystals have been polished and optically examined. The reported color change has been observed to occur in the transformation of $\beta_1' \rightarrow \gamma_1'$ (β_1 is an ordered BCC phase and is copper-red in color; γ_1' is basically an ordered HCP structure and is a yellowish-gold in color). A sample of the β_1 (parent) phase was transformed under an optical microscope by adding liquid nitrogen to the glass dish holding the sample. The martensite phase was seen to grow into the parent phase in a slow (thermoelastic) manner. The martensite plates were seen to retract in a similar manner when the sample was reheated above A_s. A thermal recycling of the $\beta_1 \rightarrow \gamma_1'$ transformation indicated that the microstructure did not have a "memory." The lack of a "microstructural memory" may be due to the rapid and erratic manner in which the sample was thermally cycled.

In order to gain some idea of possible mechanisms which contribute to high damping in the thermoelastic alloys, a simple stressing device was constructed. A Cu-Al-Ni sample was stressed about 200 psi in compression and observed simultaneously under a low-power light microscope. As the sample was stressed, twins could be seen to appear and to increase in length and number as the stress was increased. These same twins disappeared immediately upon the release of the stress. The interface between the γ_1' martensite and the β_1 parent phase was allowed to move upon the application of an applied stress. The amount of γ_1' increased with the applied stress. After the stress was removed, the $\gamma_1' \rightarrow \beta_1$ interface retracted slightly, but did not fully recover its original unstressed position.

Figures 48 and 49 show the results of Loss Factor and Dynamic Modulus versus temperature measurements on single crystal samples of the Cu-Al-Ni alloy. The loss factor is quite high below the M_s temperature. However, the alloy exhibits a very low modulus and the loss factor drops off rapidly above +50°C.

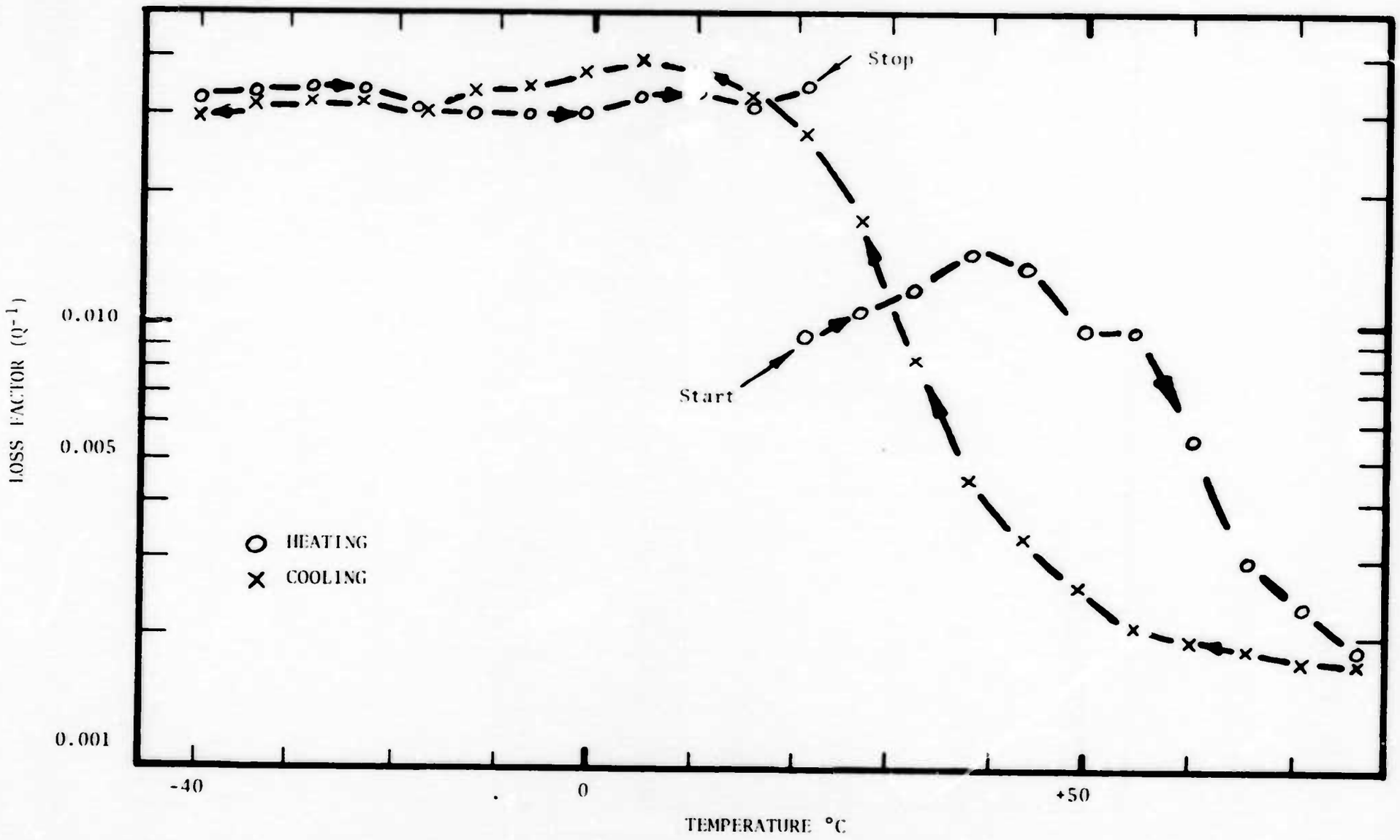

Figure 48. Loss Factor vs. Temperature Curve for a Single Crystal Sample of Cu-14.2 w/o Al-3.0 w/o Ni measured at 115-150 Hertz and a stress of 2000 psi. The M_S temperature for this material is approximately +10°C.

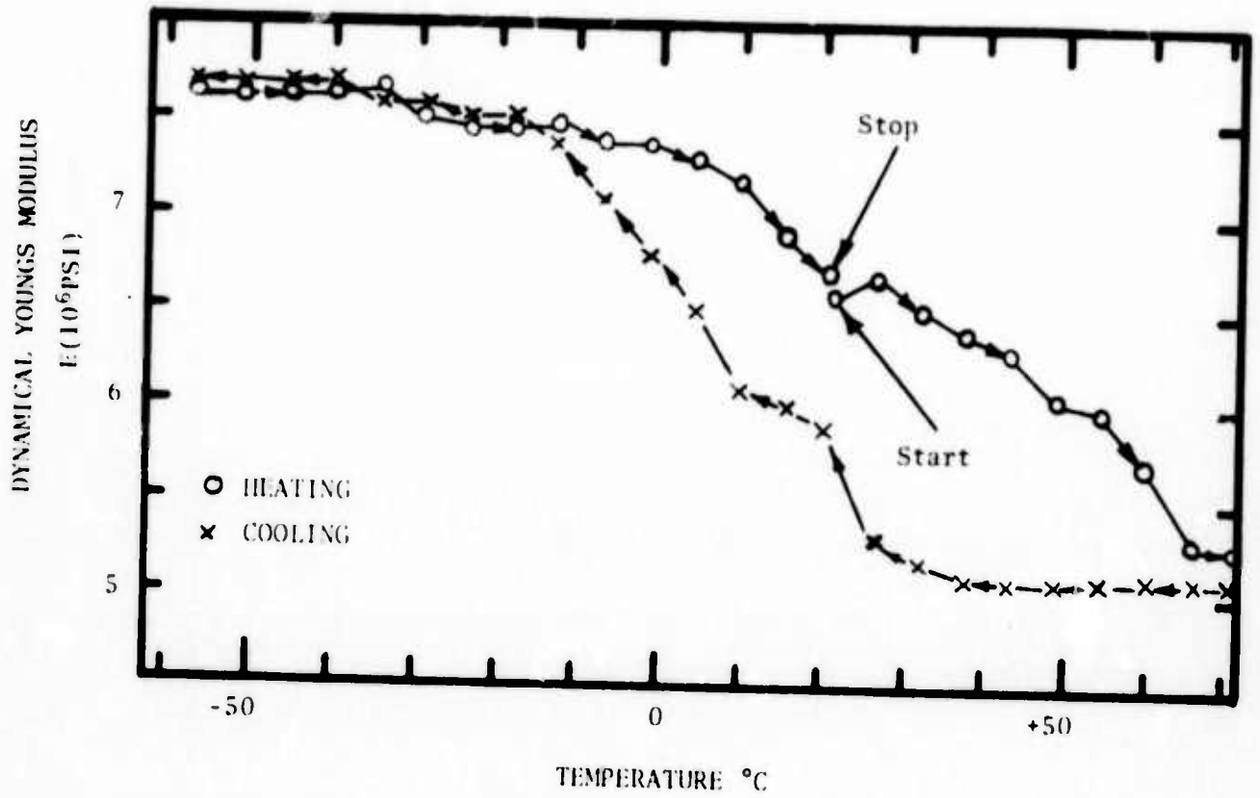

Figure 49. Dynamical Youngs Modulus vs. Temperature Curve for a Single Crystal Sample of Cu-14.2 w/o Al-3.0 w/o Ni measured at 115-150 Hertz. The M_s temperature for this material is approximately +10°C.

IV. MEASUREMENT OF THE DAMPING BEHAVIOR AND STRENGTH OF NICKEL AND SEVERAL COBALT BASE ALLOYS

In order to evaluate relative damping behavior of nickel and the cobalt base alloys discussed by Cochardt as compared with the 55 w/o Ni-45 w/o Ti alloy discussed in Sections II and III, measurements of the loss factor of a 70 w/o Co-30 w/o Ni alloy and a sample of pure nickel were carried out. The results for the 70 w/o Co-30 w/o Ni sample are shown in Figure 50. The sample has a very flat damping curve and there seems to be no large change in damping even above the M_s temperature which occurs at about 30°C (13). Figure 51 shows the results of the damping test on pure (approximately 99.9%) Ni. From other work done on Ni (14) and CoNi alloys (9) it appears that a significant amount of the damping in these materials is due to magnetic damping (i.e. from magnetic domain motion), however in several of these alloys there is a martensitic phase transformation (from fcc to hcp) and it is of considerable interest to determine if a material can be developed which would produce damping by both magnetic domain motion and by thermoelastic martensite formation.

One method for attaining these features simultaneously is to consider the fcc/hcp transformations in cobalt rich Co-Ni alloys like the 70 w/o Co-30 w/o Ni discussed above. This alloy has a very high magnetic Curie Point and a fcc/hcp transition near room temperature. This alloy was one evaluated by Cochardt, who reported a logarithmic decrement at 25°C, a frequency of one cycle/sec, and a stress of 2000 psi for a 65 w/o Co-35 w/o Ni alloy of 0.18. The logarithmic decrement is the product of π times Q^{-1}. Thus

$$\zeta = \pi Q^{-1} \tag{1}$$

and if ζ=0.18 then $Q^{-1} \approx 0.06$. This value is approximately fifteen times larger than the value shown in Figure 50. However, the latter values were observed at 200 Hertz (200 cycles/sec) and 2000 psi rather than 1 cycle/sec and 2000 psi stress. Cochardt also

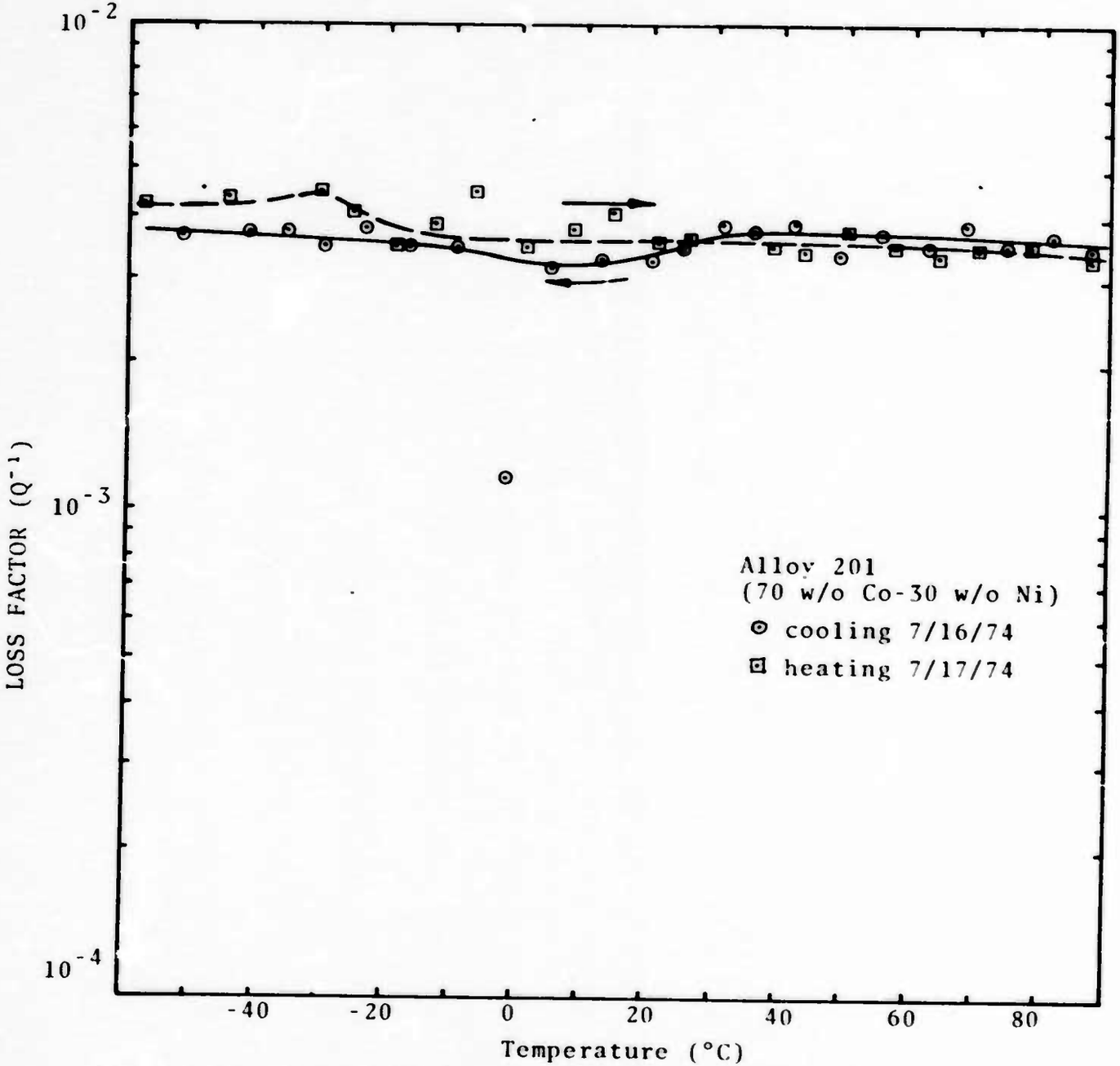

Figure 50. Damping behavior of alloy 201 (70 w/o Co-30 w/o Ni).

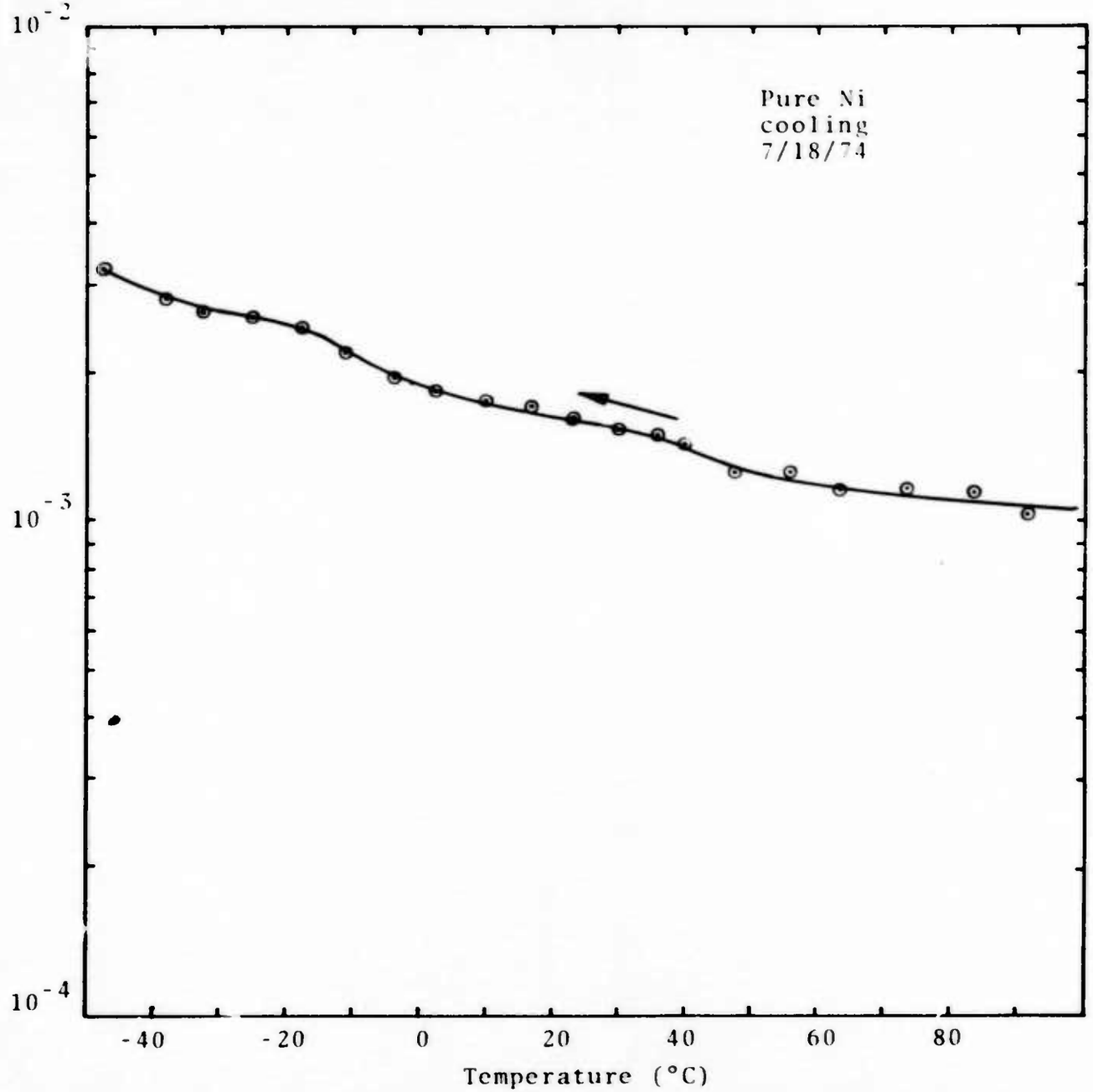

Figure 51. Damping behavior of pure nickel (approximately 99.9%).

reported on a 80 w/o Co-20 w/o Fe alloy which exhibited ζ=0.09 (i.e. Q^{-1}=0.03) at 1 cycle/sec and 2000 psi and 25°C. This alloy also exhibits a high Curie temperature. However, in the condition as fabricated by Cochardt (9), this alloy was a stable bcc structure which was probably ordered with no chance for transformation. The processing sequence followed by Cochardt called for homogenization at 1100°C for two hours. Figure 52 shows that the alloy was in the fcc field at this temperature (1373°K). Subsequently the alloy was annealed for two hours at 900°C (1173°K). Figure 52 shows that at this temperature the alloy was still in the stable fcc field but just about to enter the two phase fcc+bcc field. The final step in the processing sequence employed by Cochardt was a slow cool to room temperature at the rate of 120°C/hour. During this treatment the sample enters the region where the bcc phase is stable and coexists with a fcc phase enriched in cobalt. In addition, the bcc orders below 800°K as is seen in Figure 52. Unfortunately Cochardt did not discuss the structure of his 80Co-20Fe alloy. However, based on his heat treatment schedule, it is likely that his alloy was largely bcc.

Figure 52 shows a curve labeled $T_o^{FCC/BCC}$ which describes the locus of points along which the fcc and bcc Co-Fe alloys have equal free energies. This curve has been computed using a thermochemical description of the fcc and bcc phases derived earlier. Figure 53 shows the free energy difference between the fcc and disordered bcc phases as a function of temperature and composition. The curve labeled $\Delta F^{BCC \rightarrow FCC}$=0 is the same as that shown in Figure 52. The remaining curves show the locus of points corresponding to various free energy differences between disordered fcc and bcc phases. As the free energy difference becomes larger, the bcc becomes more stable relative to the fcc phase for a given composition. In the case of iron base alloys (i.e. Fe-Ni and Fe-C alloys), the fcc phase can be retained by rapid cooling until the "driving force" for transformation to the bcc form reaches the vicinity of 300 cal/g.at. (i.e. the free energy of the bcc phase is 300cal/g.at.

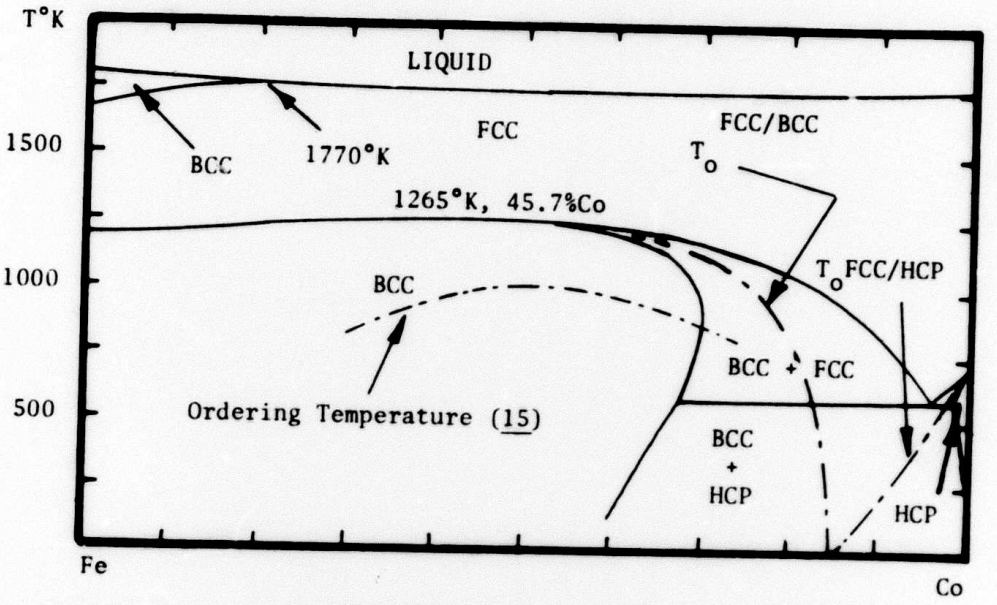

Figure 52. Calculated Iron-Cobalt Phase Diagram Showing Locus of Curve for T_o(FCC/BCC) where FCC and BCC Phases of Same Composition Have Equal Free Energies (10,15).

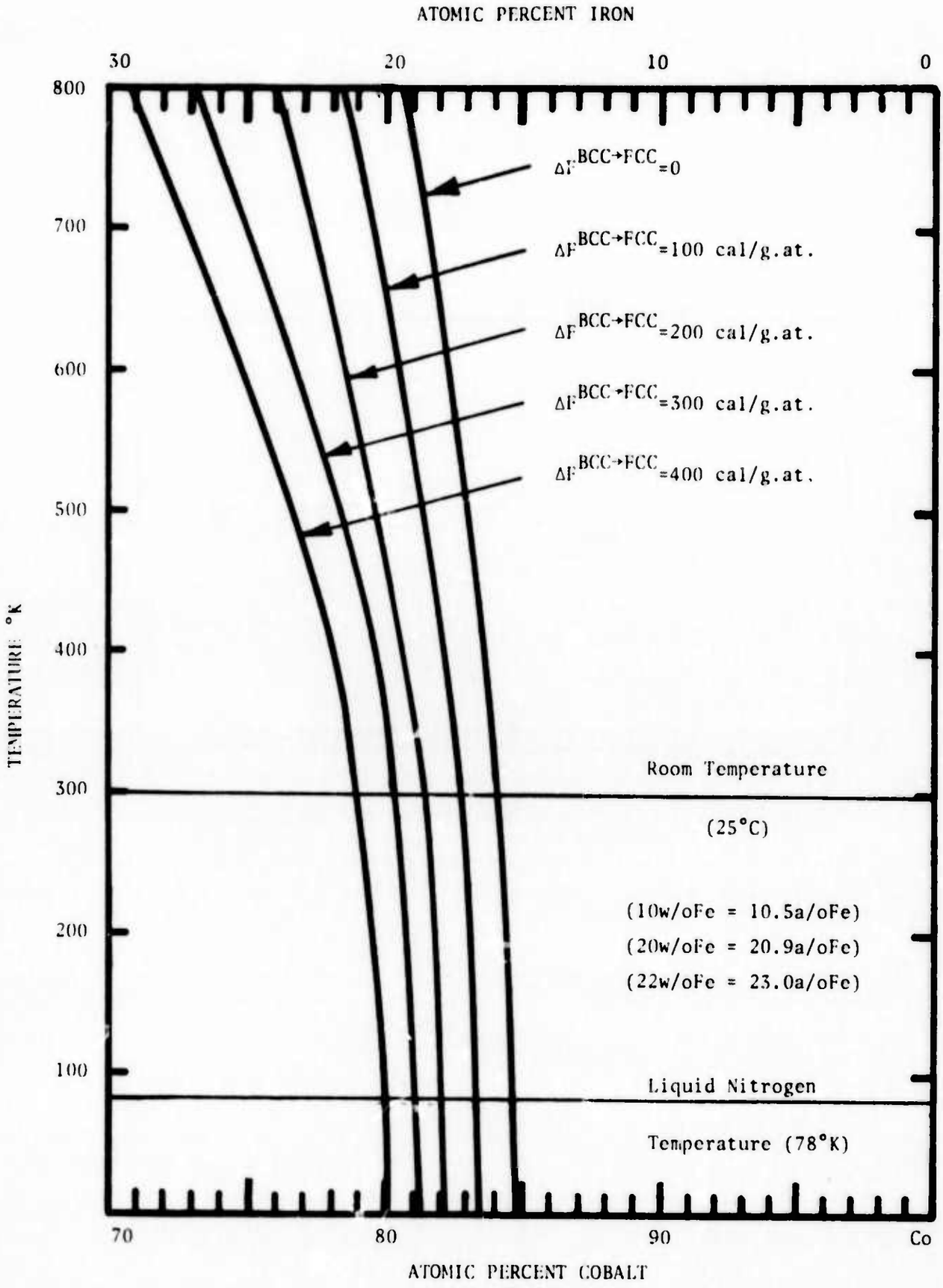

Figure 53. Calculated Temperature and Composition of the Free Energy Difference between FCC and BCC Iron Cobalt Alloys.

less than the fcc phase). Figure 53 suggests that this situation should prevail at room temperature in an alloy with 80 a/o Co-20 a/o Fe (80.9 w/o Co-19.1 w/o Fe). Alloys containing less than 20 a/o Fe could be expected to remain fcc while alloys with greater than 20 a/o (19.1 w/o) Fe would be expected to transform to the bcc phase on cooling from 1000°C. In order to test this prediction, a series of cobalt-iron alloys was prepared and air cooled from 1000°C. Figures 54-57 show the resulting microstructures. The first two photomicrographs show typical austenitic fcc structures obtained by air cooling the 82 w/o Co-18 w/o Fe and 90 w/o Co-10 w/o Fe alloys. On the other hand, Figure 56 shows the martensitic bcc structure obtained on air cooling the 78 w/o Co-22 w/o Fe alloy. The crystal structure of these alloys was verified by X-ray diffraction using CrKα radiation. Inclusions shown in Figures 54-57 are oxide particles which are present in the Ferrovac E iron used to make the alloy by combination with electrolytic cobalt.

Figure 57 shows the microstructure of the 80 w/o Co-20 w/o Fe alloy which contained some surface martensite formed during the polishing. This was established by annealing the specimen at 1000°C, air cooling it and taking an X-ray pattern from the surface without polishing. This pattern showed no bcc diffraction lines. However, polishing the surface produced strong bcc peaks. This result suggests that the 20 w/o Fe alloy (19.1 a/o Fe) is close to transforming at room temperature. This result is in keeping with the predictions of Figure 53.

An attempt was made to produce martensite in this alloy by cooling it in liquid nitrogen (i.e. to 77°K). However, no bcc phase formed. This may be due to the steep free energy difference versus temperature curve which does not yield very many more cal/g.at. of driving force as the temperature is lowered from 300°K to 77°K.

The results shown in Figures 54-57 are in keeping with earlier studies of the Co-Fe system (16-18) which showed a lowering of the fcc/hcp transition temperature of cobalt by the addition

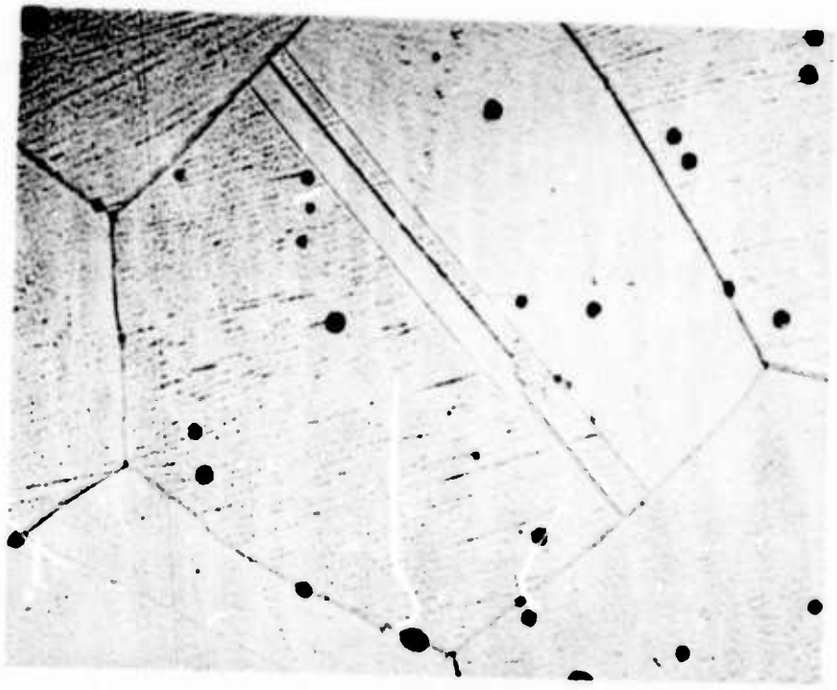

Plate No.
10486

Figure 54. 82 w/o Co-18 w/o Fe Alloy Annealed at 1000°C Air Cooled to 25°C. Etched in 5% Nital. Photomicrograph Shows Twinned Austenitic Structure (X1000).

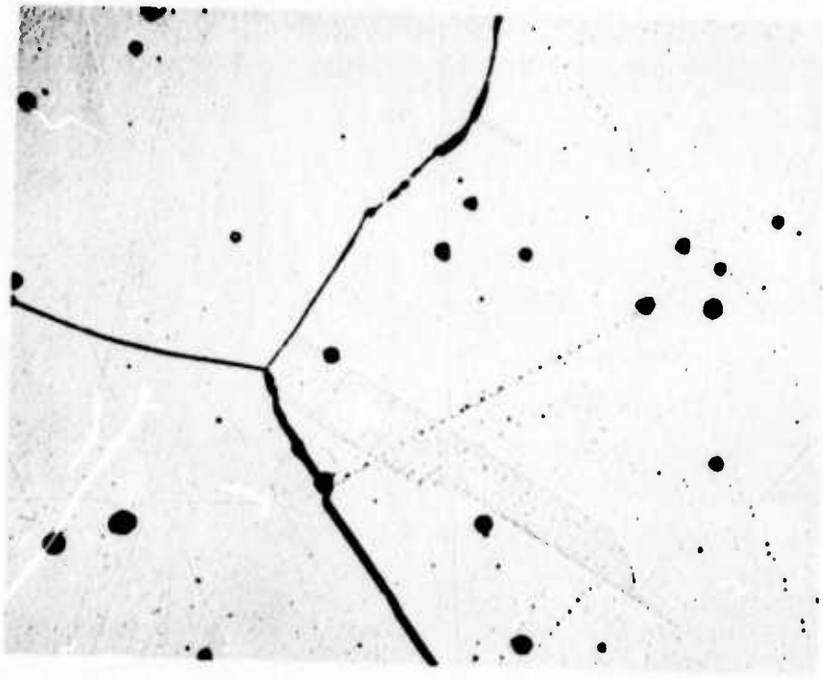

Plate No.
10489

Figure 55. 90 w/o Co-10 w/o Fe Alloy Annealed at 1000°C Air Cooled to 25°C. Etched in 5% Nital. Photomicrograph Shows Twinned Austenitic Structure (X1000).

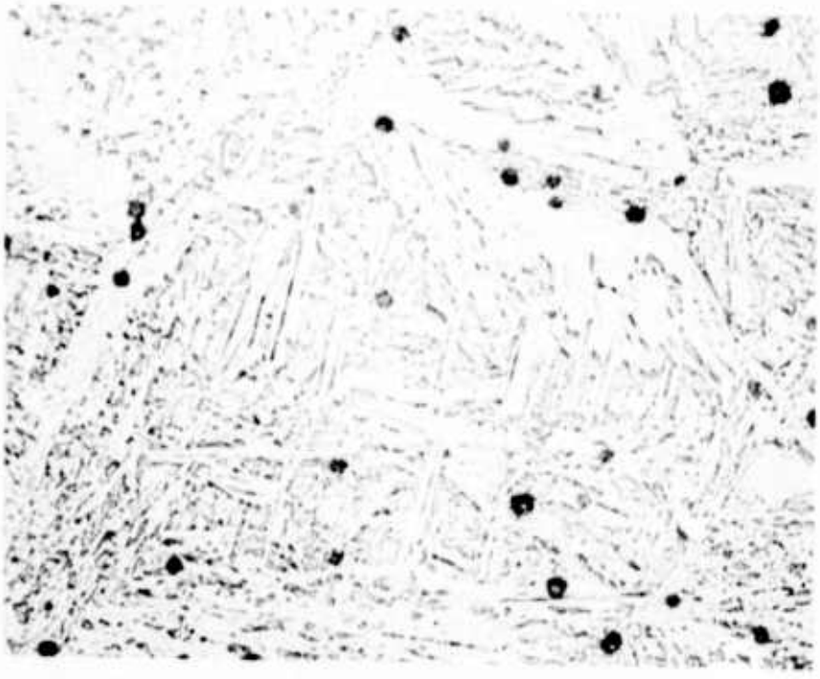

Plate No.
10483

Figure 56. 78 w/o Co-22 w/o Fe Alloy Annealed at 1000°C Air Cooled to 25°C. Etched in 5% Nital. Photomicrograph Shows Structure of BCC Phase (X1000).

Plate No.
10484

Figure 57. 80 w/o Co-20 w/o Fe Alloy Annealed at 1000°C Air Cooled to 25°C. Etched in 5% Nital. Central Grain Shows Surface Martensite (BCC) Formed during Polishing in an Austenite (FCC) Matrix (X1000).

of iron. Addition of 5 a/o Fe to cobalt reduced T_o from 733°K to 500°K (17,18). Alloys with 7.5, 10.0, 12.5 and 15 a/o Fe cooled to 25°C (248°K) by water quenching after two hours at 1100°C were found to be completely fcc (16). Plastic deformation in Liquid nitrogen by hammering to effect a 17% deformation produced hexagonal phase in the 7.5 a/o Fe alloy and some bcc phase in the 15 a/o alloy. However the 10.0 and 12.5 a/o Fe alloys were found to remain fcc.

Thus, the series of Co-Fe alloys shown in Figures 54 and 57 with 18 and 20 w/o iron fall in exactly the range required to test the hypothesis, i.e. that high damping could be attained in a metastable phase with a high magnetic Curie point. The Curie point for the fcc appears to be near 950°C (1223°K)(18).

Accordingly, a series of "resonant dwell damping" bars were fabricated from alloys in this series and tested at 25°C along with an additional set of alloys at a stress level near 2000 psi. The geometry of the samples resulted in natural frequencies in the 190-270 Hertz range. The results for the original set of samples are shown in Table 1. This group of samples labeled 51-64 were prepared by annealing alloy stock, machining the damping bars and then making the measurements.

Subsequently, the damping bars were X-rayed. It was found that samples 57, 58, 59 and 60 (i.e. 80 w/o Co-20 w/o Fe and 82 w/o Co-18 w/o Fe) exhibited fcc and bcc diffraction lines. This was apparently due to the surface deformation which occurred during machining. Consequently, these four samples were reannealed at 1000°C and oil quenched. These samples yielded completely fcc X-ray patterns. Subsequent measurement of the loss factor yielded values of 280 to 500 x 10^{-4} as shown by samples 57A, 58A, 59A and 60A in Table 1. Following this experience, the remainder of samples 51-64 were reannealed and oil quenched and the loss factor at 25°C measured once again. The results are shown in Table 2. The reannealing did not affect the loss factors of the 78 w/o Co-22 w/o Fe samples very much. These were 14 and

TABLE 1

SUMMARY OF RESONANT DWELL DAMPING MEASUREMENTS AT 25°C

Sample No. Composition (weight percent)	Resonant Frequency (Hz.)	Dynamical Youngs Modulus ($PSIx10^{-6}$)	Peak Stress (PSI)	Loss Factor ($Q^{-1}x10^{4}$)	Comments on Test
51(70Co-30Ni)	265	28.0	2190	66	All Samples
52(47.2Fe-52.8Pt)	185	15.7	1290	28	Annealed at
53(47.2Fe-52.8Pt)	214	19.2	1660	25	1000°C--Air
54(46.2Fe-53.8Pt)	191	14.7	1290	69	Cooled--Then
55(78.0Co-22.0Fe)	259	26.6	2050	14	Machined
56(78.0Co-22.0Fe)	251	26.3	1980	16	"
57(80.0Co-20.0Fe)	237	24.2	1790	92	"
58(80.0Co-20.0Fe)	251	24.3	1900	68	"
59(82.0Co-18.0Fe)	245	23.1	1800	81	"
60(82.0Co-18.0Fe)	237	22.8	1740	64	"
61(90.0Co-10.0Fe)	264	27.8	2140	8	"
62(90.0Co-10.0Fe)	264	28.1	2140	14	"
63(65Co-28Fe-7Ni)	240	23.2	1770	17	"
64(70Fe-20Co-10Cr)	276	29.9	2410	6	"
57A(80.0Co-20.0Fe)	238	24.4	1810	280	All Samples
58A(80.0Co-20.0Fe)	243	25.5	1990	450	Annealed at
59A(82.0Co-18.0Fe)	236	21.4	1670	480	1000°C and
60A(82.0Co-18.0Fe)	242	23.8	1810	500	Oil Quenched

TABLE 2

SUMMARY OF RESONANT DWELL DAMPING MEASUREMENTS AT 25°C

Sample No. Composition (weight percent)	Resonant Frequency (Hz.)	Dynamical Youngs Modulus ($PSI \times 10^{-6}$)	Peak Stress (PSI)	Loss Factor ($Q^{-1} \times 10^{4}$)	Comments on Test
55A(78.0Co-22.0Fe)	253	25.4	1960	20	All Samples
56A(78.0Co-22.0Fe)	252	26.5	2000	13	Annealed at
61A(90.0Co-10.0Fe)	266	28.2	2170	7	1000°C--Then
62A(90.0Co-10.0Fe)	272	29.8	2270	7	Oil Quenched
63A(65Co-28Fe-7Ni)	244	24.0	1830	28	"
72A(79.0Co-21.0Fe)	249	24.3	1900	19	"
73A(79.0Co-21.0Fe)	264	27.8	2140	10	"
75A(80.0Co-20.0Fe)	249	24.3	1900	24	"
76A(80.0Co-20.0Fe)	251	26.3	1980	274	"
77C(81.0Co-19.0Fe)	232	21.2	2000	11	Machined in 33%
78C(80.5Co-19.5Fe)	248	24.3	2000	12	Cold Worked Condition
79 NIVCO	275	28.3	2000	14	As Received from
79 NIVCO	272	28.2	5000	26	Westinghouse
80C(81.5Co-18.5Fe)	245	23.1	2000	12	Machined--Cold Worked
73B(79.0Co-21.0Fe)	263	27.0	2100	9	Annealed--Water Quench
77A(81.0Co-19.0Fe)	257	24.8	2000	31	Annealed 1000°C--Then
78A(80.5Co-19.5Fe)	248	24.4	2000	320	Oil Quenched
80A(81.5Co-18.5Fe)	247	24.3	2000	110	"

16 x 10^{-4} (Numbers 55 and 56) before the reannealing and 20 and 13 x 10^{-4} (Numbers 55A and 56A) after reannealing. The diffraction patterns both showed substantial quantities of the bcc phase. Similarly, the reannealing had little effect on the 90 w/o Co-10 w/o Fe alloys. Thus samples 61 and 62 exhibited Q^{-1} = 8 and 14 x 10^{-4} before reannealing and 7 and 7 x 10^{-4} after annealing. Both sets of X-ray patterns showed completely fcc structures. Thus the results show a marked peak in the loss factor in the vicinity of 80 w/o Co-20 w/o Fe providing the alloy is all fcc. This is not dependent on the magnetic Curie temperature since both the fcc and bcc phases have high Curie temperatures which are near 1000°C.

Table 2 shows additional results for other Co-Fe alloys with compositions in the vicinity of 80 w/o Co-20 w/o Fe which were made and tested in order to establish the effects of composition, structure and degree of cold work on the loss factor. These preliminary results show that the high damping behavior can be reproduced in other alloys but it is eliminated by cold work. This work is proceeding in order to establish the processing limits for obtaining high loss factors.

Table 2 also contains the results of damping tests on NIVCO, which is a commercial alloy developed by Cochardt at Westinghouse (20). It was kindly furnished by Dr. Lou Willertz of Westinghouse Research Laboratories. According to Cochardt's description, NIVCO is 72 w/o Co-23 w/o Ni and the balance titanium and aluminum which are added to provide strength by precipitation hardening. Cochardt reports values of the logarithmic decrement of 0.02 and 0.05 at room temperature for this alloy at shear stresses of 2000 psi and 5000 psi (Figure 1 of Reference 20). Since Q^{-1} is equal to the decrement divided by π, Cochardt's results would correspond to loss factors of 0.007 and 0.017 or 70 x 10^{-4} and 170 x 10^{-4} respectively at 25°C and stresses of 2000 psi and 5000 psi. These values are much higher than those shown in Table 2. The values measured in the present tests, i.e. 14x10^{-4}

at 2000 psi and 26 x 10^{-4} at 5000 psi, are five times smaller than Cochardt's results. The main difference is that the frequency of the present measurements at 230-270 Hz is in the audible range while that used by Cochardt was near 1 cycle/sec (1 Hertz).

Thus, the current results indicate that loss factors of Q^{-1} = 500 x 10^{-4} are attainable in the 80 w/o Co-20 w/o Fe alloys which are two to three times higher than observed in nitinol (i.e. 55 w/o Ni-45 w/o Ti) and fifty times higher than NIVCO. Measurements of the loss factor of 80 w/o Co-20 w/o Fe will be carried out between -80°C and +80°C for comparison with the 55 w/o Ni-45 w/o Ti alloy. However, preliminary results show almost no change in the audible "ring" (or lack of "ring") of the alloy at liquid nitrogen or +200°C. Thus it is not anticipated that the Q^{-1} value will decrease significantly in this temperature range.

The other advantages the Co-Fe alloy has in relation to the Ni-Ti alloy are a higher modulus of 25 million psi (Tables 1 and 2) versus 8 million psi and ease of fabrication.

In order to evaluate the strength of the 80 w/o Co-20 w/o Fe composition, a set of tensile bars were fabricated of annealed material. Subsequent tests were expanded to test swaged rod. These were compared with tensile results measured for NIVCO. Figures 58-66 display the results. The 82 w/o Co-18 w/o Fe and 80 w/o Co-20 w/o Fe alloys show reproducible 0.2 percent offset yield strengths of 17000-18000 psi in the annealed condition in Figures 58-62. This is the strength level of the samples which exhibited loss factors of Q^{-1} = 500 x 10^{-4}.

Figures 63-65 show the yield strength obtained for samples of the 18.5 w/o Fe, 19 w/o Fe and 19.5 w/o Fe alloys in a cold worked condition following a 33% reduction in diameter by cold swaging. Reference to Table 2 shows that these alloys exhibited loss factors of 11 to 14 x 10^{-4} in the cold worked condition. Annealing raised the loss factor of the 19.5 w/o Fe sample to 320 x 10^{-4} as shown in Table 2.

Figure 66 shows the results of a tensile test on NIVCO. The measured 0.2 percent yield strength of 108,900 psi is in good

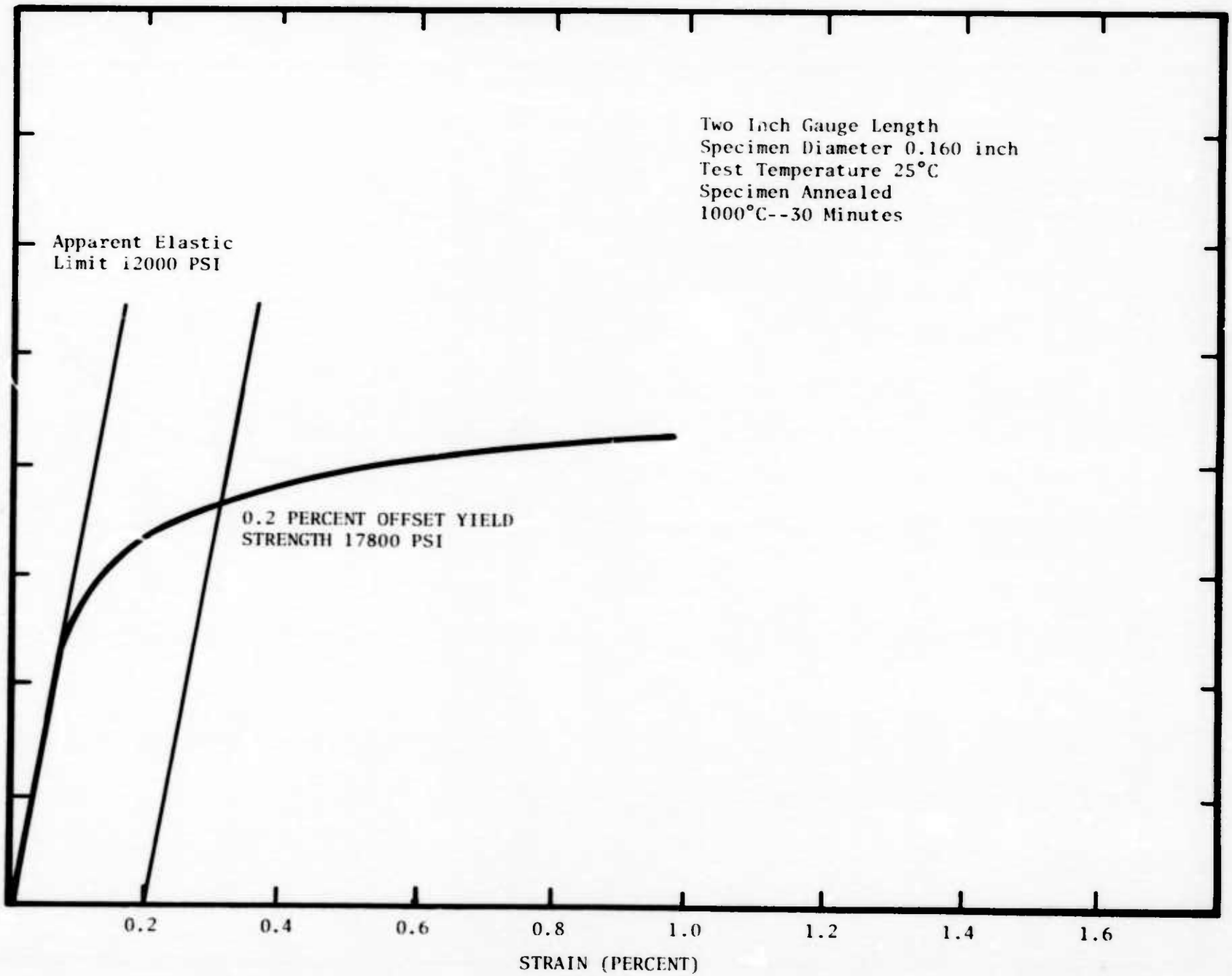

Figure 58. Stress-Strain Curve for a 82%Co-18%Fe Alloy at 25°C.

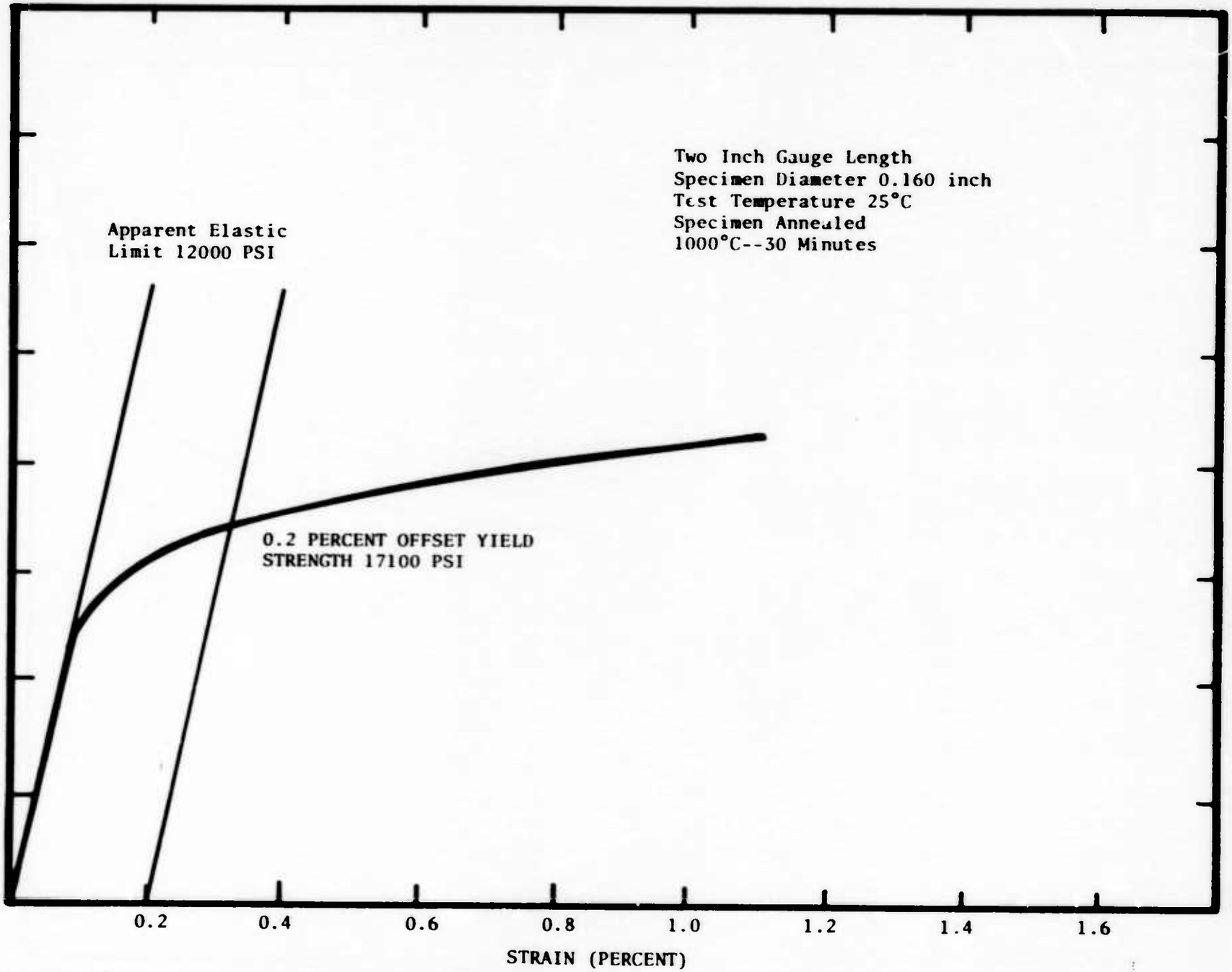

Figure 59. Stress-Strain Curve for a 82%Co-18%Fe Alloy at 25°C.

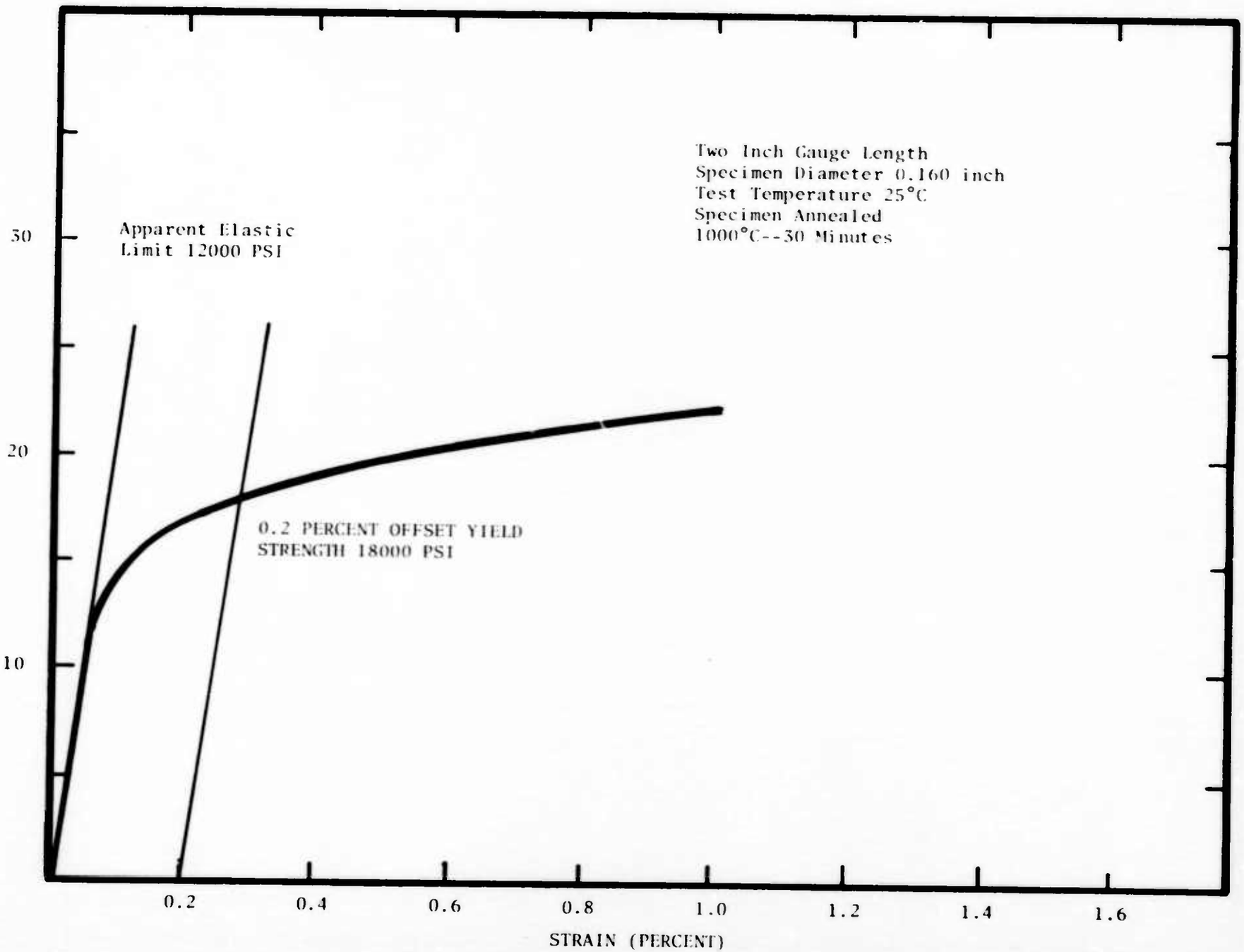

Figure 60. Stress-Strain Curve for a 80%Co-20%Fe Alloy at 25°C.

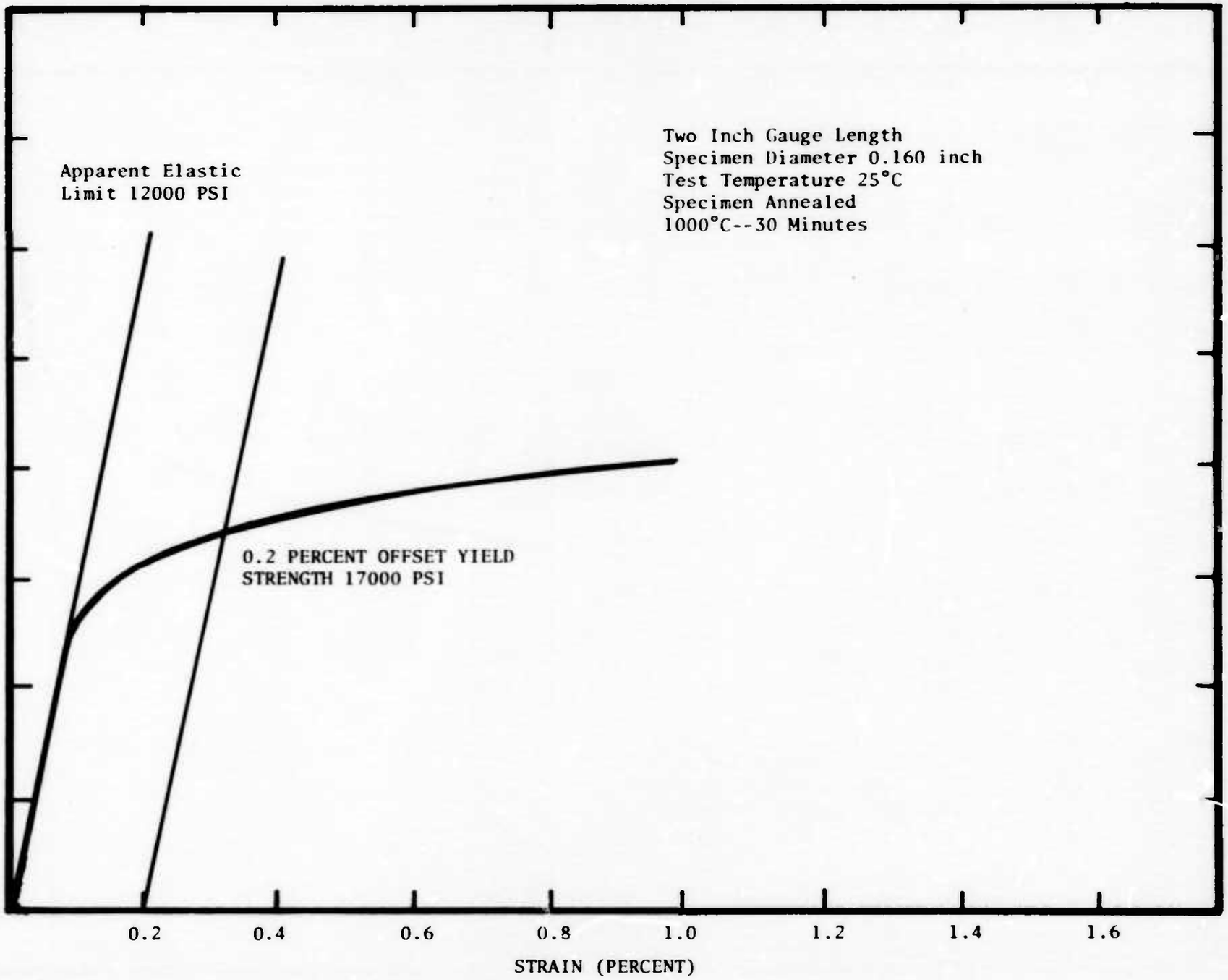

Figure 61. Stress-Strain Curve for a 80%Co-20%Fe Alloy at 25°C.

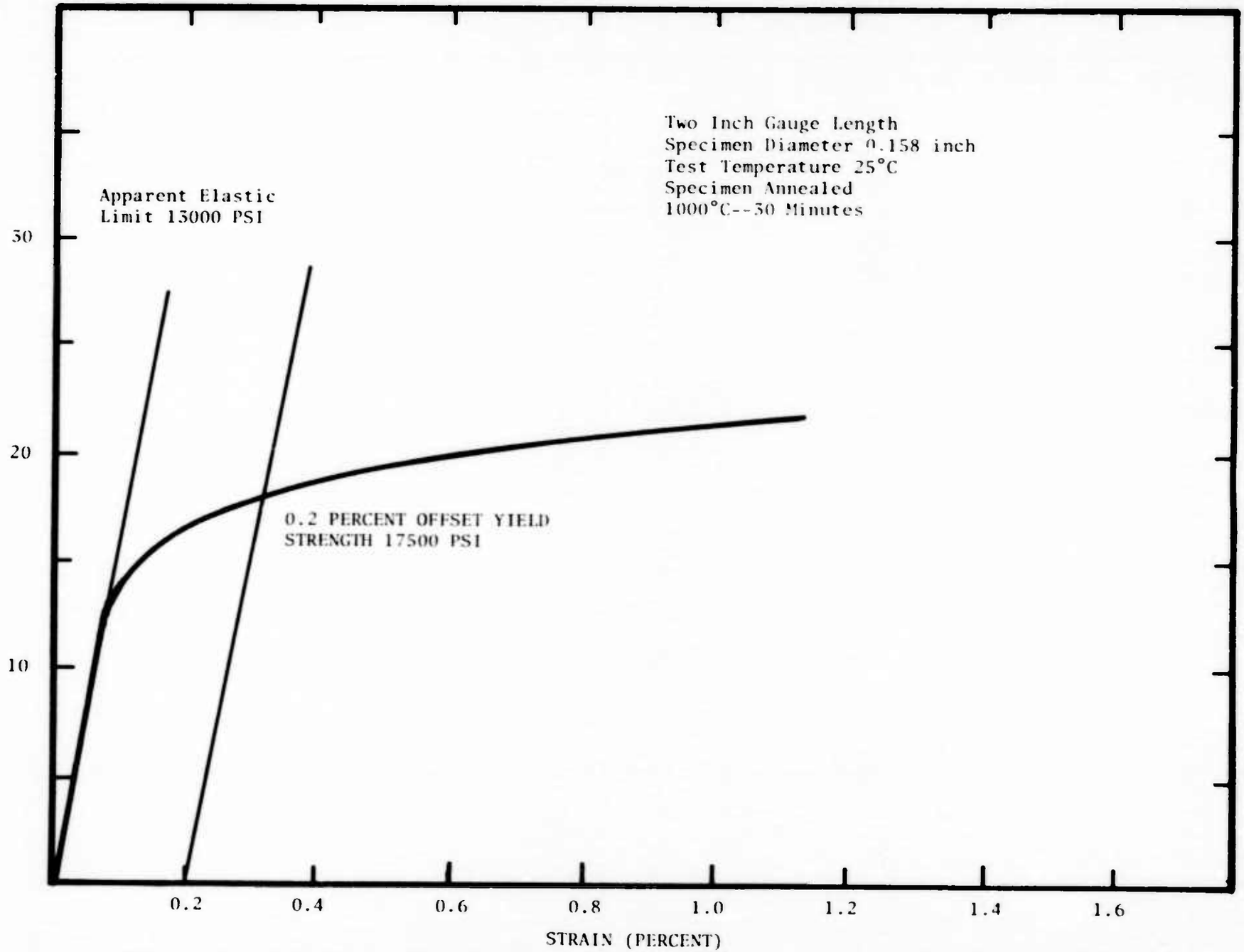

Figure 62. Stress-Strain Curve for a 80%Co-20%Fe Alloy at 25°C.

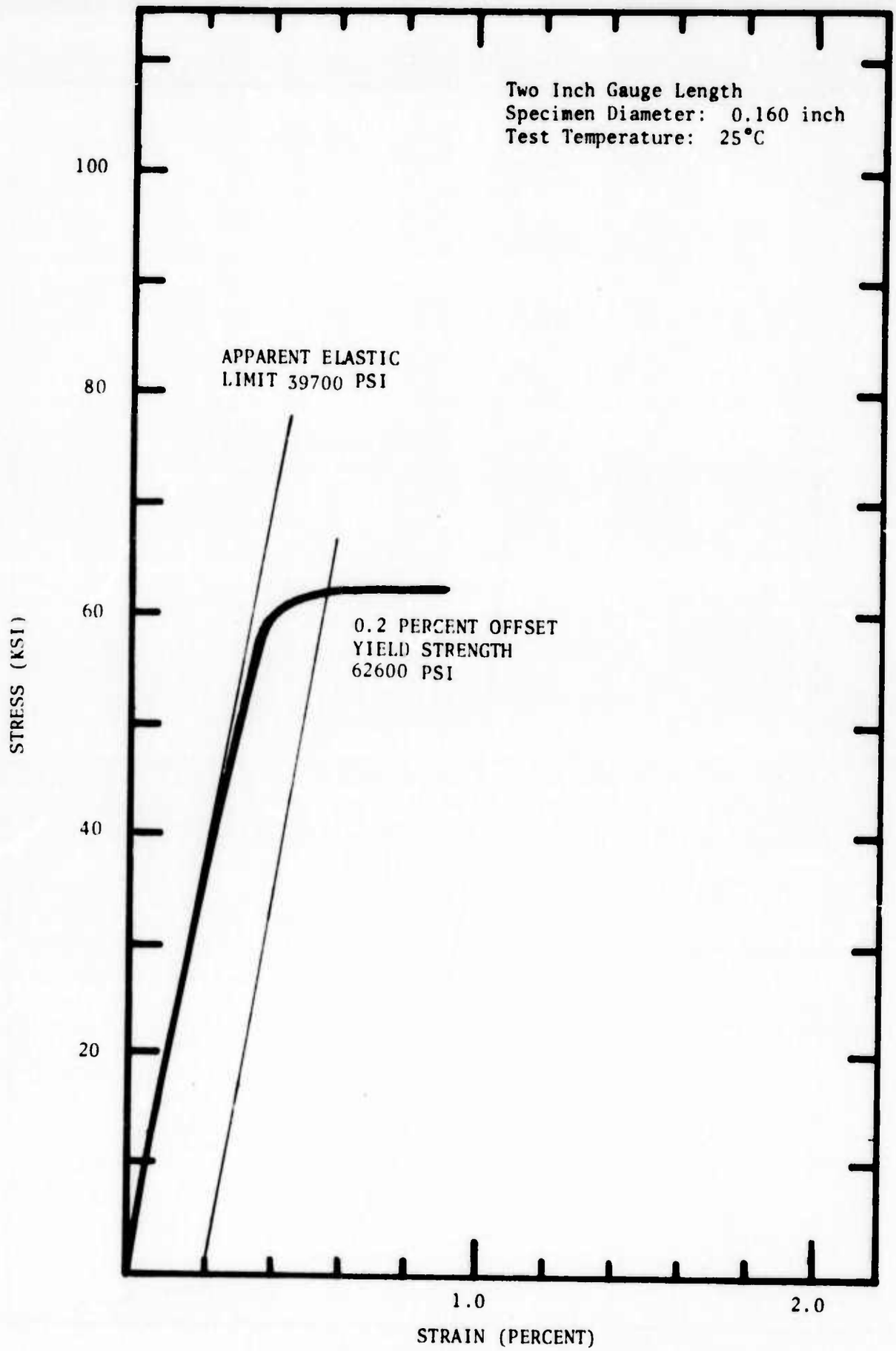

Figure 63. Stress-Strain Curve for a 81.5 w/o Co-18.5 w/o Fe Alloy Tested in the Cold Worked Condition at 25°C. Cold reduction of thirty-three percent (diametral) by swaging.

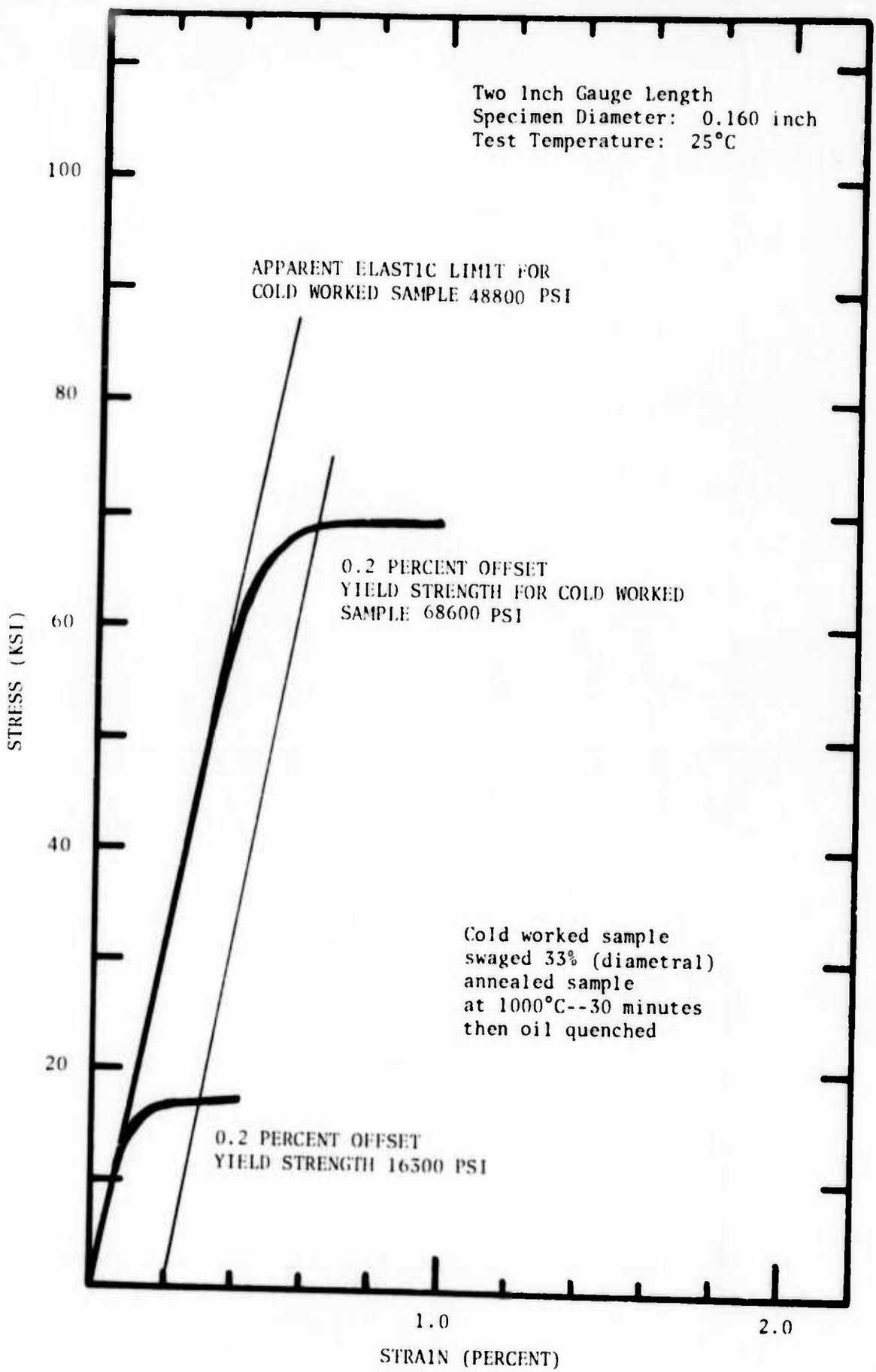

Figure 64. Stress-Strain Curves for 81 w/o Co-19 w/o Fe Alloy in the Cold Worked and Annealed Condition at 25°C.

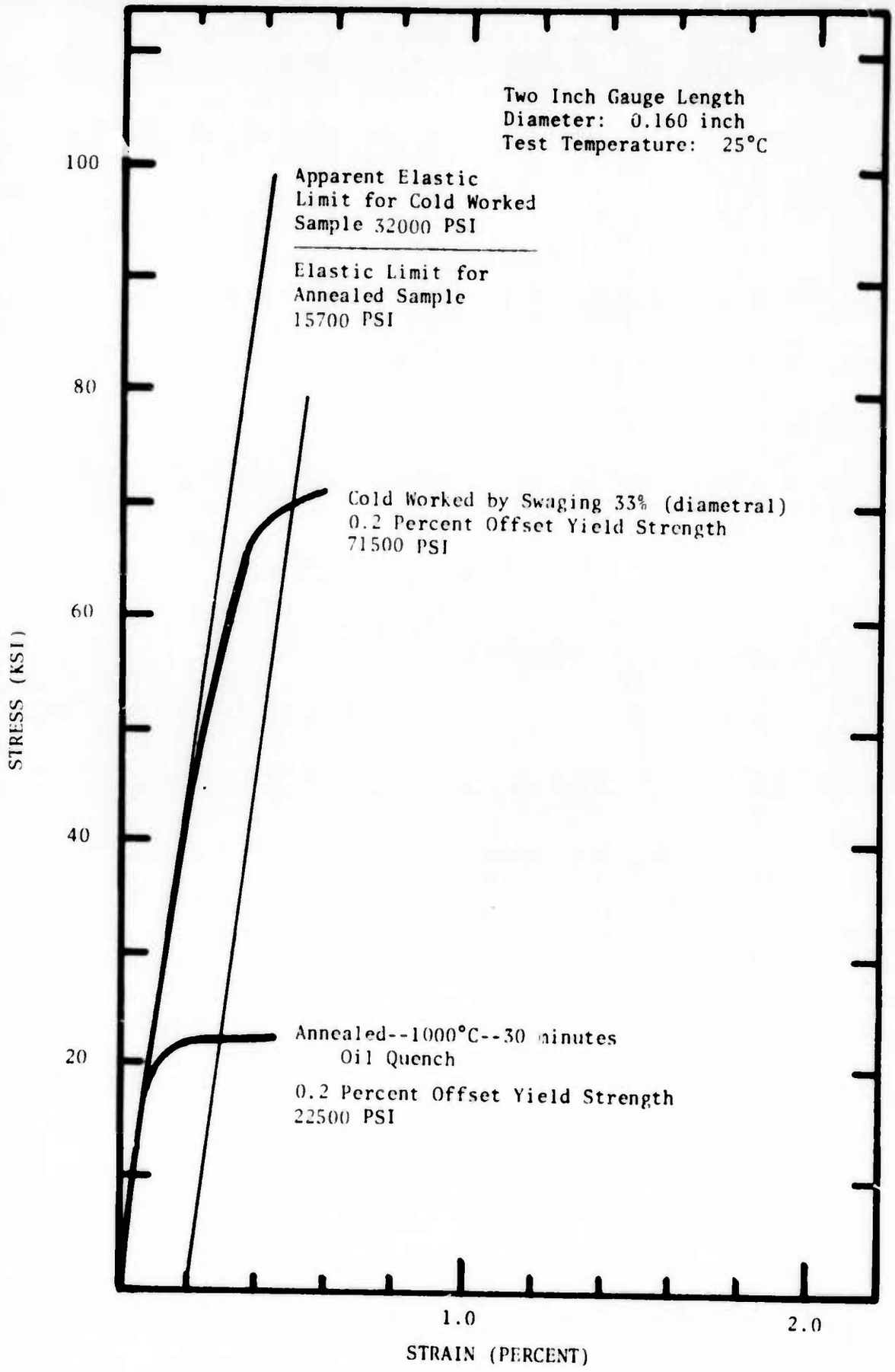

Figure 65. Stress-Strain Curves for 80.5 w/o Co-19.5 w/o Fe Alloy in the Cold Worked and Annealed State at 25°C.

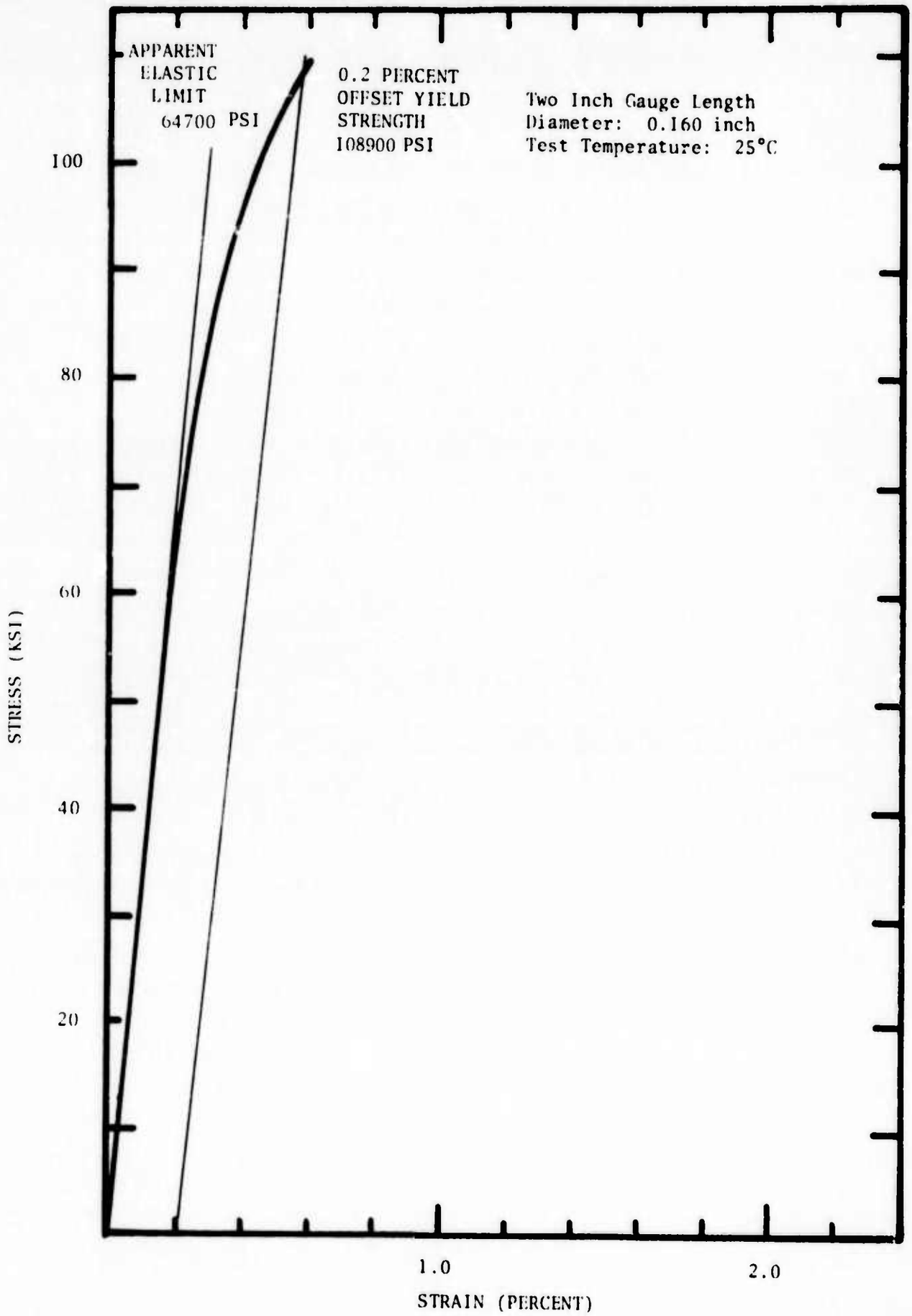

Figure 66. Stress-Strain Curve for NIVCO (Westinghouse) at 25°C.

agreement with Cochardt's reported value of 110,000 psi (20).

These values of the yield strength were combined with the measured loss factors measured at a stress level of 2000 psi in the range 150 to 250 Hz for NIVCO, 80 w/o Co-20 w/o Fe and 55 w/o Ni-45 w/o Ti are compared in Figure 67. The comparison shows the relatively high damping capacity (and low strength) of the Co-Fe alloy to the other two materials. However, it is likely that this shortcoming can be overcome through alloying. For example, the strength of NIVCO is not due to the properties of the 72 w/o Co-23 w/o Ni matrix, which is comparable to the 80 w/o Co-20 w/o Fe material. The strength is due to the presence of precipitates formed by the Al and Ti additions. A similar effect can be expected in the Co-Fe alloy. Another possible source of strengthening is additional solid solution hardening which might be effected by addition of nickel. The nickel additions would be controlled so as to maintain the "metastable condition" of the fcc phase. This is illustrated in Figure 68 which shows the ternary Fe-Ni-Co counterpart of Figure 53 calculated on the basis of the thermochemical description published previously (10).

Figure 68 shows the locus of the $\Delta F^{BCC \rightarrow FCC}=0$ and the $\Delta F^{BCC \rightarrow FCC}=+300$ cal/g.at. curves in the Fe-Ni-Co system at 25°C. These alloys should be metastable in the fcc form at 25°C. If they can be fabricated in this state, they may develop high Q^{-1} values comparable to 80 w/o Co-20 w/o Fe and higher yield strengths than the 17,500 psi level exhibited by the 80/20 Co-Fe alloy. Such a series of alloys is currently being fabricated for evaluation. If this effort produces the desired result, it would also have a beneficial effect on the cost of the alloys since it would increase the iron content of the alloy and substitute nickel for cobalt. Both of these composition changes would lower the cost.

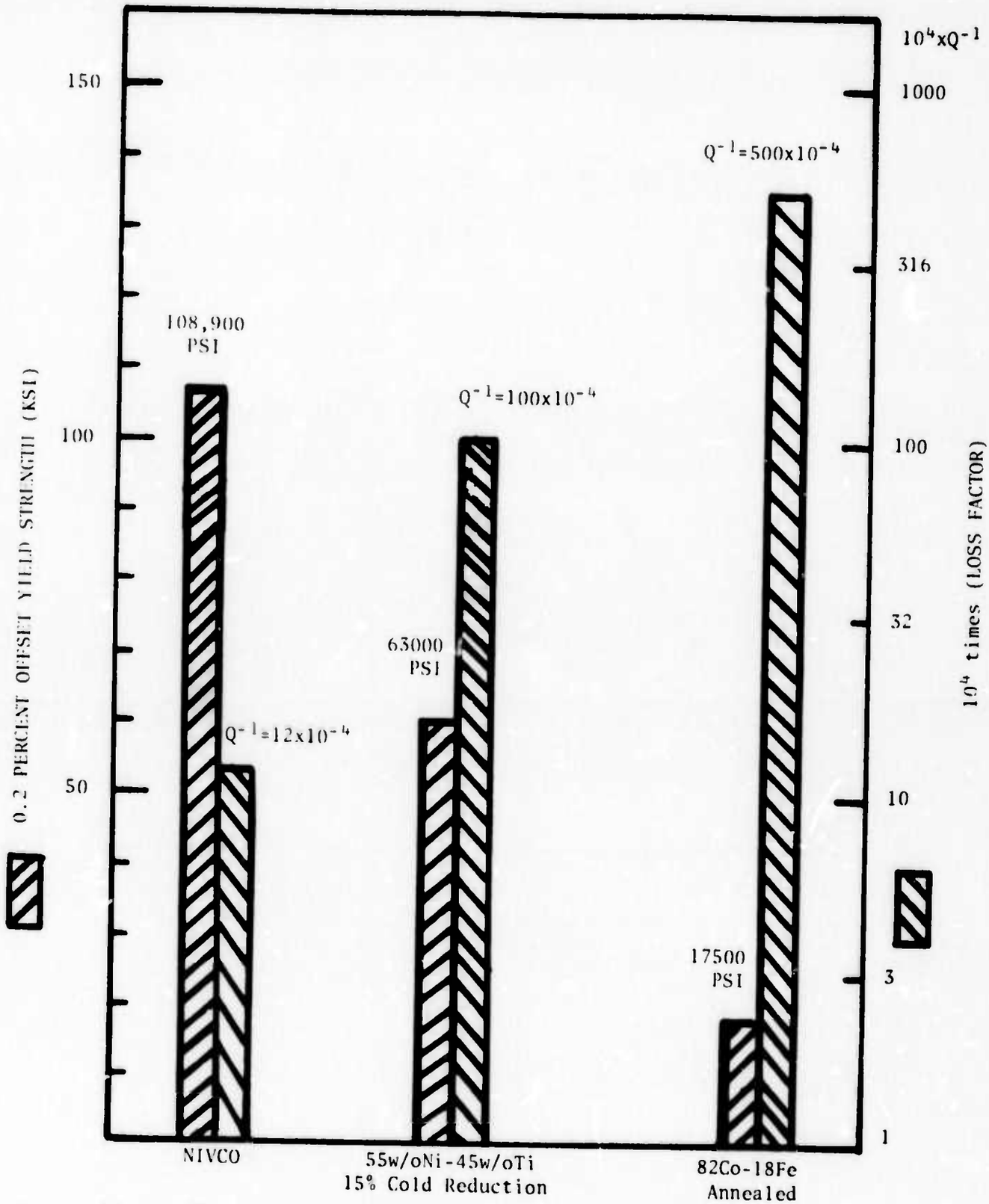

Figure 67. Comparison of Damping Capacity (Loss Factor) and Yield Strength for Several High Damping Materials at 25°C. Note that Damping Factor is Displayed on a Logarithmic Scale. Damping Capacity measured at frequencies near 150-250 Hz at a stress of 2000 psi.

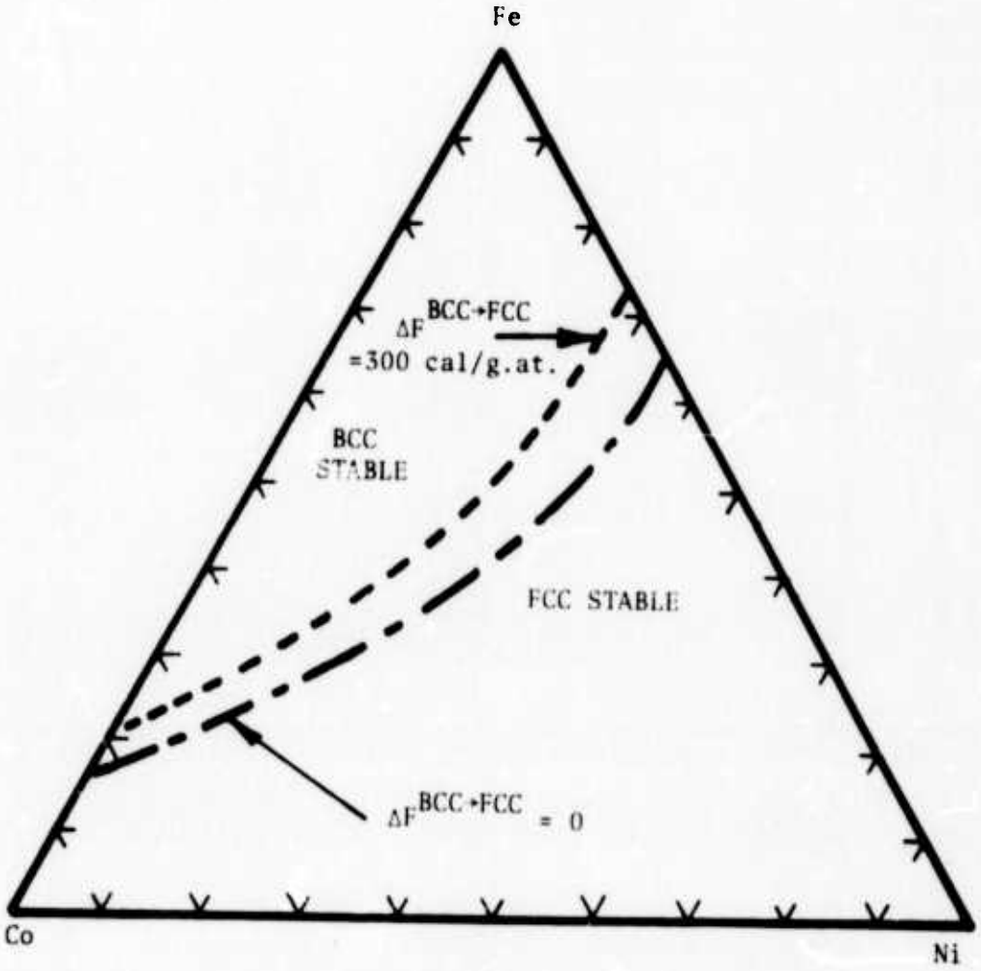

Figure 68. Calculated Regions of BCC and FCC Stability for Fixed Compositions at 25°C in the Iron-Nickel-Cobalt System.

V. DESCRIPTION OF THE EXPERIMENTAL METHODS FOR PERFORMING THE DAMPING MEASUREMENTS

During the period which is covered by the present report the main effort at Bolt, Beranek and Newman has been concentrated on design, construction and testing of the Resonant Dwell Apparatus. This type of apparatus can be employed to measure the specimen loss factor, g_S, as a function of temperature. This property is a direct measure of the acoustic absorption capacity of a given material. As a result of previous developments and current activities the apparatus can now be operated between -100°C and +300°C, thus covering the general range of interest for most engineering applications. In addition to upgrading the operating characteristics of the Resonant Dwell Apparatus some determinations of g_S were made as a function of temperature on standard "reed-type" and standard "flat-type" samples.

The measured material loss factors were obtained by means of a resonance dwell apparatus. Heine (21) and Cremer, Heckl and Ungar (22) have discussed resonant measurements of loss factors, and they have discussed a number of other techniques for measuring loss factors. The following discussion is based on their publications.

The resonance dwell technique is a forced vibration method of indirectly determining the loss factors of simple structural elements by measuring their response to excitation at a modal frequency. For a thin beam, where the mode and dynamic stress distributions are well known, the specific damping capacity of the material (energy dissipated per unit volume in one stress cycle at a given peak stress divided by 2π times the peak potential energy in the unit volume at the same stress) may be inferred from the determined loss factor.

In this test, the specimen loss factor in a mode (usually the fundamental) is determined from the resonant amplification factor, or Q, of the specimen in that mode. The mechanical Q of a

vibrating system is defined in terms of a characteristic deflection δ of the system due to distributed exciting forces proportional to the inertia forces of the mode in question. The amplification factor at resonance is

$$Q = \frac{\delta_{res}}{\delta_0} \tag{2}$$

where δ_0 is the deflection due to the distributed exciting force being applied statistically and δ_{res} is the deflection when the same pattern of forces is applied in simple harmonic motion at the modal natural frequency. The relationship between Q, the specimen loss factor g_s, and the logarithmic decrement ζ of single-degree-of-freedom system is

$$\zeta = \frac{\pi}{Q} = \pi g_s \tag{3}$$

The advantages of the resonance dwell method are: first, the ratio δ_0/δ_{res}, for a properly designed specimen, is dependent only upon the damping in the specimen; second, the vibration amplitude δ_{res} may be maintained at any constant level so that specimen damping may be determined as a function of a well-defined stress history; and third, because nothing is attached directly to the vibrating specimen, extraneous energy losses are minimized.

The method for ensuring that the beam specimen is excited at a mode is straightforward. The apparatus is constructed in such a way that the specimen acts as a vibration absorber placed on an excited single degree-of-freedom supporting system (see Figure 69). At a natural frequency of the beam, the response of the supporting system is minimized. The frequency of the response minimum, and hence of the beam mode, can therefore be determined by monitoring the acceleration of the supporting system.

A sketch of the apparatus is shown in Figure 70. A cantilever beam specimen of a test material is clamped to a bar which

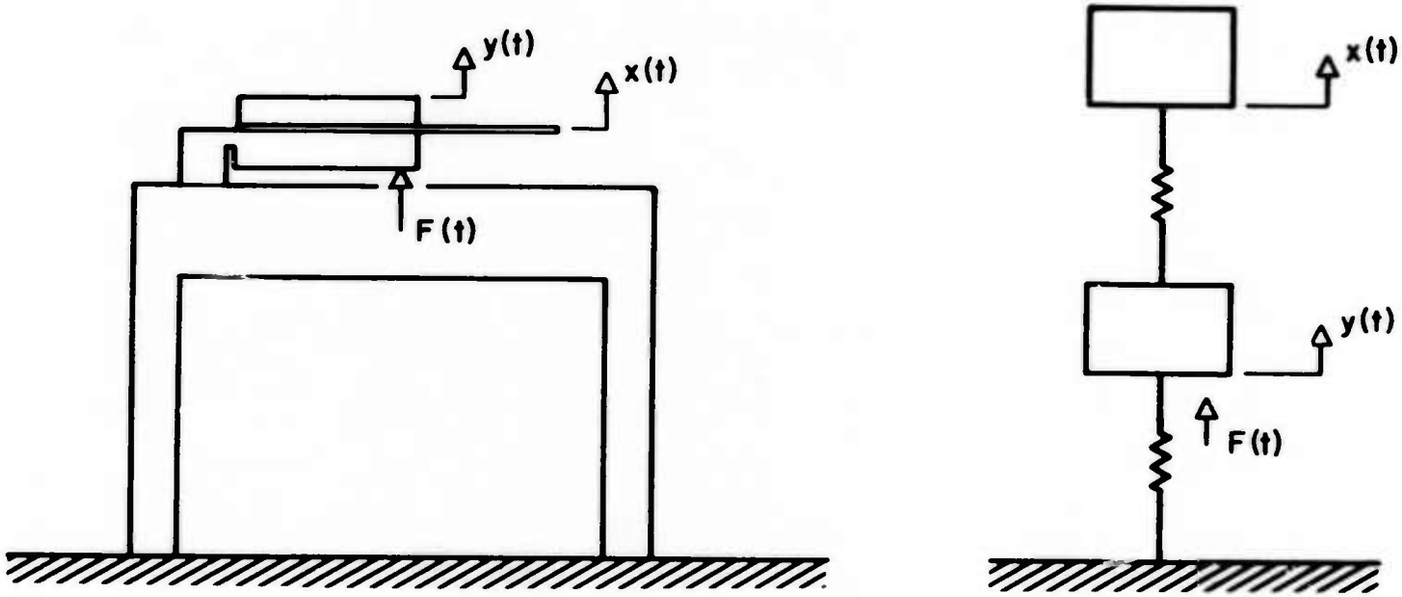

FIGURE 69 . AN EXCITED MECHANICAL SYSTEM WITH A RESONANT VIBRATION ABSORBER (EQUIVALENT TO THE RESONANT DWELL DAMPING APPARATUS).

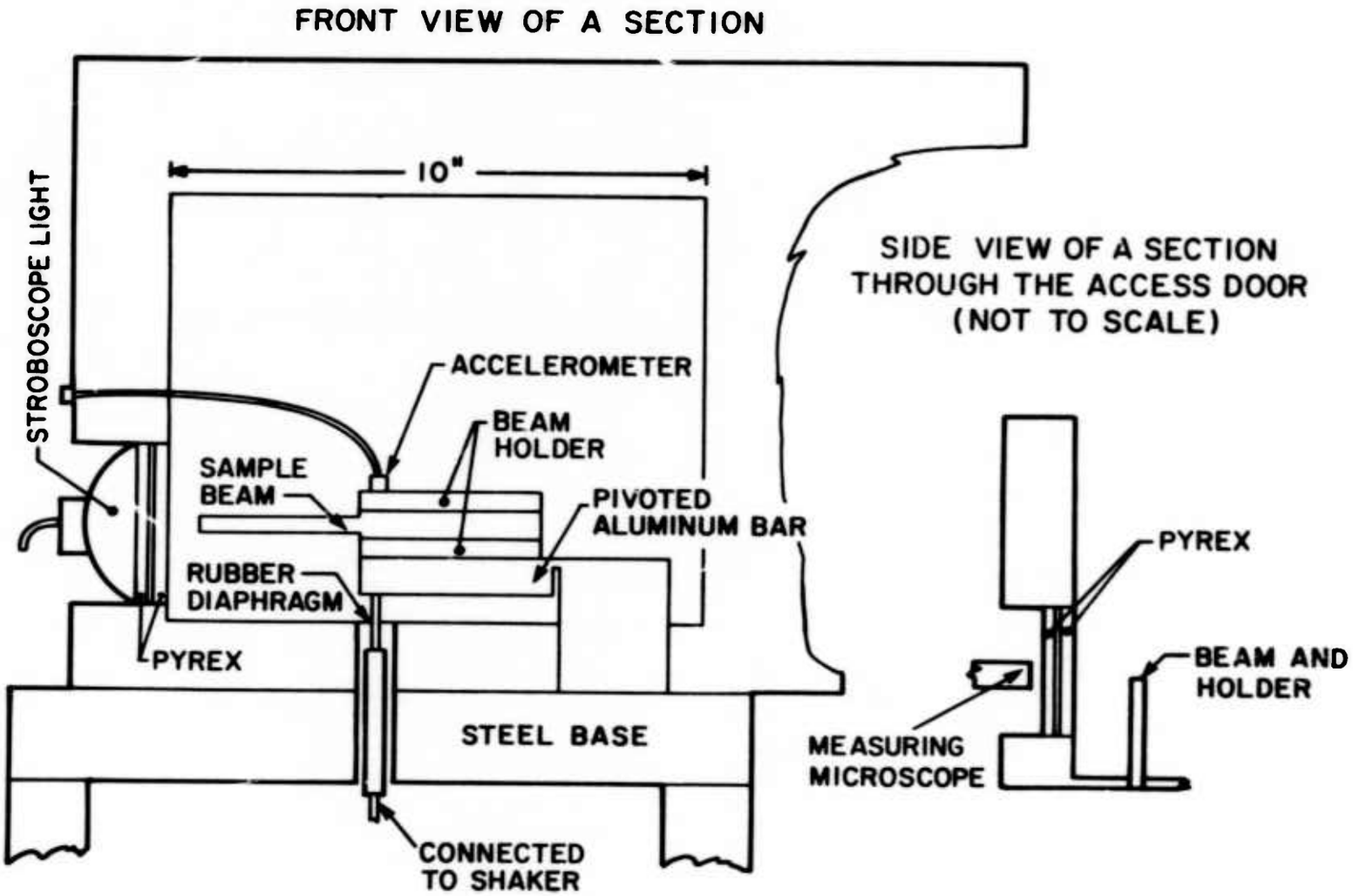

FIGURE 70. SKETCH OF THE RESONANT DWELL APPARATUS AND ENVIRONMENTAL CHAMBER.

is connected at one end to an electromagnetic shaker and the other to a heavy base. The thickness of the bar at the base end has been reduced by a saw cut to provide a pivot around which the remainder of the bar can rotate when excited by the shaker. Figure 71 shows the configuration of a typical reed-type test beam.

The shaker is connected to the bar by a rod which passes through a hole in the base. The hole is sealed by a rubber diaphragm which keeps the gases that are used for temperature control from leaking out of the chamber.

Control of the temperature of the test beam is provided by a commercially available environmental chamber that has been modified to provide some viewing ports. The chamber can be raised to a temperature of over 600°F by air that is blown over electric heaters. It can be cooled to -100°F by allowing carbon dioxide to expand through the chamber.

The base shown in Figure 70 may be placed on any convenient solid surface, such as a laboratory table. Excitation of the base by the shaker reaction is minimized by the large mass of the base and by supporting the body of the shaker on a jack which passes between the legs of the base. The jack provides some isolation of the shaker from the table. The isolation can be improved by supporting the shaker on a "bridge" that is tied to the floor. Measurements of the acceleration of the base showed the present configuration to be adequate.

The response of the supporting system [y(t) in Figure 69] to shaker excitation is measured with an accelerometer mounted on the bar at the root of the specimen. Specimen response [x(t) in Figure 69] is measured optically with a low power microscope with a retical.

Figure 72 shows a block diagram of the electronic instrumentation that is used in conjunction with the resonance dwell apparatus. Only two electronic measurements are required--identification of the resonant frequency of the test beam, and accelero-

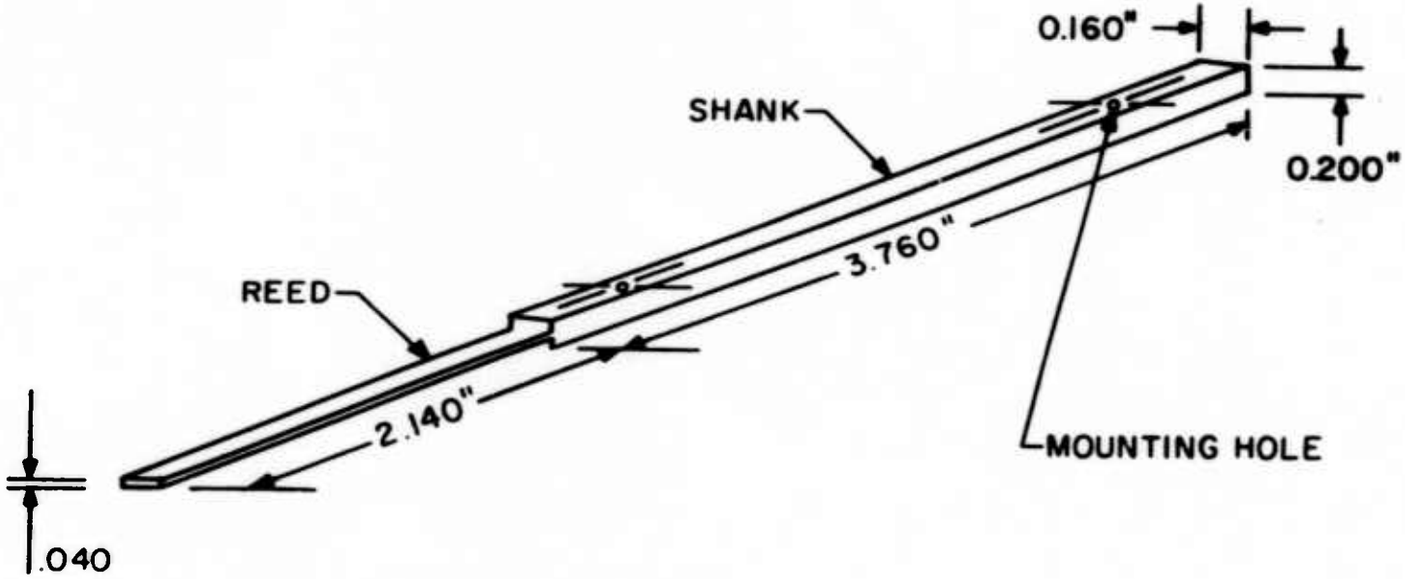

FIGURE 71. SPECIMEN DESIGN FOR MEASURING DAMPING CAPACITY.

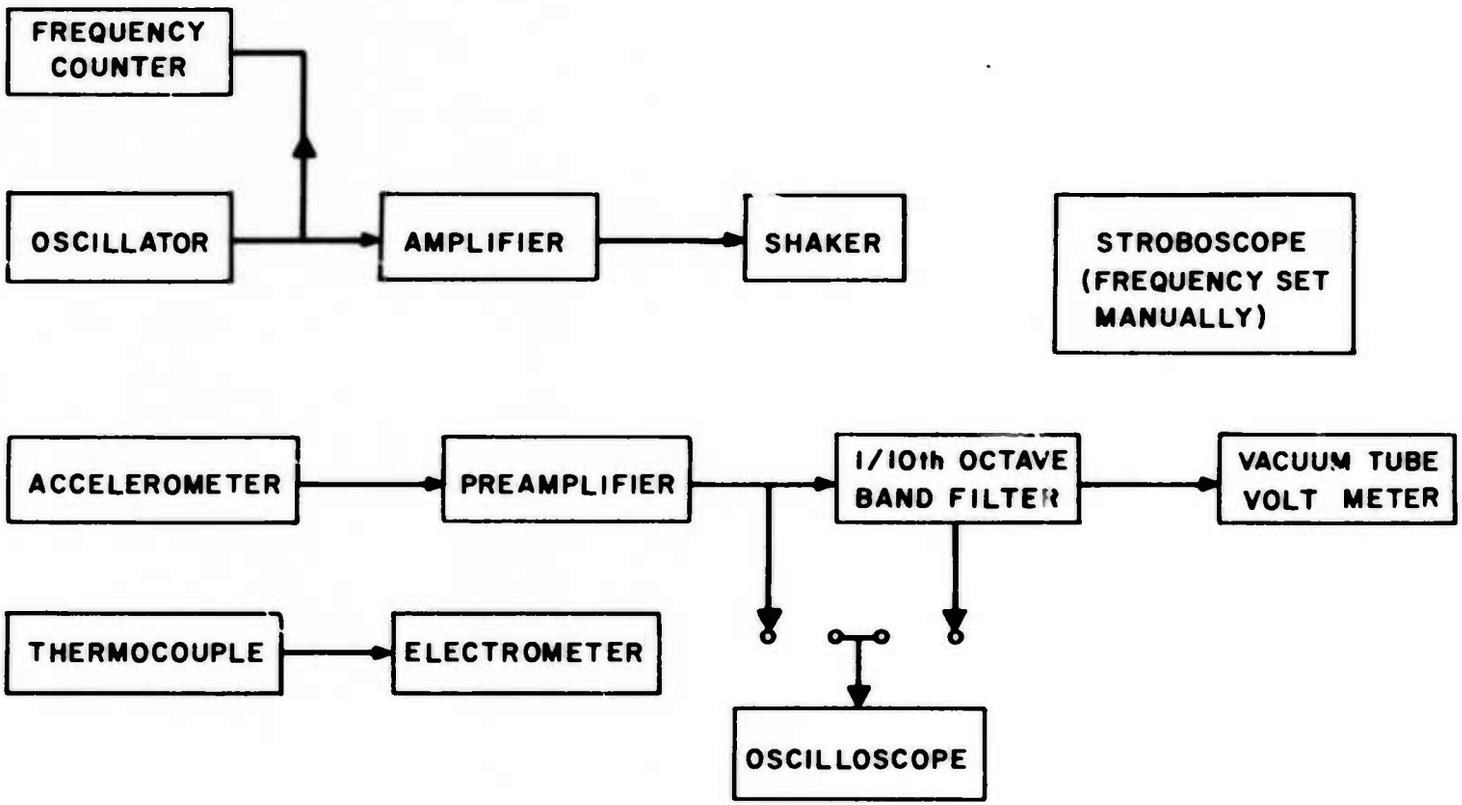

FIGURE 72. BLOCK DIAGRAM OF ELECTRONIC INSTRUMENTATION FOR RESONANT DWELL DAMPING MEASUREMENTS.

meter output. The remaining measurement is the nonelectronic optical measurement of displacement of the beam tip. That measurement is facilitated by the "stop-action" feature of a stroboscope light that is set to flash at nearly the same frequency as the frequency of the mechanical oscillation of the test beam. Figure 73 shows a photograph of the environmental chamber and the associated electronics.

The response of a test beam in the resonant dwell apparatus can be described by the following mathematics. For cantilever beams in their fundamental mode of vibration, tip amplitudes as a function of peak stress and specimen natural frequency are given by

$$y_{t,DA} = 3.63\left(\frac{\sigma_p}{f_n}\right)\frac{1}{\sqrt{E\rho}} \qquad (4)$$

where $y_{t,DA}$ = peak to peak amplitude (in.), σ_p = maximum stress (psi), f_n = specimen design natural frequency (Hz), E = Young's Modulus (psi), and ρ = material density (lb/in^3). The fundamental natural frequency of a cantilever beam of length L (in.) and thickness h (in.) is

$$f_n = \frac{1}{2\pi}\left(\frac{1.8751}{L}\right)^2 h\left(\frac{32E}{\rho}\right)^{1/2} \qquad (5)$$

The relationship between the specimen loss factor g_s and root acceleration a_0, fundamental specimen frequency f_n, and beam tip double amplitude $y_{t,DA}$ is

$$g_s = 0.083\ (1 + 0.2L)\ \frac{a_0}{f_n^2}\ \frac{1}{y_{t,DA}} \qquad (6)$$

where a_0 is the bar acceleration in $in./sec^2$ measured at the frequency f_n (the response minimum).

Each beam specimen may be run at the frequencies of modes higher than the fundamental. In practice, however, the highest

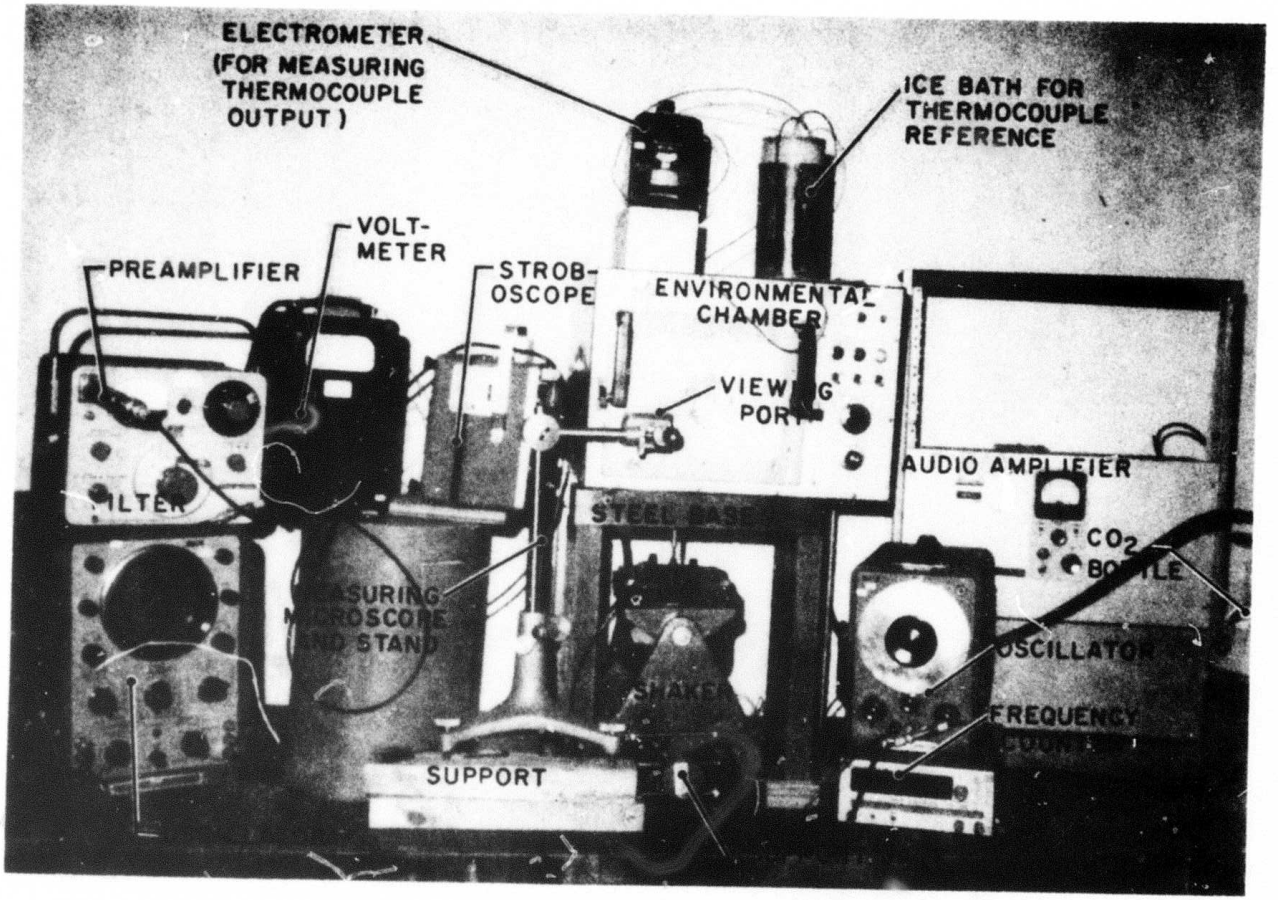

FIGURE 73. PHOTOGRAPH OF THE ENVIRONMENTAL CHAMBER AND ELECTRONICS COMPRISING THE RESONANT DWELL APPARATUS.

useful mode is usually the second (though for specially designed specimens the third might be used), because the tip amplitude for a given stress becomes very small with increasing frequency and because the force required for the excitation of a given stress increases with both mode number as well as frequency. For example, a force higher by a factor of more than 3 is required to excite a 10,000 psi peak stress in a specimen with a 650 Hz second mode than for a specimen designed to have a 650 Hz first mode even though the tip amplitudes required are the same for the two specimens.

The formulas equivalent to Equations 4 and 5 for the second mode are

$$f_2 = \frac{1}{2\pi} \left(\frac{4.6941}{L}\right)^2 h\left(\frac{32E}{\rho}\right)^{1/2} \tag{7}$$

and

$$g_{s,2} = 0.045\ (1 + 0.056L)\ \frac{a_0}{f_2^2 y_{t,DA}} \tag{8}$$

The measurements described in this section were obtained with a nickel-titanium reed-type sample like the specimen shown in Figure 32. The test specimen was prepared by standard heat treatment and temperature cycling 70 times between -90°C and +65°C.

Preliminary measurements of the temperature distribution within the test volume of the commercial temperature chamber revealed that the temperature was not uniform, and the temperature at a given point in the chamber varied with time for a fixed setting of the temperature control. Therefore, it was necessary to measure the temperature of the test specimen by attaching an iron-constantan thermocouple to its surface (near the root of the beam).

These measurements also showed that the specimen loss factor of the nickel-titanium test beam depended on the amplitude of vibration of the tip of the beam at a fixed temperature at which the higher loss factors were exhibited. In addition, the value of the loss factor and the relationship between the loss factor on

tip amplitude at a given temperature depended on the past history of the temperature changes. That is, the damping properties at a given temperature were not necessarily the same when the sample was cooling as when it was heating.

The resonant frequency of the test beam varied as the tip amplitude and temperature were changed. Some of the change in loss factor with changing tip amplitude may have been caused by the accompanying frequency change, and not by the amplitude change. However, the changes in resonant frequency were small. The resonant frequency of the test beam was between 150 Hz and 200 Hz for the entire range of temperature and tip amplitude covered during the tests.

Figure 74 shows that the specimen loss factor determined from the observations of the test specimen was not a function of tip displacement for the higher temperatures at which lower values of loss factor were observed. Figure 74 also shows that the measured specimen loss factor was a relatively strong function of tip displacement at the lower temperatures at which high specimen loss factors were measured.

The strain-independence of the loss factor at 77°F would seem to rule out dislocation motion and magnetic domain motion as the mechanisms that generate the observed loss factor since those mechanisms are predicted to be stress (and therefore strain) dependent (21). Of the known mechanisms for generating internal friction in metals, theory predicts that only thermal diffusion is independent of stress (ibid). Substitution of the values of the thermal coefficients for the test sample into the equation to predict the sample loss factor due to thermal diffusion yielded a value which is an order of magnitude lower than the constant value in Figure 33. Therefore, the loss factor measured at 77°F agrees with no known theory. Either the test material is controlled by some internal loss mechanisms that are not described by available theories, or the measuring equipment introduced some artifact. It seems unlikely that the equipment gave extraneous high readings at 77°F,

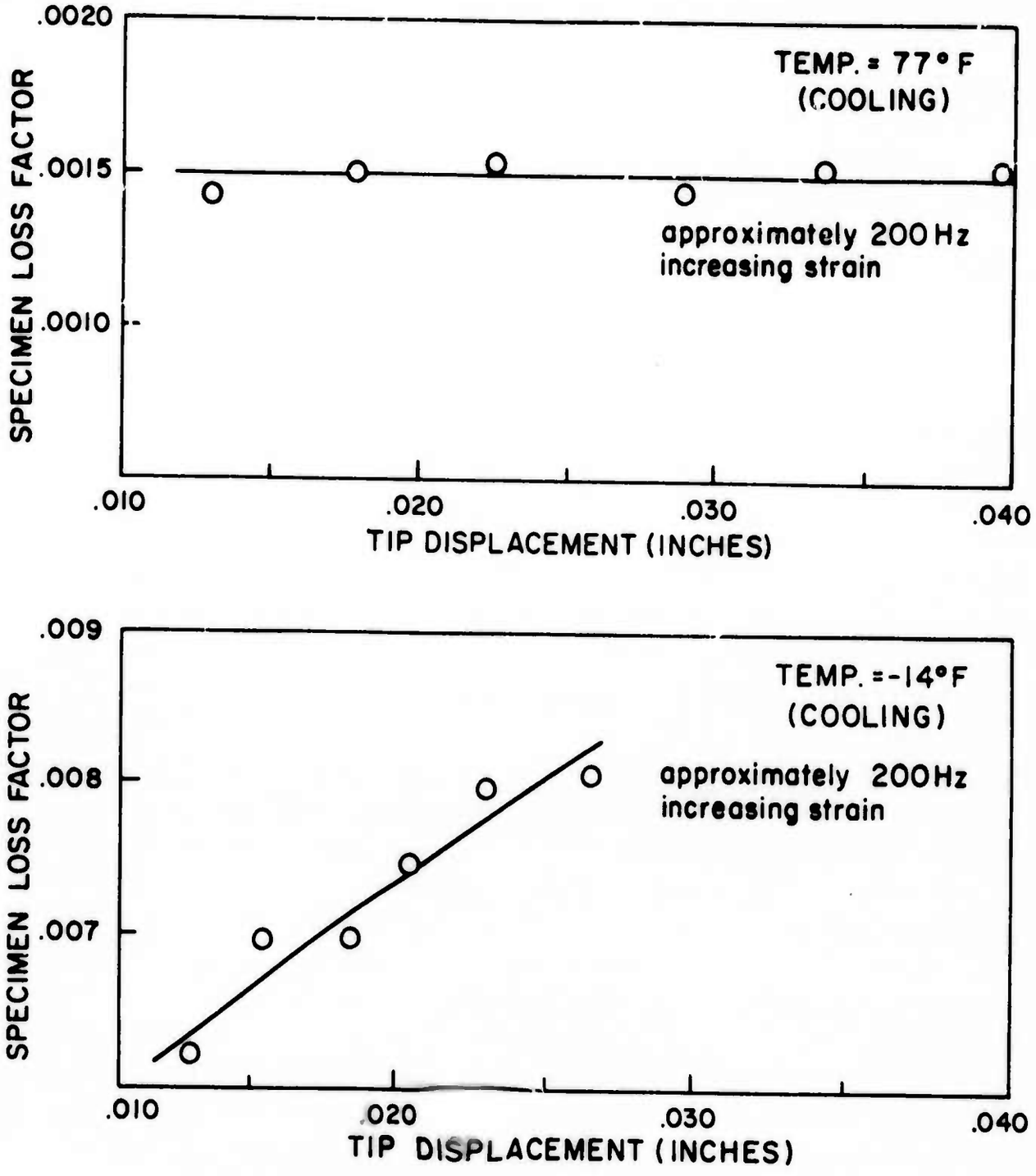

FIGURE 74. AMPLITUDE-DEPENDENCE OF THE SPECIMEN LOSS FACTOR OF NICKEL-TITANIUM SAMPLE NUMBER V4609-80.

since readings an order of magnitude lower (in agreement with thermal diffusion theory) were obtained above 100°F.

A number of graphs like those shown in Figure 74 were used to pick off the specimen loss factor corresponding to a constant tip displacement (zero to peak) of .02 in. for various temperatures. It was necessary to use separate graphs for heating sequences and cooling sequences. The value of the loss factor depended slightly on the strain sequence (increasing or decreasing strain). Straight lines were fit through the points on the graphs like those in Figure 74. Curved lines may have been equally appropriate. The straight line provided better definition of the temperature dependence of the damping factor than was obtained before any attempt was made to plot the damping factors at constant tip amplitude.

Figure 75 shows the specimen loss factors determined from observations of the nickel-titanium test specimen. The curve reveals some apparent hysteresis in the damping properties of the specimen--the specimen loss factors effective at temperatures near 80°F appeared to be different for the cooling and heating cycles. Relatively small errors in the measured output of the thermocouple attached to the root of the test beam could have contributed to the apparent hysteresis. If portions of the test beam were not at the same temperature that was measured at the root of the beam, there might have been apparent hysteresis generated by the non-uniform temperature of the beam.

The point that lies well above the curve in Figure 75 was determined from observations of the test sample that were made on a different day from the observations that yielded most of the other points in the figure. That point provides some evidence that the response of the test sample depended on the past history of the sample, which is consistent with the observed temperature hysteresis of the damping properties of the test sample.

Laboratory measurements showed that the internal damping of mechanical vibrations of a nickel-titanium test beam was unusu-

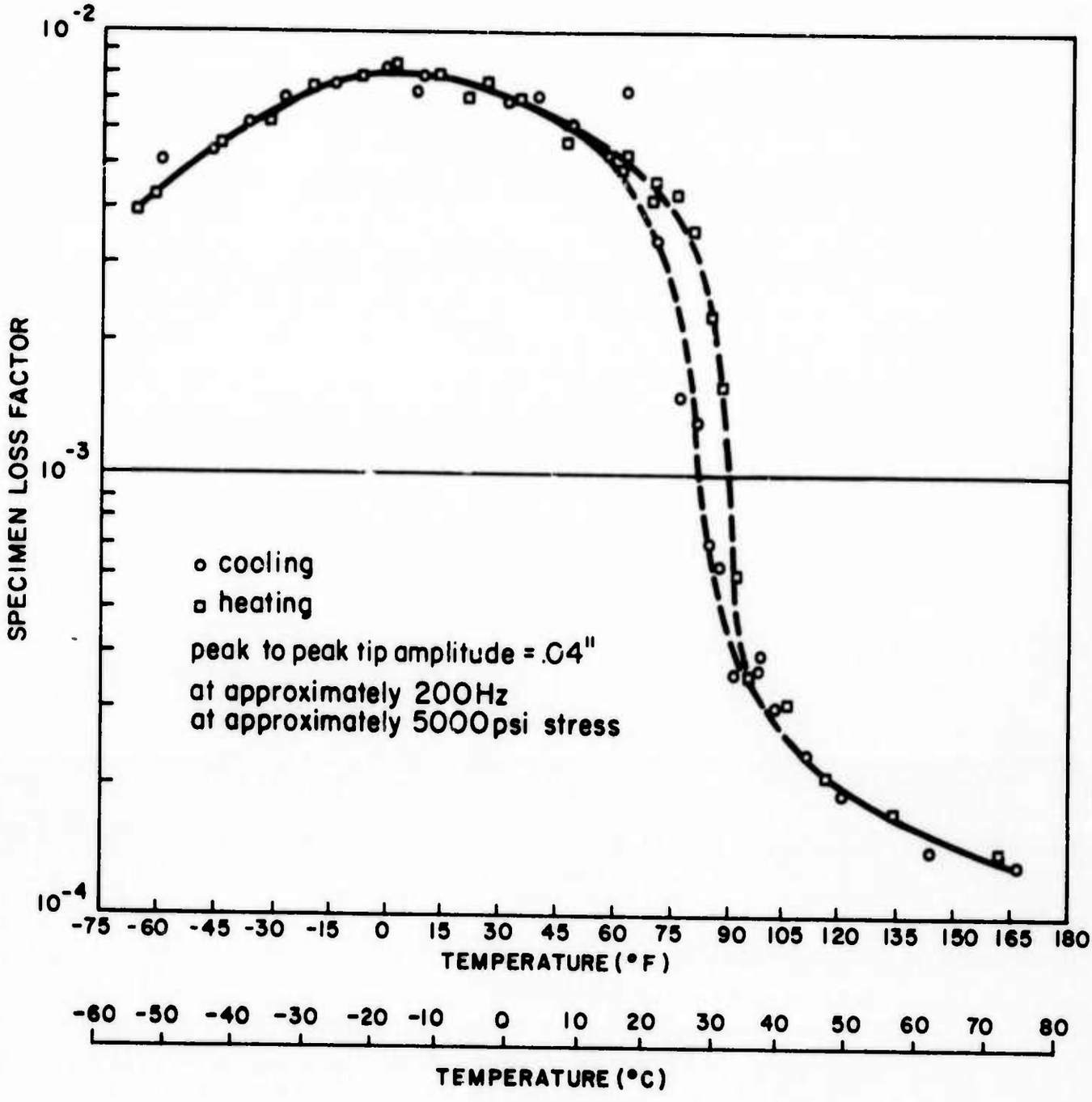

FIGURE 75. TEMPERATURE-DEPENDENCE OF THE SPECIMEN LOSS FACTOR OF NICKEL-TITANIUM SAMPLE NUMBER V4609-80 (AT CONSTANT TIP AMPLITUDE).

ally high at temperatures below about 80°F. The specimen loss factor approached .01 near 0°F at about 200 Hz and about 5000 psi stress. That value for the loss factor is more typical of built-up composite structures than homogeneous samples (23,24). The values of the loss factor determined from the measurements depended on temperature, past history of temperature, the amplitude of the tip of the vibrating test reed, possibly upon the resonant frequency of the test beam, and depended slightly upon the strain history of the test beam.

Some of the experimental data do not agree with theories of the mechanisms of generation of internal friction. Although equipment artifacts cannot be ruled out, it seems unlikely that extraneous equipment responses were responsible for the unexpected data.

There is a possibility that the apparent temperature hysteresis of the specimen loss factor described in this report was due to slight errors in the measurements of the temperature of the test beam. In addition, it is possible that the temperature of the test beam was not uniform during the tests. The beam and test chamber should be provided with a number of thermocouples in order to precisely define the thermal conditions of the test beam.

The question of the origin of those particular data which do not conform to theory should be resolved. If the appropriate stress range can be covered for several samples of different dimensions but identical material, then there would be more basis for deciding whether to look for equipment artifacts or to revise the theories.

It is possible that the loss factor of the test sample at a given temperature and a given level of stress or strain is a function of the resonant frequency of the beam (21). In addition, temperatures and/or stress hysteresis might be more pronounced at frequencies and stresses other than those for which the reported measurements were gathered. If several samples of different lengths and thickness can be prepared from a single batch of Ni-Ti alloy,

then curves of loss factor versus increasing and decreasing temperature can be prepared for several combinations of frequency and stress level. Moreover, since the loss factor of the test specimen depends not only on the temperature sequence leading up to a given test temperature, but upon the length of time that the sample is maintained at a given test temperature as well, it would be instructive to investigate the temperature dependence of the loss factor for different rates of increasing and decreasing the temperature.

VI. SUMMARY

The results obtained during the initial phase of this study indicate that structural changes which occur during phase transformations (particularly those of a thermoelastic nature) can offer a significant means for absorbing acoustical energy. In particular the complete set of resistivity, modulus, heat capacity and damping measurements performed on the 55 w/o Ni-45 w/o Ti alloy shows that over a useful temperature range between 12°C and 32°C high yield strength and high damping can be combined. Moreover, present results indicate that plastic deformation can be employed to expand the temperature range over which the attractive properties can be combined and to increase the strength levels.

Although the above mentioned desirable characteristics appear attainable, the mechanistic origin of the damping remains a mystery. The present results show that damping increases above the M_S temperature. Although twin formation readily occurs below M_S, no discernable structural changes occur above M_S. Hence the only postulated source for enhanced damping at temperatures above M_S is some precursor mechanism like soft mode formation. Externally applied tensile stresses characteristic of those employed in the damping measurements (up to 5500 psi) were found to have a negligible effect on M_S.

Preliminary studies of iron-platinum, copper-aluminum-nickel, cobalt-nickel, and cobalt-iron alloys suggest that other examples of high strength-high damping materials based on structural transformations may be developed. In particular, a range of cobalt-iron alloys has been identified which exhibits loss factors that are five to fifty times higher than commercially available materials. Although the strength of this alloy is currently low, mechanisms exist for increasing the strength. These methods are currently under investigation.

REFERENCES

1. G. D. Sandrock, Met. Tr. (1974) 5 299.

2. G. D. Sandrock, A. J. Perkins and R. F. Heheman, Met. Tr. (1971) 2 2769.

3. K. Otsuka, T. Sawamura, K. Shimuzu and C. M. Wayman, Met. Tr. (1971) 2 2583.

4. L. Kaufman and M. Cohen, Progress in Metal Physics, Volume 7 (1958) p. 165, Pergamon Press, London.

5. I. A. Arbuzova, V. S. Gavril'yuk and L. G. Khandros, Fiz. Met. i. Metalloved. (1970) 30 181.

6. I. A. Arbuzova, V. S. Gavril'yuk and L. G. Khandros, Fiz. Met. i. Metalloved. (1959) 27 1126.

7. M. E. de Morton, J. Appl. Phys. (1969) 40 208.

8. M. E. de Morton, J. Australian Inst. of Metals (1969) 14 228.

9. A. W. Cochardt, Tr. A.I.M.E. (1956) 206 1295.

10. L. Kaufman and H. Nesor, Zeit. Metallkunde (1973) 74 249.

11. A. Kussman and K. Jessen, J. Phys. Soc. Japan (1962) 17, Supplement B1, 136.

12. R. J. Weiss, Proc. Phys. Soc. (1963) 82 281.

13. T. Takeuchi and M. Honma, Science Reports of the Research Institute of Tohaku University, A9 (1957) p. 492.

14. B. K. Basu, Applied Physics Letters (1973) 15 961.

15. K. C. Mills, M. J. Richardson and P. J. Spencer, "Thermodynamic Properties and Phase Diagram of the Fe-Co and Ni-Pt System," Faraday Society Symposium (1973)(to be published).

16. H. Schumann, "Cobalt" (1968) 40 156.

17. U. Hashimoto, J. Japanese Inst. of Metals (1937) 1 177.

18. K. Ishida and T. Nishizawa, Tr. Jap. Inst. of Metals (1974) 15 225.

19. R. M Bozorth, Ferromagnetism, D. Van Nostrand Company, New York (1959) Figure 5-77.

20. A. Cochardt, Magnetic Properties of Metals and Alloys, A.S.M., Cleveland, Ohio (1959) 251-279.

21. J. C. Heine, "The Stress and Frequency Dependence of Material Damping on Some Engineering Alloys," Ph.D. Dissertation, Massachusetts Institute of Technology (1966).

22. L. Cremer, M. Heckl and E. E. Ungar, Structure-Borne Sound, Springer-Verlag, New York, Chapter III (1973).

23. E. E. Ungar, "Damping of Panels," in Noise and Vibration Control, Ed. Leo L. Beranek, McGraw-Hill, New York (1971).

24. E. E. Ungar, "The Status of Engineering Knowledge Concerning the Damping of Built-up Structures," J. Sound & Vib. 26 (1) 141-154 (1973).